Karlsruhe Institute of Technology

Annual Report 2012

October 2013

Karlsruhe Nano Micro Facility (KNMF)

Dr. Jürgen Mohr, Dr. Susan Anson, Thomas Schaller

A colour version of this report is available for download
on the KNMF website (www.knmf.kit.edu)

KIT – University of the State of Baden-Wuerttemberg and
National Research Center of the Helmholtz Association

Karlsruhe Institute of Technology (KIT)
Karlsruhe Nano Micro Facility (KNMF)
Hermann-von-Helmholtz-Platz 1
76344 Eggenstein-Leopoldshafen
Germany

Phone: +49(721)608-23123
Fax: +49(721)608-26273
Email: knmf-useroffice@kit.edu

Table of Contents

KNMF – a research infrastructure offering open access to micro and nano technologies and expertise for academic and industrial R&D groups

Multi-material nano/micro fabrication and characterisation is developing rapidly worldwide. In addition to the ongoing fundamental research in this area, a transition to application focussed R&D activities and industrial use can be observed with nano and micro technologies as key enablers to innovations in various application areas like health care, medical diagnostics, information and communication technologies, energy, automation, optics and photonics, etc. To exploit new research ideas and innovative products profound process knowledge, skilled employees and highly advanced equipment is needed. Thus, it is increasingly difficult for individual research groups at universities, in research centers and in industry to keep up with state-of-the-art technologies and processes developments. To overcome this problem, the Karlsruhe Nano Micro Facility (KNMF) has been established by KIT. KNMF facilitates access to high end technologies and expertise in the area of micro and nano structuring and characterisation. External users from academia and industry across the globe can access the nano- and micro technology equipment and expertise. KNMF complies with the Helmholtz rules on operating large scale user facilities. Free and open access is given via a proposal system and after positive project evaluation by an independent peer review board; the results need to be published. Access is also possible on proprietary base by full cost recovery

Technologies offered

KNMF has started operation in 2009 involving the facilities of seven institutes at KIT, which work closely together in three virtual laboratories

- KNMF laboratory for micro- and nanostructuring (opened in 2009)
- KNMF laboratory for microscopy and spectroscopy (opened in 2010)
- KNMF laboratory for synchrotron characterisation (opened in 2012)

The latter offers the unique possibility to combine traditional characterisation methods for micro/nano characterisation with synchrotron based methods at one place.

In 2012 in total 21 technologies were available. There is an on-going investment programme in which new equipment is being commissioned and dedicated to be offered to KNMF users. During 2012 the technologies direct laser writing and single crystal X-ray diffraction were newly commissioned and added to KNMF portfolio. In the light of decreasing demand by users, electron probe micro analysis was removed from KNMF's portfolio; SEM is no longer available as an individual installation but is still an important auxiliary technology and can be used in combination with other installations. The existing technologies as of the beginning of 2013 and the planned installations in the next years can be seen in figure 1. It is not only the single technology which makes KNMF of interest for external user. The possibility to combine the technologies offered by KNMF to complex process chains and characterisation clusters allows the execution of user requests in a more comprehensive manner. This is demonstrated by external and internal user projects described in the following chapters.

In 2012, KNMF offered a total machine time of roughly 60.000 hours per year not including the beam-time of the ANKA beamlines. About 38 persons (scientists, technicians) were running the KNMF processes. The number will increase up to 49 persons in the next two years.

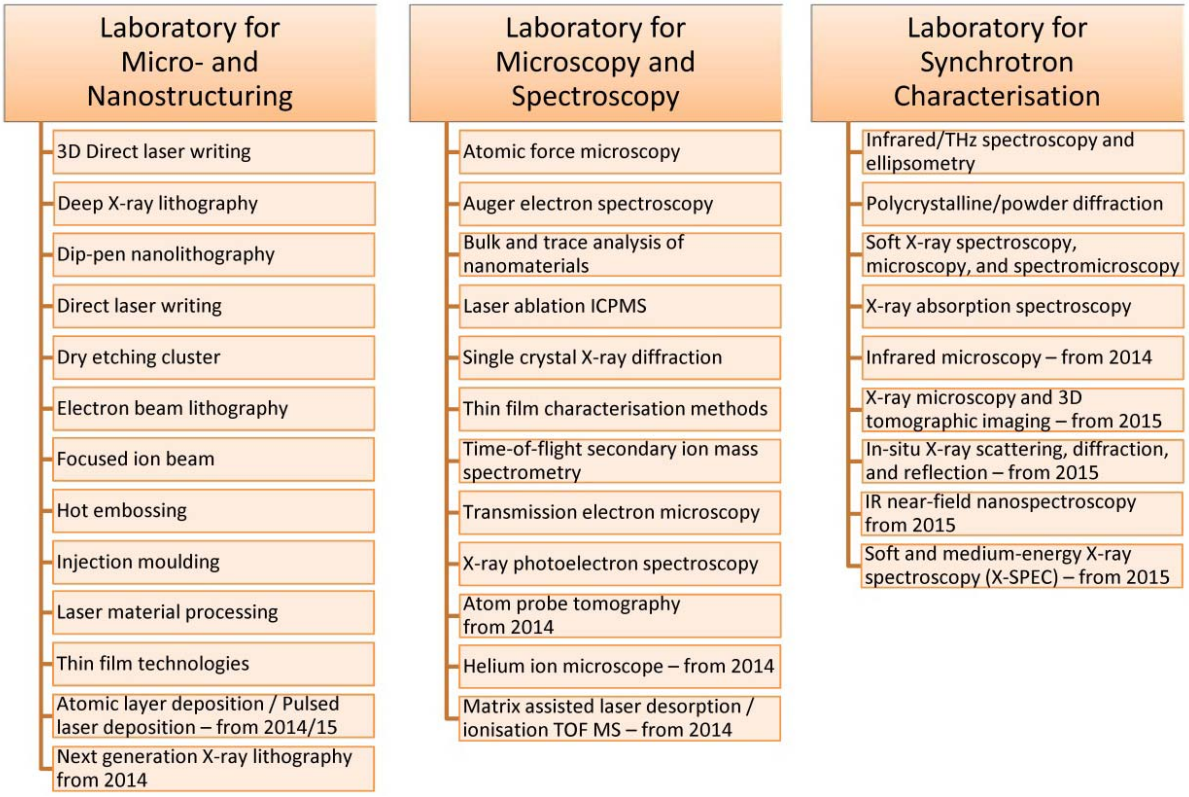

Fig. 1: Portfolio of the KNMF as of today and the future planning

Access and use of KNMF

A simple Peer Review process ensures transparent, open, and no fee access to KNMF for work intended for publication. Two calls per year are published and proposals are evaluated immediately after the close of the call by an independent peer review board. For user projects linked with public funded and already reviewed external collaborative projects, *e.g.* European, BMBF, DFG projects the proposal submission is simplified and the PRB adopts the decisions made by the respective independent review panels as long as the activities are in support of the project partners. Users can submit four types of proposals:

- standard (duration up to 6 months),
- long-term (duration up to 2 years),
- proprietary (full cost recovery, not peer reviewed, publication of results not required),
- fast-track (for small and urgent tasks upon decision of the KNMF head, review by PRB *a posteriori*).

The users are encouraged to contact the user office or the technical experts prior to proposal submission to discuss all open issues and to define a feasible workplan. This usually results in well-written proposals and increases the chance for acceptance during the review process.

Full details of how to access KNMF can be found under http://www.knmf.kit.edu/.

Since the start of KNMF's operation in 2009 the number of proposal has increased continuously reaching an average of 90 to 100 per call (fig. 2). KNMF is still in the implementation phase which is characterized by an increase of the fraction of external use and which will result in an equal fraction of external and internal use in 2014. In 2012 the annual use by external users was about 45% already.

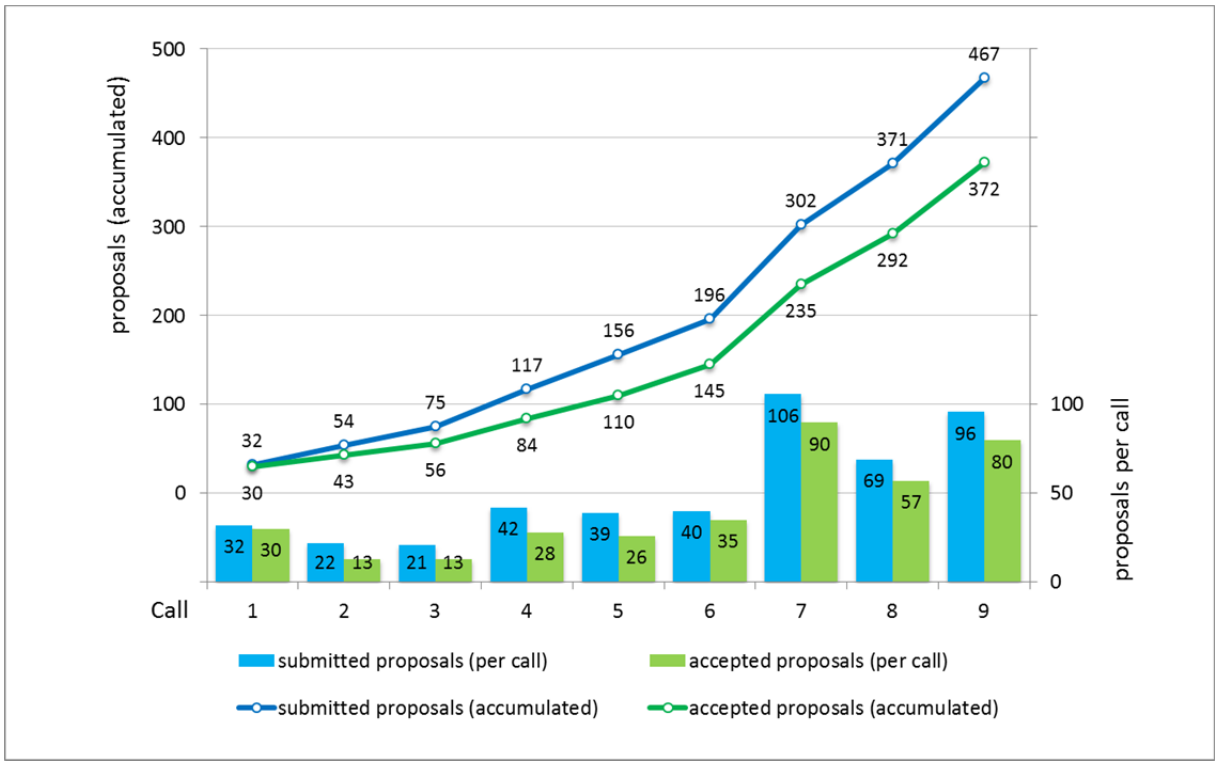

Fig 2.: Numbers of proposals submitted and accepted per Call

Figure 3 shows the type of organization which submit proposals; 23% of users are from industry. KNMF is not only intended for national users. Almost half of the users come from outside Germany, whereas 15% are from outside Europe. This demonstrates that KNMF's technology portfolio and competence is recognized as having worldwide relevance and also enables international groups to improve their scientific output. (Fig.4)

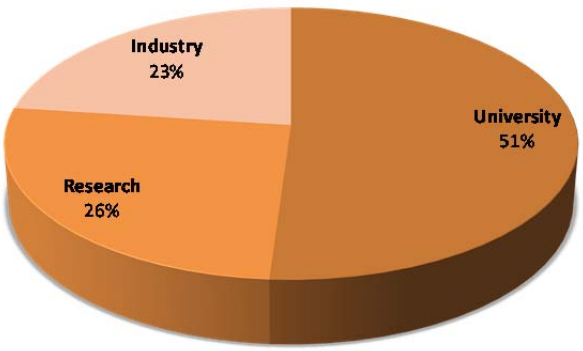

Fig 3 type of organisation of users

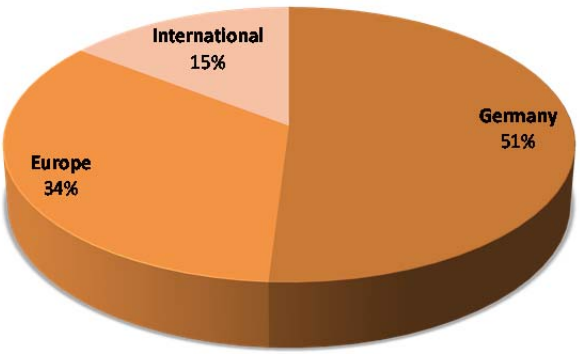

Fig. 4 geographical orign of users

Usually KNMF user requests do not ask for access to a specific technology only but require solutions to achieve particular goals. Such projects need a very close interaction between KNMF staff and the user for pre-preparation of the project and post-processing of the project results. It is an important observation that the human factor, the direct interactions and the time a KNMF expert spends with the user, is at least as critical for the overall success of the KNMF project as the raw technology time as measured in machine hours.

KNMF – a research facility

The key ingredient for KNMF's technical competence is that it builds on technologies and skills developed in the Helmholtz Programme Science and Technology of Nanosystems (STN), in particular, on technologies which have reached a sufficient level of maturity and robustness to handle the large variety of user requests. The ongoing close collaboration between STN and KNMF ensures a continuous development of the expertise in micro- and nanotechnologies.

In view of strategic development KNMF has started to identify promising R&D topics relevant to strategic research fields, which address complex research challenges and warrant long term collaborations ("public-public" partnerships). These public-public-partnerships are being established along the value chain with partners responsible for fundamental scientific research, methodology studies, instrumentation and innovative application oriented developments. The virtual institute "New X-ray analytic methods for material science" (VI-NXMM) is a first realization of this concept. It started from the x-ray imaging activities in medical applications brought to KNMF by Prof. Pfeiffer's group (Technical University Munich) and was further complemented by external (EMPA, CAU, HZG) and internal partners (IAM-WK, IPS, ANKA) with a focus on materials analysis. Additional public-public partnerships are under discussion and will be established in the future.

KNMF has already demonstrated a huge impact on the scientific output in different nano and micro technology related fields. This is demonstrated by around 120 publications in referenced journals and additional presentations which are related to KNMF's activities.

User Committee

The User Committee was elected in 2011. It is the interface between KNMF and its users and communicates the interests and needs of the users to the KNMF board. It gives also advice to the future development of KNMF's technology portfolio.

Elected members are:

Prof. Dr. Sven Achenbach (Chair), University of Saskatchewan, Canada
Prof. Dr. Florian Banhart, University of Strasbourg, France
Dr. Erik Bründermann, Ruhr-University of Bochum, Germany
Prof. Dr. Jost Göttert, Hochschule Niederrhein, Krefeld, Germany
Prof. Dr. Lorenz Kienle, University of Kiel, Germany
Dr. Karen Lienkamp (Co-Chair), University of Freiburg, Germany

In-house Activities / Results from Internal Users

Electron Beam Lithography (EBL)

Peter-J.Jakobs, Julian.Hartbaum, Kira Koehnle, Christian Lay

E-Beam – Lithography is operated in KNMF by the Institute of Microstructure Technology (IMT) for fabrication of high accurate structures in nano- and microscale. We use a state of the art 20 bit Vector Beam – Tool from Vistec for 6” Substrates with Ultra High Resolution and Extreme Wide Field (VB6UHR-EWF), that means we can exposure a real big mainfield of 1310 µm with a resolution of 1.25 nm. We tune in to two different ways. One way is to realize a pattern in extreme thick resist (3200 nm), only a few working groups are doing this worldwide. The other way is to expose a very small pattern, down to about 20 nm (depends on substrate stack). In 2013 we want to establish the Proximity- Effect-Correction (PEC). This is rather complex, because the layer composition of some of our substrates consist of up to 7 different layers with different heights, but first results are looking promising. In addition we try to improve our exposure alignment down to about 10 nm. Below you will find some elected R&D activities which have been performed in 2012.

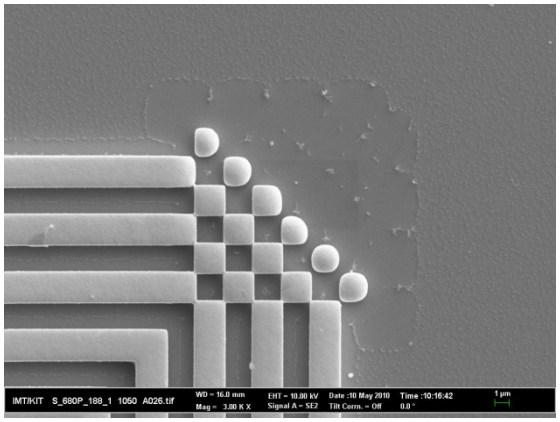

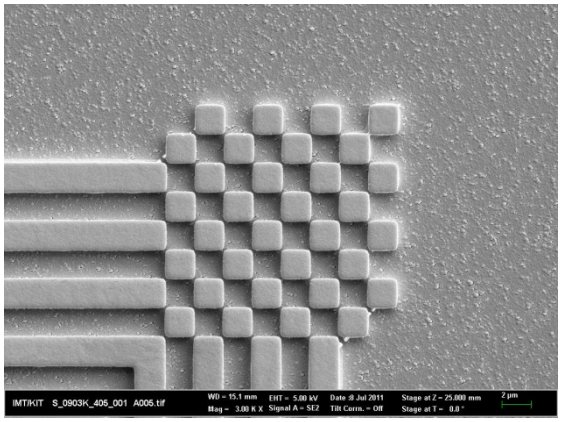

Fig. 1: Pattern without PEC (Resist height 3200 nm) Pattern with PEC (Resist height 3200 nm)

Double beam actuator

This work focused on the fabrication of free-standing Ti double beam cantilevers with critical dimensions of 50-500 nm covered by an integrated magnetic cube at the front end. Main challenges were the patterning of nanostructures as well as their release from the substrate to get movable cantilevers. Resist nanostructures are written by e-beam lithography at 100 kV (Vistec VB6 UHR EWF). A reactive ion etching tool was used to transfer the nanopattern in a metallic layer system consisting of gold and titanium. Direct-write technology (an aligned e-beam exposure) enabled the integration of magnetic Permalloy cubes on top of the cantilevers front ends. The release of the functionalized cantilevers was performed by dry etching methods.

The deflections of the magnetic functionalized cantilevers will be realized by external magnetic fields. At the same time, resistance measurements of a double beam in a Wheatstone-configuration allow the determination of the deflection due to the piezoresistivity of the thin gold layer. Additionally, in stationary magnetic fields, the beams can be heated by an electrical current causing a deflected/undeflected state of the beams due to heating the Permalloy above the Curie-temperature.

Combining the magnetic double beam actuators with other functional nano devices opens a route to fabricate nano-magneto-mechanical systems for active handling of fluids or manipulating of objects in the nano domain.

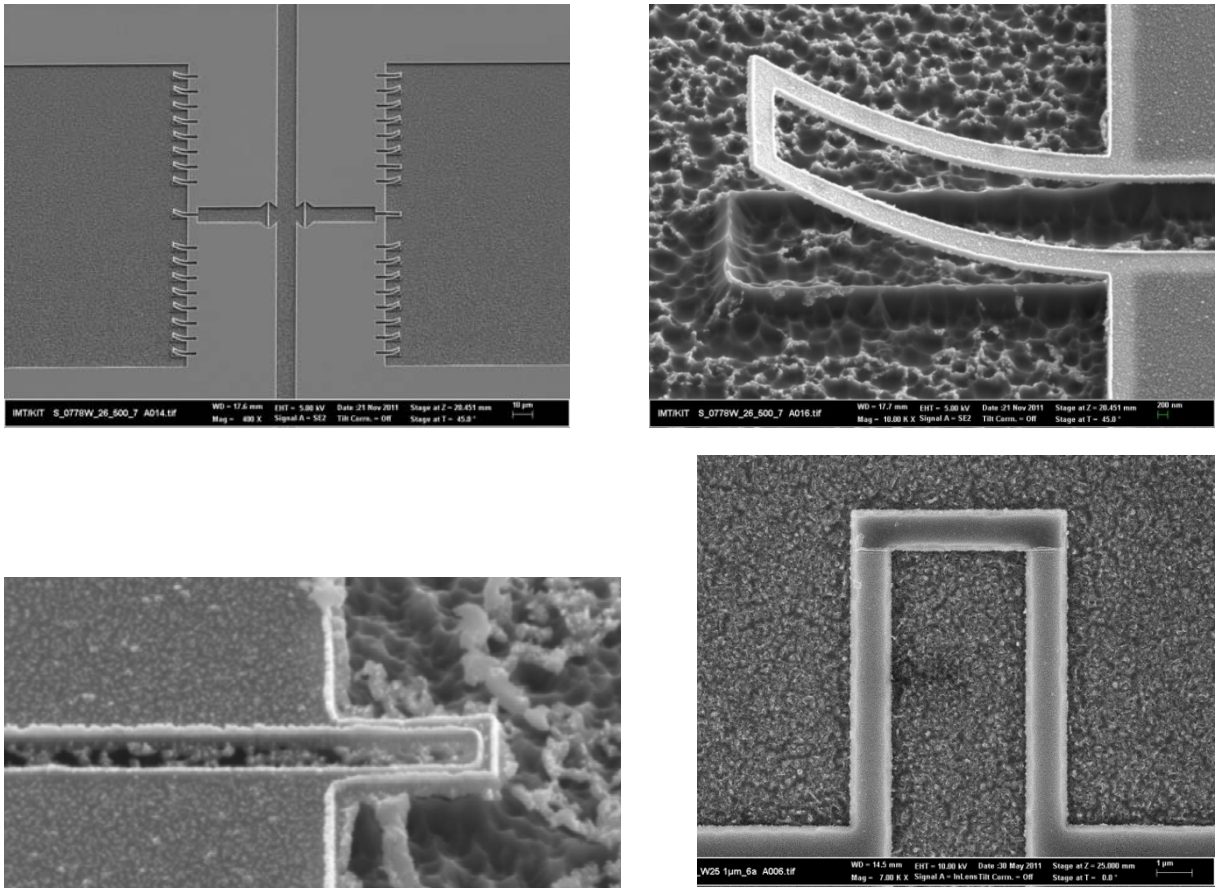

Fig. 2: SEM-pictures of double beam structures. Upper left: Array of double beams. The two middle-beams can be electrical contacted. Upper right: Released double beam, 50 nm thickness, 400 nm width. Bottom left: 100 nm thickness, 100 nm width. Bottom right: 300 nm Permalloy on top of the front end of a double beam with 500 nm width, realized by a direct-write exposure, which was aligned to the prestructured beams.

Sub-wavelength Grating Waveguides

Reported under DRIE

Silicon-rich Silicon-nitride Ring Resonators

Reported under DRIE

Nanoimprint Silicon Stamps

Nanoimprint technology allows the parallel production of nanoscale structures at high speed. However, the fabrication of nanoimprinted structures requires the development of high precision stamps with low surface roughness for low demoulding forces.

Electron beam lithography is essential to create structures with feature sizes down to 100 nm. We use PMMA positive resist as well as AR-N 7520 negative resist on silicon wafers to create silicon stamps for nanoimprinting. An example of developed resist structures can be seen in Figures 3 and 4.

The challenge in creating these imprint stamps are the different demands of electron beam exposure and imprinting. For the latter, large filling structures have to be adjacent to the desired nanostructures to achieve a homogeneous distribution of polymer in the stamp's trenches and a low residual polymer height under the stamp's elevated structures. However, when large structures are exposed with the electron beam, nearby small structures receive

part of the dose. This proximity effect has to be mitigated by careful layout design as well as adjusting the dose according to results of a proximity effect simulation.

After development of the resist, the pattern is transferred to the silicon with reactive ion etching in the Oxford Plasma Lab 100 RIE chamber.

To achieve rectangular as well as smooth sidewalls, we use a cryogenic silicon etch process with a very low etch rate to improve control of the profile depth. Figure 5 shows an etched silicon stamp with structure sizes down to 280 nm.

The result of an imprint process with a silicon stamp is shown in Fgure 6. While it was possible to reproduce the structures, the residual resist height was still too high. Thus, further optimization of filling factor and profile depth are required.

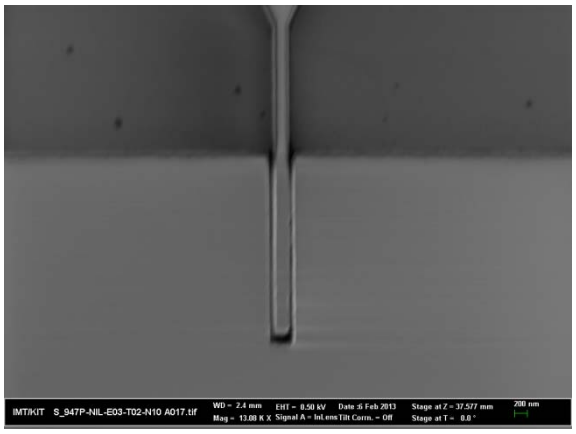

Fig. 3: SEM image of negative resist after exposure and development.

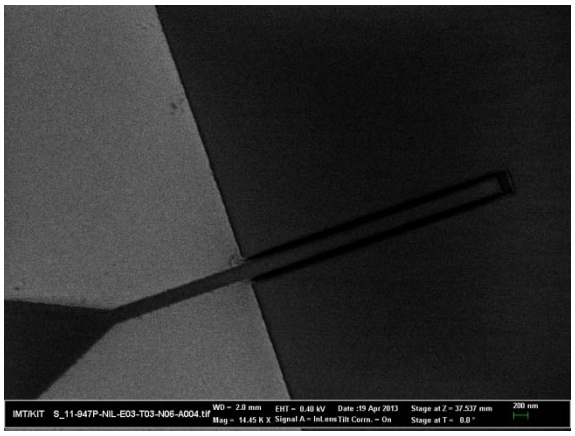

Fig. 4: SEM image of positive resist after exposure and development.

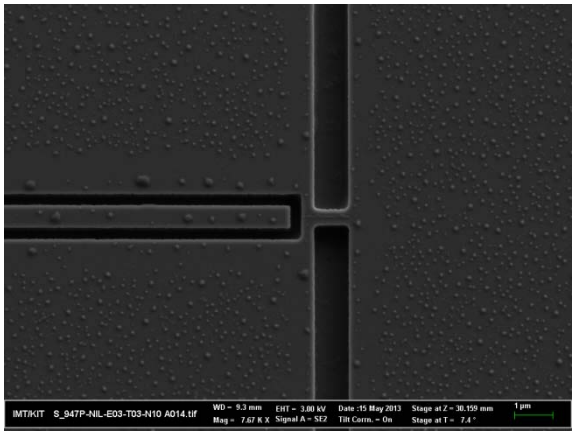

Fig. 5: The stamp after silicon etching. The surface is contaminated with resist residue, which can be removed by oxygen plasma treatment.

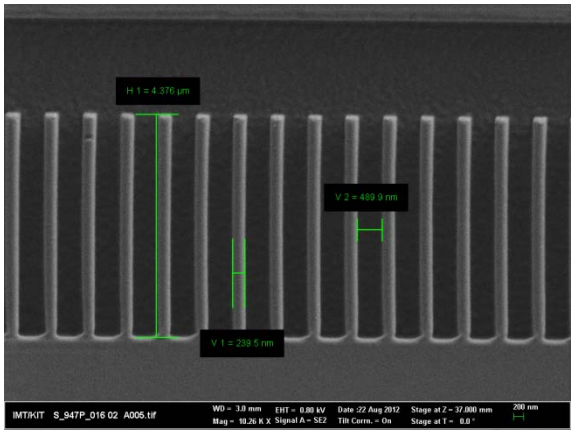

Fig. 6: Imprinted resist structures. The beams have a height of 4.4 µm and a width of 240 nm.

References

[1] R. Palmer, A. Luca, D. Korn, P. Schindler, M. Baier, J. Bolten, T. Wahlbrink, M. Waldow, R. Dinu, W. Freude, C. Koos, and J. Leuthold, "Low Power Mach-Zehnder Modulator in Silicon-Organic Hybrid Technology," Photonics Technology Letters, IEEE, vol. PP, pp. 1-1, 2013.

[2] D. Korn, M. Lauermann, P. Appel, L. Alloatti, R. Palmer, W. Freude, J. Leuthold, and C. Koos, "First Silicon-Organic Hybrid Laser at Telecommunication Wavelength," in CLEO: Science and Innovations, 2012.

[3] W. Freude, J. Brosi, C. Koos, P. Vorreau, L. C. Andreani, P. Dumon, R. Baets, B. Esembeson, I. Biaggio, T. Michinobu, F. Diederich, and J. Leuthold, "Silicon-Organic Hybrid (SOH) devices for nonlinear optical signal processing," in Transparent Optical Networks, 2008. ICTON 2008. 10th Anniversary International Conference on, 2008, pp. 84-87.

4] D. Hillerkuss, R. Schmogrow, M. Meyer, S. Wolf, M. Jordan, P. Kleinow, N. Lindenmann, Philipp C. Schindler, A. Melikyan, X. Yang, S. Ben-Ezra, B. Nebendahl, M. Dreschmann, J. Meyer, F. Parmigiani, P. Petropoulos, B. Resan, A. Oehler, K. Weingarten, L. Altenhain, T. Ellermeyer, M. Moeller, M. Huebner, J. Becker, C. Koos, W. Freude, and J. Leuthold, "Single-Laser 32.5 Tbit/s Nyquist WDM Transmission," J. Opt. Commun. Netw., vol. 4, pp. 715-723, 2012.

[5] C. Koos, J. Leuthold, W. Freude, T. J. Kippenberg, J. Pfeifle, C. Weimann, K. Hartinger, V. Brasch, T. Herr, R. Holzwarth, D. Hillerkuss, and R. Schmogrow, "Terabit/s data transmission using optical frequency combs," pp. 860009-860009, 2013.

Deep X-ray Lithography (XRL)

Maximilian Amberger, Martin Börner, Jochen Heneka, Birgit Hübner, Alexandra Karbacher, Arndt Last, Danays Kunka, Felix Marschall, Barbara Matthis, Jan Meiser, Pascal Meyer, Daniel Münch, Jürgen Mohr, Vladimir Nazmov, Franz Josef Pantenburg, Christin Straus, Julia Wolf

Three beamlines at the synchrotron source ANKA are operated in KNMF by the Institute of Microstructure Technology (IMT) for fabrication of high aspect ratio microstructures (HARMST). LITHO 1 and LITHO 2 are open to users, LITHO 3 is under commission up to 2014 to allow upscaled fabrication for multiscale dimensions. The in-house research focuses on process improvement and optimization as well as on the fabrication of new and innovative HARMST with HGF internal customers. The following R&D activities performed in 2012.

X-Ray Lenses

We are developing refracting imaging lenses for X-ray full field microscopy for high photon energies up to 30 keV. As the refractive power of all lens materials is very weak, a few hundred biconcave parabolic shaped lens elements are necessary for a focal length of a few centimetres. The aperture of the lenses is only 70 µm and the radius in the apex of the parabola 6 µm, so the fabrication is very challenging. As the exact shape of the surface and the alignment of all lens elements with respect to each other are very important, deep X-ray lithography is a very suitable process. Deep X-ray lithography easily allows for varying the lens elements geometry and aperture along the optical axis. 2012 new type of so called Taille-lenses has been developed using this potential. In X-ray full field microscopy Taille-lenses provide a larger field of view and increased resolution compared to conventional X-ray lenses.

In order to reduce the absorption influence accompanying any increase in aperture, the optically passive material can be removed systematically, retaining only the refracting surface areas and arranging the residual shapes onto a kinoform curve [1,2]. But, the microstructures in the periphery become even thinner and lose their mechanical stability. To avoid this fact, a new design, containing pillar-like microstructures with triangular and similar cross-section was developed. The pillars are to be placed separated from each other like inclined triangular prism, geometrically as it is shown in Fig.3. The microstructures have been arranged in a weaving pattern, but with some spaces between each other, resembling a mosaic. The deep X-ray lithography approach with its high-collimated and deep penetrating X-ray beam employed for the X-ray patterning is highly relevant to the design of large aperture 2-D lenses with an aperture of 1.5 x 1.5 mm and the microstructures cross-section below 40 µm, so the fabrication is very challenging (Figure. 1, 2).

The preliminary testing of the manufactured lenses was conducted at the synchrotron source Spring-8, in Japan. The results of measurement are collected in Table 1. The measured gain already achieved the gain delivered by X-ray capillaries,. however this is only a part of the achievable theoretical gain.

Very thin and long pillars cannot provide the designed wave-guide arrangement for conducting of the X-ray beam. In order to stabilize their position, the manufacturing parameters have been optimized.

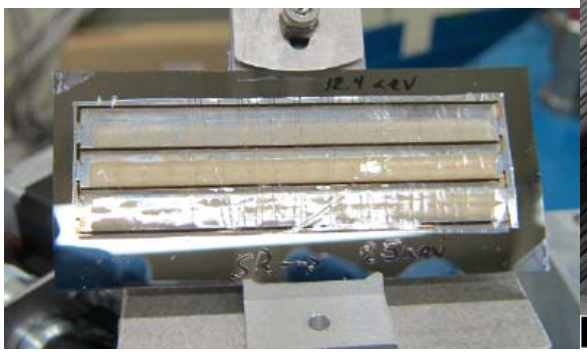

Fig.1: Three X-ray mosaic lenses for three photon energies, namely 12.4, 25, and 50 keV mounted on one substrate.

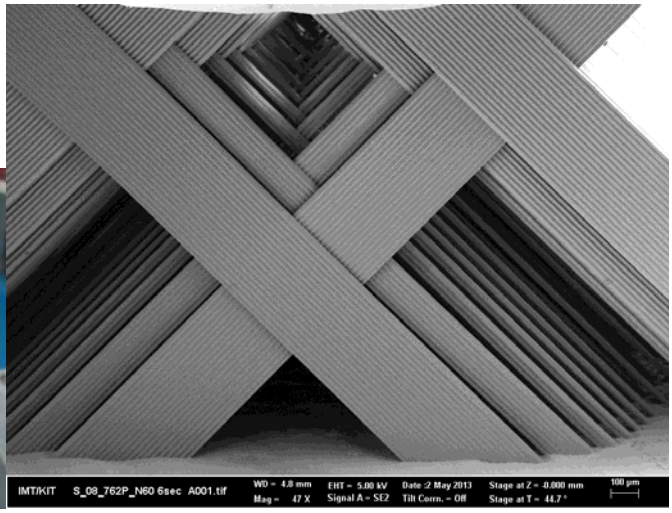

Fig.2: SEM-picture of a 2-D mosaic lens of SU-8 for a photon energy of 25 keV.

Table 1: Measured parameters of the point focus mosaic lenses

Parameter	12.4 keV	25 keV	50keV
Gain	176	14.25	8.38
Spot size, µm	44.6 x 44.6	46.4 x 46.4	63.8 x 290

The produced 2-D X-ray mosaic lenses have already been employed in the experimental studies at the synchrotron sources Spring-8, PETRA-III, and ANKA.

X-ray microscopy experiments with our lenses take place at several synchrotrons, for example ANKA, Petra III, ESRF and Spring-8. Besides the gain of knowledge concerning the lens design, the experiments gave promising results in material science, for example. The best resolution achieved at 30 keV was in the range of 200 nm (line and space), see Figure 3.

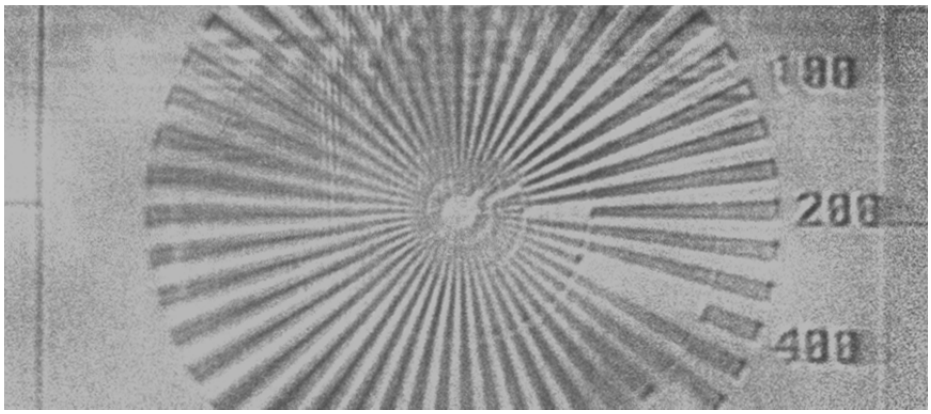

Fig. 3: Full field X-ray microscopy with a Siemens star (0.5 µm gold, 30 µm diameter, resolution: 200 nm/line pair)

X-ray Gratings

We are developing gratings for X-ray Phase Contrast Imaging. This imaging technique provides three types of image information: absorption contrast, phase contrast and dark-field contrast. The challenging fabrication of high aspect ratio structures >80 becomes necessary,

because small periods (2 – 10 µm) for compact setups and high absorbers for energies >30 keV are needed.
Deep X-ray lithography allows the fabrication of such high aspect ratios, but the following development and electroplating of the LIGA process may cause structure deformations and collapses. Freeze drying can avoid deformations in the development step (cf. *Freeze-Drying for Advanced Fabrication of HARMST*). Today's electroplating baths run at 55 °C. The elevated temperature causes an expansion of the resist material, so tensions may lead to deformations like waviness and trenches. To overcome this limitation in 2012 we developed a low temperature bath operating at 30 °C. In order to compare the baths we fabricated two gratings with the same layout and the same height and electroplated one in each bath. Both gratings have been measured at ANKA Topo Tomo with the same experimental setup and conditions. The experiment shows two tendencies, an improved visibility and an improved homogeneity. Both factors influence the final picture quality.

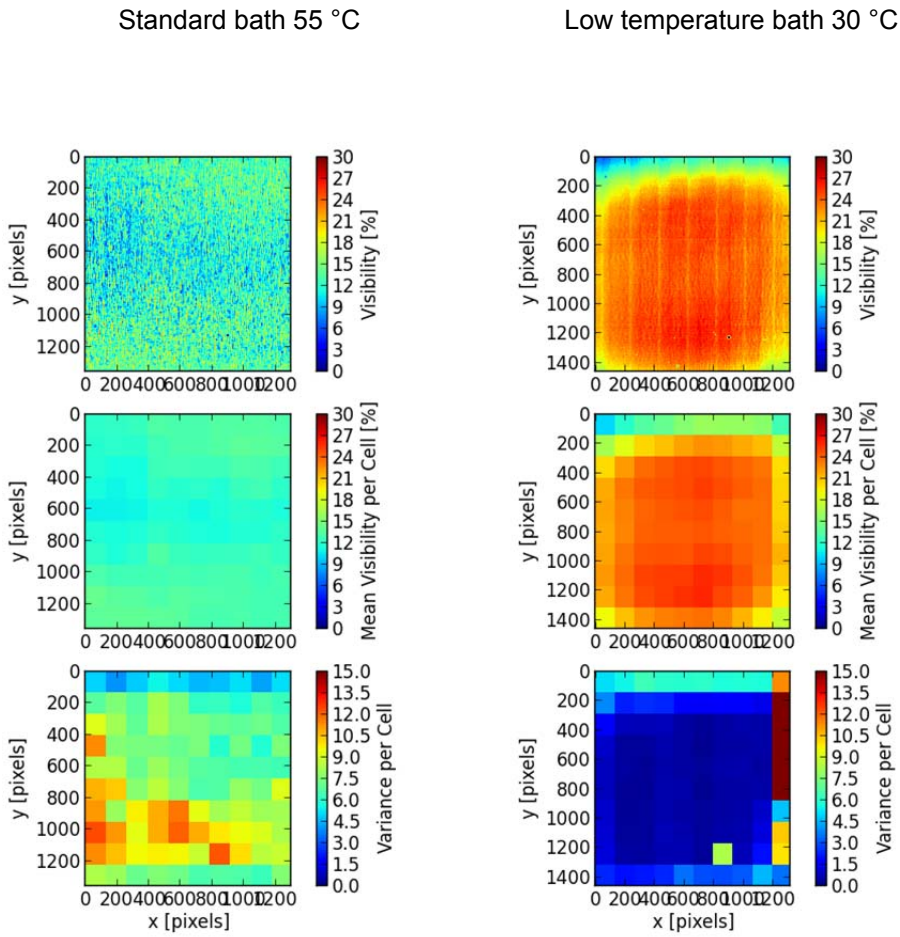

Fig. 4: From top to bottom, the figure a) shows the visibility, b) mean visibility of the different regions and c) homogeneity for each of the regions maps

Freeze-Drying for Advanced Fabrication of HARMST

Current developments in micro- and nanotechnology show a trend to progressively increasing aspect ratios. Unfortunately, in lithography based micro processes, the achievable

aspect ratio is limited by structure collapse due to capillary forces which occur during drying after development. Capillary forces can be avoided by freeze drying, hence avoiding the direct phase change from liquid to gas. By freeze drying, microstructures with high aspect ratios show significantly fewer defects in comparison to drying in air. Applications which require high aspect ratio microstructures are thus rendered possible. For example X-ray gratings and X-ray mosaic lenses structured by deep X-ray lithography might be improved with this technique.

The X-ray gratings consist of long parallel lamellas with a thickness of 1.2 µm a length of 20 mm to 60 mm and an aspect ratio up to 100 see [Figure 5]. At the moment the lamellas are stabilized by additional structures to avoid collapsing. In the future these structures might get unneeded due to freeze drying, which would increase the quality of the gratings significantly. Improved grating quality give better imaging contrast and resolution in X-ray phase contrast imaging (PCI). PCI will be used in breast cancer recognition with outstanding resolution in future.

X-ray mosaic lenses consist of a huge number of tall, freestanding, pillars with small triangular cross-section, forming lenses similar to Fresnel lenses. In view of their applications, the aperture of a lens should be as large as possible. This is however limited by the possible aspect ratio. By freeze drying the reachable aspect ratio for these lenses already has been increased from 8 to 25. Due to the current experiments further improvements are possible. X-ray mosaic lenses are used as condenser in hard X-ray full field microscopy to upgrade illumination and thus reduce exposure time and noise.

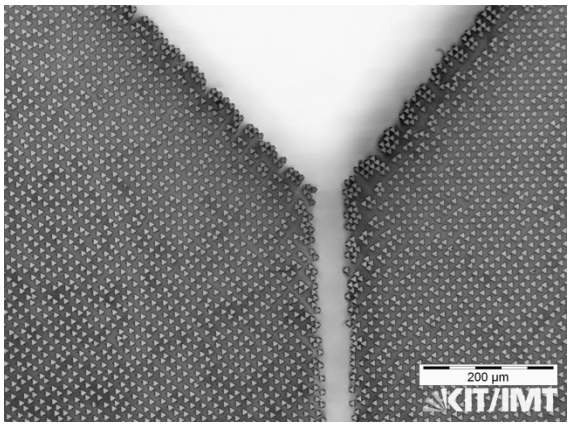

Fig. 5a: Freeze dried part of an X-ray mosaic lens consisting of triangular pillars (10 µm edge length, 230 µm height)

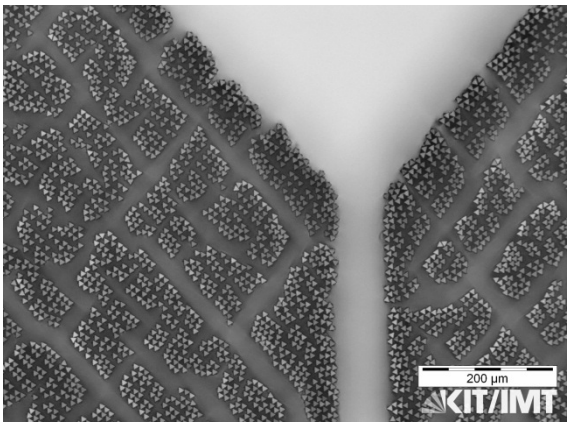

Fig. 5b: As fig. 9a but conventionally dried

Currently we are running systematic experiments for finding the optimal drying process and pushing the fabrication limits. The experiments also intend to find the now reachable aspect ratio for different geometries and structure sizes.

A new Generation of X-RAY LIGA Mould Inserts for Micro Injection Moulding

Recent developments in the LIGA technique lead to a completely new modification of the classical LIGA process chain the LIGA2.X process [Figure. 6]. This new approach aims at the large scale fabrication of single polymeric microparts (volumes below 0.5 mm^3) using a new kind of X-ray LIGA-mould inserts and micro injection moulding.

The advantages of the new approach LIGA2.X compared to the classical LIGA process are the elimination of any rework during fabrication of single polymeric micro parts, reduction of scrap production, industry and mass production suitable mould technology for injection

moulding using a new developed demoulding concept, optimized injection moulding parameters for every single cavity and the possibility for a flexible arrangement of LIGA2.X mould inserts in multicavity moulds. The residual layer free production of single polymeric micro parts in the LIGA2.X approach overcomes also the typical prejudice of the LIGA process like costs and time with characteristics like near shape replication of the parts, short cycle times, elimination of process steps and easy changeable mould inserts during production.

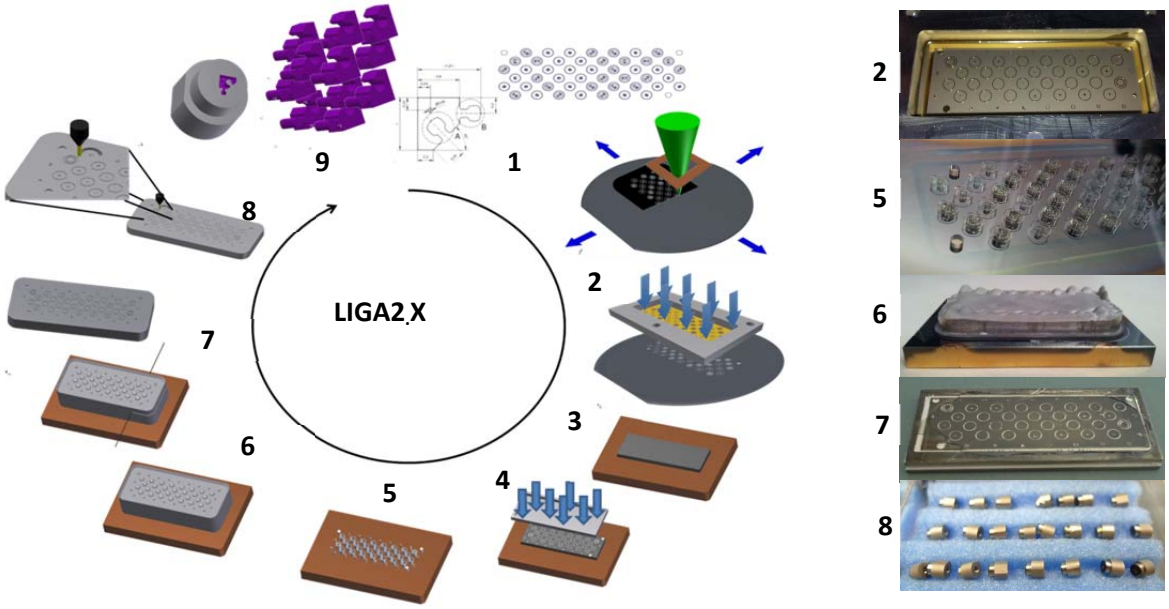

Fig. 6: Schematic description of the LIGA2.X process for the fabrication of LIGA2.X mould inserts. 1) x-ray intermediate mask fabrication using e-beam lithography; 2) x-ray working mask fabrication using x-ray lithography; 3) resist plate glued on the substrate; 4) deep X-ray lithography using synchrotron radiation; 5) resist structures after wet chemical development; 6) nickel-electroplating; 7) wire EDM to fabricate the mould insert total height; 8) HSC milling to get small adaptive mould inserts; 9) ready mould insert for micro injection moulding

In the micro injection moulding process the quality of the mould especially the mould inserts is crucial because of the small shot weights of the parts and the small cavities which make the mould filling difficult. The use of LIGA mould inserts to produce single polymeric micro parts has one disadvantage. The use of ejector pins is not practical because of the required hole in the mould insert (high risk to destroy the cavity during hole machining), the size of the pins and the wear which occurs in the combination of nickel mould insert and hardened steel ejector pins. Therefore it is necessary to partially/fully pull the part out of the cavity and collect the parts with a suitable handling system. Figure 7 shows the new developed mould concept for LIGA2.X process, a modified three plate multi-cavity injection moulding tool.

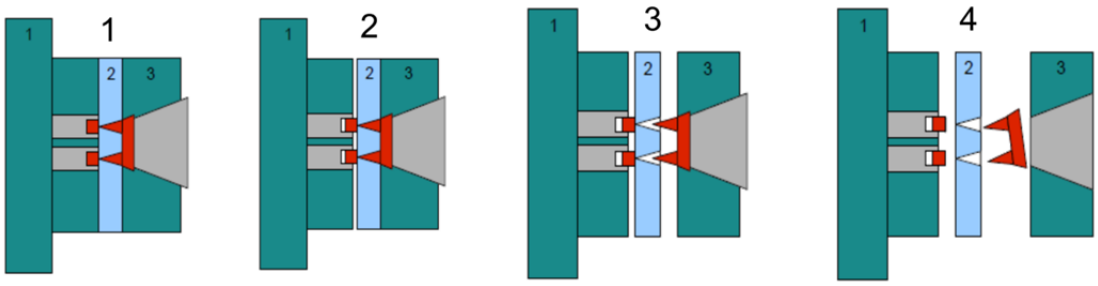

Fig. 7: Schematic description of the injection moulding concept for the fabrication of single polymeric micro parts; 1) mould filling with closed mould; 2) mould opening movement 200 µm to reduce the demoulding force during the removal of the part; 3) separation of the part from the sprue system due to pulling, 4) demoulding of the sprue system and part removal

The material of the new developed LIGA2.X mould inserts is electroplated nickel with a

hardness > 350 HV 0.1, the outer dimensions of the mould inserts are shown in Fig. 8b. The structured cavities have completely vertical lateral sidewalls with a high surface quality. The diameter 3 mm step is fabricated by HSC milling and the lower step diameter 4 mm is fabricated by wire EDM [Figure 8c].

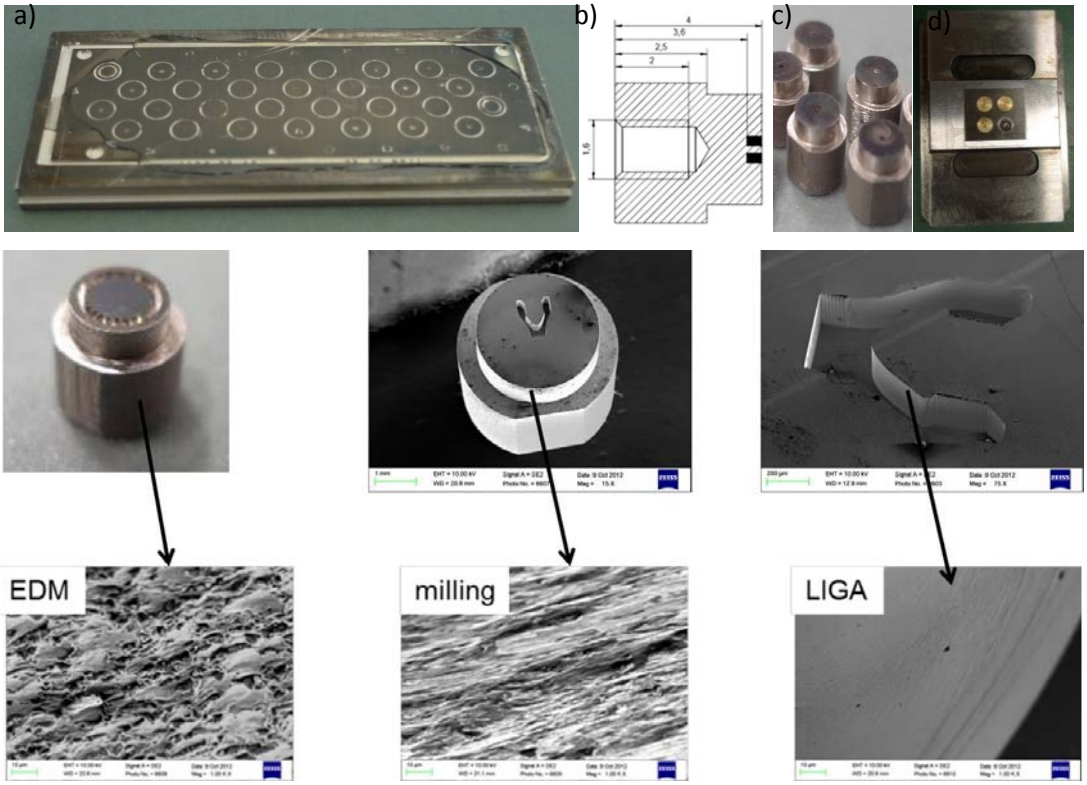

Fig. 8: a) X-ray LIGA structured nickel plate with PMMA based casting material; b) outer dimensions of the LIGA2.X mould inserts; c) LIGA2.X mould inserts; d) mould insert integrated in holder plate of the mould

The LIGA2.X process allows the fabrication of polymeric micro parts with shot weights below 0.25 mg. A high precision in the position of the cavity relative to the outer dimensions of the novel small mould inserts can be reached. Milling of electroplated nickel shows high contour and dimensional accuracy which leads to new possibilities in the LIGA mould insert fabrication compared to the classical LIGA-process. The next steps will be the replication of the LIGA mould inserts with the semi-crystalline polymer POM using a Microsystem 50 (Wittmann Battenfeld) and a micromän 50 (Otto Männer GmbH) injection moulding machine.

Strategic Themes

Since KNMF started we used our close collaboration with the research group of electrical engineering of USask (University of Saskatchewan, Saskatoon, Kanada; Group leader: Prof. David Klymyshyn) to build up a strategic theme called “Fabrication of RF-MEMS with LIGA” to exploit the third dimensions for this kind of devices. One proposal of the second call gives an inside into the wide range of applications (2009-009-000137). For that theme the KNMF technologies “EBEAM, DXRL and Electroforming” were used already. Maybe in the future “Hot Embossing and DWL” will follow.

Collaborations outside KIT in internal projects:

Helmholtz-Zentrum Geesthacht; Helmholtz Virtuelles Institut: Christian-Albrechts- Universität Kiel, Technische Universität München, Eidgenösische Materialforschungsanstalt (EMPA).

References

[1] T. Liu, R. Simon, D. Batchelor, V. Nazmov and M. Hagelstein, “A desktop X-ray monochromator for synchrotron radiation based on refraction in mosaic prism lenses”, *J. Synchrotron Rad.*, Volume **19** (2012) 191-197, doi:10.1107/S0909049511052307.

[2] H Fukui, M Simon, V Nazmov, J Mohr, K Evans-Lutterodt, A Stein, A. Q. R. Baron “Large-aperture refractive lenses for momentum resolved spectroscopy with hard X-rays”, *J. Synchrotron Rad*. Volume **20** Iss. 4 (2013) 591–595. doi:10.1107/S0909049513011722.

[3] P Meyer, J D. Claverley and R K. Leach “Quality control for deep x-ray lithography (LIGA): a preliminary metrology study”, Microsystem Technologies: Volume 18, Issue 4 (2012) 415-421

[4] M. Simon, V. Altapova, T. Baumbach, M. Kluge, A. Last, F. Marschall, J. Mohr, V. Nazmov, H. Vogt, Refractive Optical Elements and Optical System for High Energy X-ray Microscopy AIP Conf. Proc. 1437, 116 (2012); doi: 10.1063/1.3703354

Laser Material Processing (LMP)

W. Pfleging, H. Besser, N. Kandora, R. Kohler, J. Proell, P. Severloh, M. Torge

Within KNMF, the Institute of Applied Materials - Applied Materials Physics (IAM-AWP) offers different kinds of laser micro-machining workstations:

Short pulsed UV excimer lasers (pulse duration 4-6 ns) operating at 193 nm and 248 nm are suitable for laser structuring and modification processes on micrometer and nanometer scale, especially for thin films and polymers. In 2012, the 248 nm laser source was upgraded to a 1000 Hz system, which means that the maximum laser repetition rate was doubled.

High power diode laser which can be applied for laser-assisted hot embossing (just new developed process, see report below), laser annealing of thin films (e.g. battery materials) and laser transmission welding for microstructured and transparent polymers.

A new ultrafast and high repetition laser machining system (femto/picosecond/ nanosecond laser) was installed in the "Laboratory for Micro- and Nanostructuring" at IAM-AWP in the mid of October 2012 (Figure 1, Figure2). By using this special configured workstation (three wavelengths, tunable pulse duration), laser micro- and nanostructuring of multimaterial systems such as biomaterials, transparent materials as well as materials for energy devices (batteries) are possible. Thereby, material processing without inducing a thermal impact or thermal-induced damage or melt formation is possible. Material processing with high repeatability and reproducibility can be achieved. In 2013, laser material processing with ultrafast laser radiation will become a main focus in KNMF In-House research. A development of new process strategies for laser patterning of different types of materials as function of laser pulse length and laser wavelength is necessary in order to achieve an outcome for future KNMF user projects.

Fig. 1: Femtosecond laser workstation.

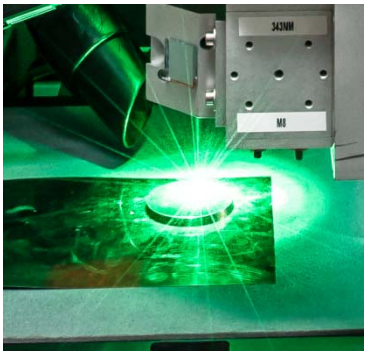

Fig. 2: Laser material processing of metallic surface using femtosecond laser radiation

The In-House research is focused on the development of new laser-assisted processes with special focus on polymers and battery materials. The following R&D activities have been performed in 2012.

Laser-assisted control of wettability on polymeric surfaces

For research and development microstructuring of polydimethylsiloxane (PDMS) is of general interest and is often used for the production of devices in microelectronics, micromechanics, microoptics, microfluidics and for biological applications. In cooperation with the Institute of

Biological Interfaces (KIT, IBG, Dr. Scharnweber) the UV laser processing of PDMS (KIT, KNMF, IAM-AWP) and subsequent cell culturing test (KIT, IBG) was investigated in detail in order to find suitable laser processes for enhanced protein/cell adhesion.

Within the use of a 193 nm laser wavelength, a process parameter was found which enables the formation of micro cones in PDMS (Figure3, left). It was shown that these features can induce the lotus effect on PDMS (superhydrophobic behaviour). Furthermore, it was verified that these features can act as an anchor leading to enhanced cell adhesion. Figure 4 reveals that a suitable pattern of superhydrophobic areas can be used to control the positioning of droplets on PDMS. Also the control of spreading and flow of liquids on PDMS in microfluidics will be possible.

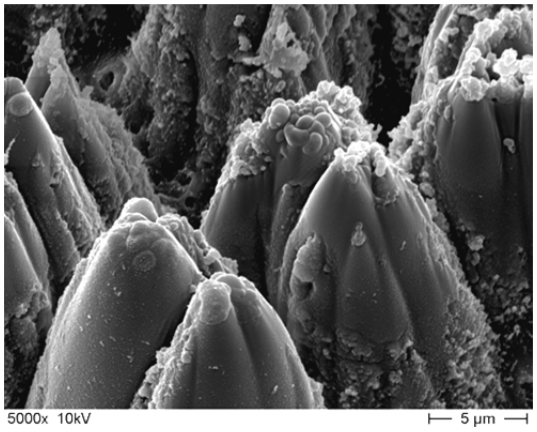

Fig. 3: SEM image of laser structured Polydimethylsiloxane (PDMS).

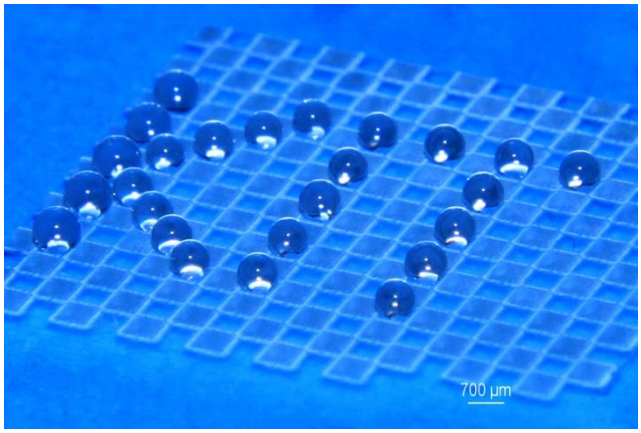

Fig. 4: Water droplets on a pattern with alternating hydrophilic and superhydrophobic areas

Laser-assisted hot embossing

Hot embossing is widely used in research and development for the replication of polymeric micro parts. With a new laser-assisted process – which was developed in cooperation with KIT-IMT (Dr. Guttmann/ Hr. Wissmann) it is now possible to significantly reduce the processing time as well as to realize a localized replication. The latter approach means that only a small part of the polymer will be heated up with the laser beam while the other parts of the polymer – maybe already functionalized – keep undamaged by undesired heat impact. Laser-assisted hot embossing was developed for the replication of micro/nanostructures in polymers for aspect ratios <10 and feature sizes from the mm-range down to the nanometer scale. The process was successfully applied for the replication of micro/nano grids (e.g. interferometer design) and was tested for thermoplastics such as PMMA, PS, COC and PEEK. Figure 5 and 6 show hierarchical microstructures in PMMA produced by laser-assisted hot embossing. The shape of the used mould design (produced by laser ablation) was perfectly reproduced.

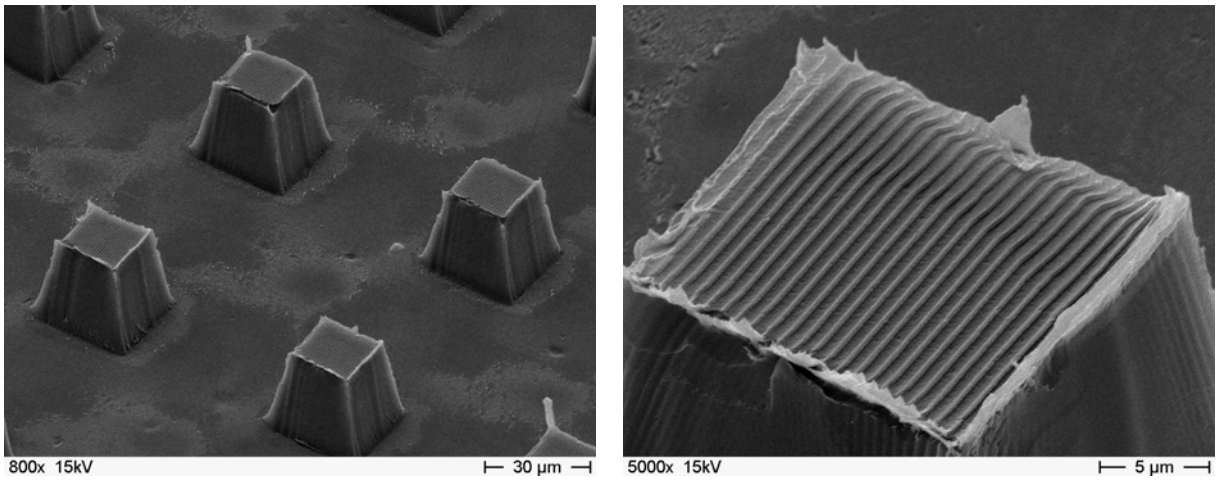

Fig. 5: SEM image of microstructures/columns in PMMA produced by laser-assisted hot embossing (left: overview; right: closer view showing a submicron structure on a micro-sized column).

Battery

Micro batteries made of 2-D thin film electrode materials shows technical drawbacks because of a 1-dimensional Li-ion diffusion and mechanical stresses due to high volume changes resulting from Li-ion insertion during charging/discharging. This in turn can lead to inhomogeneous current densities, increased high power losses, high ohmic resistance and reduced battery lifetime. The development of 3-dimensional (3D) cell architectures for electrodes for lithium-ion batteries is a promising approach to increase the surface of the active material and to provide faster Li-ion diffusion which in turn enables improved battery cycle stability especially for high discharging and charging currents. Furthermore, free-standing microstructures are suitable to compensate mechanical stresses due to volume changes during electrochemical cycling and an increased battery life-time can be achieved. At IAM-AWP / KNMF the laser material processing group develops advanced laser processes (Laser-Annealing, Micro/Nanostructuring) for battery materials in order to tune the cell/battery performance of thin film batteries as well as large area high power batteries (pouch cell design) made of thick film electrodes. For process development a strong cooperation to analytic groups in KIT was established (IAM-ISS / Dr. Bruns, IFG / Dr. Weidler, IAM-AWP / Dr. Bergfeldt).

One new developed process is the pattering of thin films electrode materials on micrometer and sub-micrometer scale by direct laser ablation using UV excimer laser radiation and chromium/quartz mask techniques. Laser structuring was performed using a short pulse excimer laser (ATLEX-500-SI, ATL Lasertechnik GmbH, pulse duration 4-6 ns, wavelength λ = 248 nm). Spherical surface structures in lithium manganese oxide (Li-Mn-O) thin films were formed with smooth surfaces and without any debris using a grating mask (Figure6). Within the use of the line patterned mask high aspect ratio structures (of up to 5) could be formed. Figure 7 shows line structures with channel widths of about 400 nm. In comparison to unstructured electrode thin film materials a significant improvement of cycle retention during battery operation (Swagelok design) was achieved.

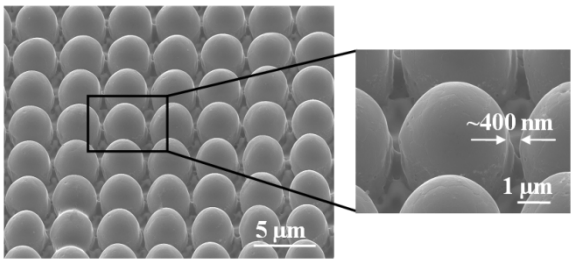

Fig. 6: Spherical 3D surface structures formed via UV-laser structuring of Li-Mn-O thin films using chromium/quartz mask technique.

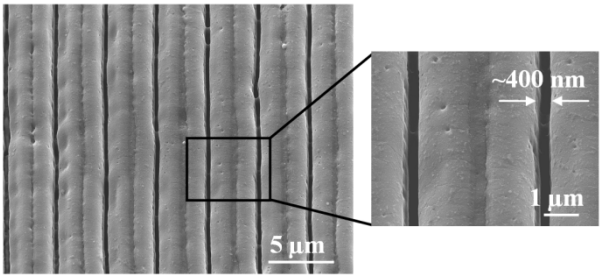

Fig. 7: Line structures formed via UV-laser structuring of Li-Mn-O thin films using chromium/quartz mask technique.

Strategic Themes

The Laser Material Processing Group in KNMF has an outstanding expertise in the field of the development of advanced laser processes for lithium-ion batteries. Three-dimensional surface structuring and surface modification of electrode materials enable a significant improvement of battery performances (battery life-time, cycle retention,...). The Laser Material Processing Group has an expertise also in electrode thick film deposition, cell assembly and electrochemical cell characterisation. In cooperation with external partners new materials, advanced thin deposition technologies or battery degradation mechanisms are investigated. External partners are: Manz Automation AG, Sihl GmbH, Princeton University (Correlation of surface topography and mechanical properties during electrochemical cycling), Naval Research Laboratory Washington (Laser-printed electrodes / all-solid state microbatteries), KIST – Korean Institute of Science and Technology (study of degradation mechanisms; new electrode materials).

A relatively new field is the combination of laser processes and print technologies (“printed surfaces for functionalized devices”). Together with KIT-INT (Dr.Dr. Hirtz) the combination of DPN lithography and laser surface patterning and modification of polymers was successfully applied and is investigated for the development of new polymeric patch clamp devices. In October 2012 an European project (EU-SMARTLAM-Projekt, FP7, Smart Production of Micropsystems based on laminated polymer films) was started which investigates the combination of laser technology and printing technology for the development of polymeric micro devices. Within SMARTLAM, the Laser Material Processing Group of KNMF is responsible for the integration and development of laser processing technologies.

External partners on that research field are: Micrux AG (microfluidic chips), DesignLED (LED-devices), PROFACTOR (product development), Neotech Services (AerosolJet Technology), FhG-IPA (micro production technologies), Sophion Bioscience A/S (patch clamp device).

Further Collaboration outside KIT in internal projects:

Paul Scherrer Institut (PSI), University of Birmingham, IREPA LASER, VITO - Lasercentrum Vlaanderen, ATL Lasertechnik GmbH, Daimler AG

References

[1] W. Pfleging, R. Kohler, I. Südmeyer, M. Rohde, “Laser Micro and Nano Processing of Metals, Ceramics, and Polymers” in Laser-Assisted Fabrication of Materials, Jyotsna Dutta Majumdar and Indranil Manna (Eds.), Springer-Verlag, 2012, ISBN : 3642283594, 9783642283598, Chapter 8, pages : 319-374, DOI : 10.1007/978-3-642-28359-8_8

[2] R. Kohler, J. Proell, M. Bruns, S. Ulrich, H.J. Seifert, W. Pfleging, “Conical surface structures on model thin-film electrodes and tape-cast electrode materials for lithium-ion batteries”, Applied Physics A (2012), in press, DOI 10.1007/s00339-012-7205-y, Print ISSN: 0947-8396

[3] Heungsoo Kim, Johannes Proell, Robert Kohler, Wilhelm Pfleging, Alberto Pique, “Laser-Printed and Processed $LiCoO_2$ Cathode Thick Films for Li-Ion Microbatteries”, Journal of Laser Micro/Nanoengineering: Volume 7, No. 3 (2012) 320–325

[4] J. Pröll, R. Kohler, A. Mangang, S. Ulrich, M. Bruns, H.J. Seifert, W. Pfleging, “Diode laser heat treatment of lithium manganese oxide films”, Applied Surface Science: 258 (2012) 5146–5152

[5] J. Pröll, R. Kohler, A. Mangang, S. Ulrich, C. Ziebert, W. Pfleging, “3D Structures in Battery Materials” JLMN-Journal of Laser Micro/Nanoengineering: Vol. 7, No. 1 (2012) 97-104

[6] R. Kohler, J. Proell, S. Ulrich, M. Przybylski, H.J. Seifert, W. Pfleging, “Influence of laser-generated surface structures on electrochemical performance of lithium cobalt oxide”, Proc. of SPIE: Vol. 8244 (2012) 82440T-1– 82440T-7

[7] J. Pröll, R. Kohler, M. Torge, M. Bruns, M. Przybylski, S. Ulrich, H.J. Seifert, W. Pfleging, Laser adjusted three-dimensional Li-Mn-O cathode architectures for secondary lithium-ion cells, Proc. of SPIE Vol. 8244 (2012) 82440S-1 - 82440S-10, DOI: 10.1117/12.906714, ISBN: 9780819488879

Injection moulding (IM)

Volker Piotter, Klaus Plewa, Jochen Heneka, Elvira Honza
Alexander Klein, Tobias Müller

Micro injection moulding has already reached a remarkable technical level and represents an impressive example for high-efficient micro fabrication processes [1]. Manufactured components are applied, for example, in micro optics, consumer products, micro fluidics or minimally invasive surgery. This is demonstrated by micro parts currently available or to be available soon.

Presently, special variants like micro compression moulding [2] or multi-component injection moulding [3] are under development. The goals of these research activities are not only to increase economic efficiency but also to expand the range of materials from polymers to metals and ceramics. In this respect, the development of the so-called Micro-PIM process is going to become a large-scale fabrication technology for metal/ ceramic microstructures.

Generation of nano-sized photonic crystal structures for surface contrast microscopy

Photonic crystal slabs (PCS) have been fabricated using micro injection moulding followed by high-index layer deposition. The required mould inserts had been made by e-beam lithography at IMT. It has to be emphasized that replication of structure sizes down to 80nm was accomplished reproducibly thus **the 100nm boarder has been vanquished**. In order to investigate the influence of the high-index layer thickness and the duty cycle of the periodicity on the sensitivity, 24 different PCSs geometries designed by Kiel University were evaluated in experiment and simulation. With this experimental series, general tendencies are established for optimal bulk and surface sensitivity values in asymmetric PCSs. The optimized injection-moulded PCSs revealed promising performance as e.g. transducers for label-free assays. They offer a high sensitivity, are cost-efficient in fabrication and mechanically stable.

Experiments on injection moulding in the sub-100nm region will continue with respect to structure widths below 80nm and higher aspect ratios.

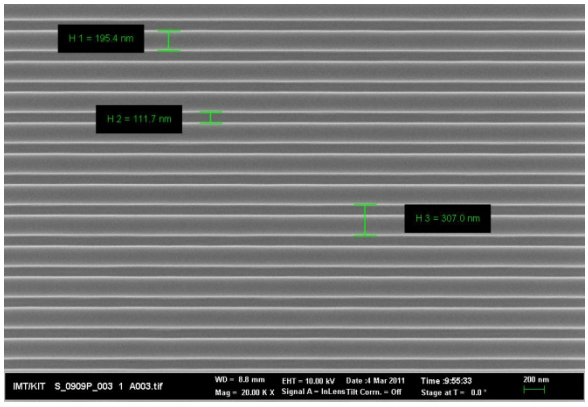

Fig. 1: SEM figure of mould insert made by e-beam writing and electroplating (IMT)

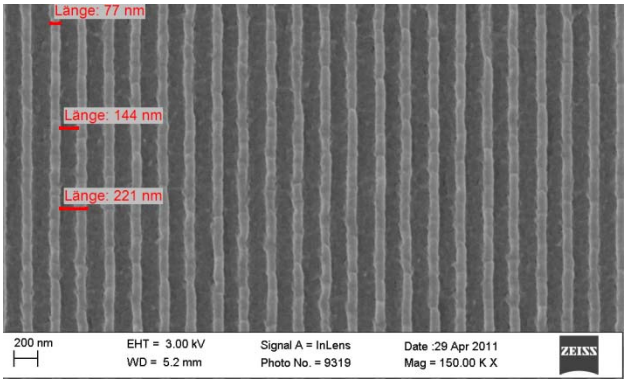

Fig. 2: SEM figure of polymer part (PMMA) made by micro injection moulding (IAM-WPT)

2C-Micro Polymer Injection Moulding

Combining two materials with different properties in a single piece is an important research and development challenge. Probably the most important advantage, however, is the considerable reduction of assembly expenditure. Within the EU-funded project COTECH a new approach for 2C-µIM has been proposed which is based on a serial junction of two 1C-units instead of a monolithic but rather complex 2C-machine. Benefits with respect to higher flexibility and reduced capital commitment are expected.

This new process conduct had been compared to the classical way by producing micro tensile specimen consisting of PA and different types of TPE´s. Both types of samples had to undergo tensile tests as well as interface characterization by SEM. No significant influence of the stand-by time between the injection steps could be observed. This allows the conclusion that **the new 2C-µIM process will enable similar interface properties while offering economic benefits** as mentioned above [4].

The results gained in COTECH will be included in new projects in 2013.

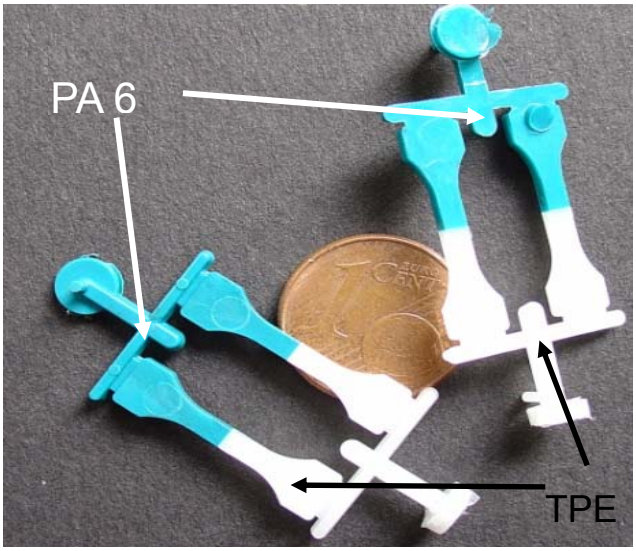

Fig. 3: 2C-tensile test specimen to investigate interface strength

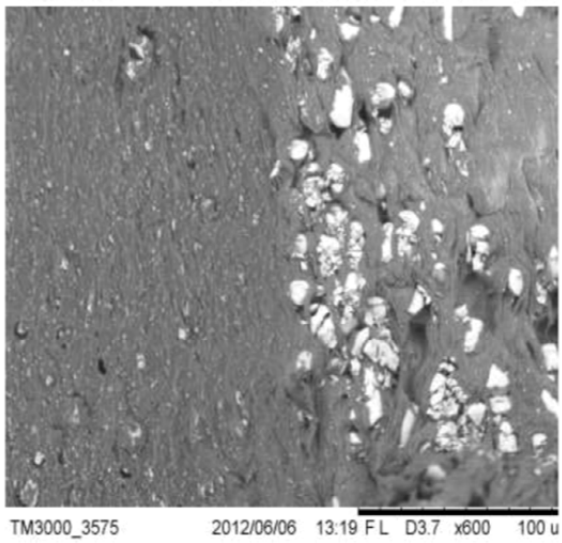

Fig. 4: SEM image of the bonding area between PA and TPE with stand-by time of 10s

In-mould-labelling combined with Micro Powder Injection Moulding (IML-MicroPIM)

To enhance replication diversity and to generate integrated multi-material products the so-called micro inmould-labelling (IML-MicroPIM) process is under development. It combines powder filled tapes with adequate PIM-feedstocks offering additional possibilities for generating functionalized surfaces as well as for the application of powders containing nano-size particles. The process has already been investigated for macroscopic applications and trials for adaptation to micro systems technology have been carried out within the former EU Large Integrated Project “Multilayer”. Main result was the combination of different $Zr0_2$ powder fractions in one part. A **tight connection between former tape and feedstock** could be obtained, i.e. compared to the green body the interface shows an indistinct outfit indicating diffusion processes during sintering [2, 3].

Investigations on IML-PIM will continue in order to improve replication accuracy and to apply even finer, i.e. nano-sized, powders to a larger extent.

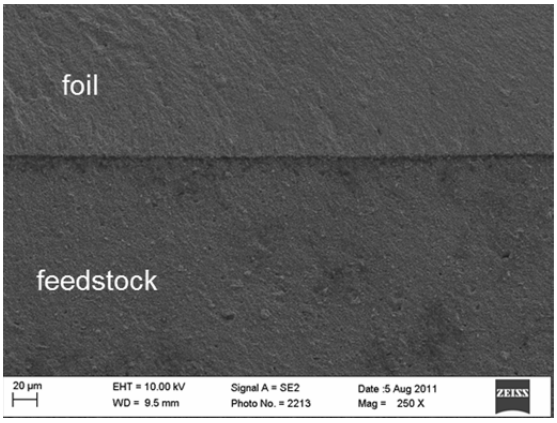

Fig. 5: Cut view of an IML-PIM green body, the interface is clearly visible (REM image).

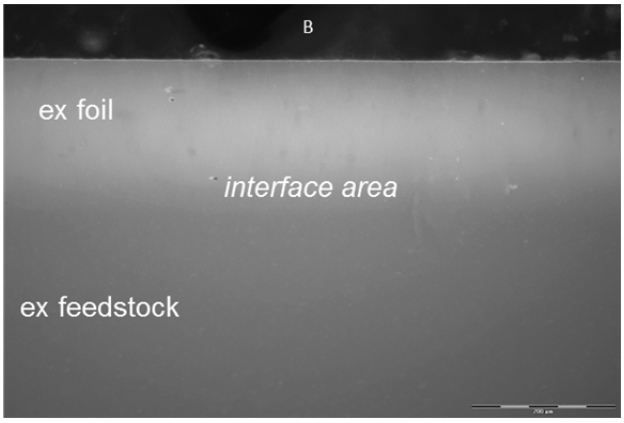

Fig. 6: Sintered IML-part, the interface appears only as an indistinct pattern between the former foil and feedstock, B = background (right).

Strategic Themes

Additive Micro Manufacturing of Metals and Ceramics

Goal: Close the entire chain from prototyping over small-medium-large series manufacturing of metal and ceramic products. Offer a “full-package-service” to future customers

Actions: Improve Additive Manufacturing Technology to obtain structure sizes for metals and ceramics below 20µm. Procurement of 3D-LCM Printer with special focused lenses. Create a data base to comply material and process capabilities in dependence of piece numbers to determine the optimal solution for particular customer demands.

Hybrid Additive and Injection Moulding Manufacturing

Goal: High-efficient manufacturing of individualized micro parts

Actions: Combine geometrical flexibility and individual design of Additive Manufacturing with the high economic efficiency of Micro Injection Moulding. Utilization of STL-System purchased under point 3. Development of binder systems suitable for both processes, creation of co-debinding and co-sintering procedures, set-up of pilot line, production of demonstrators.

Further Collaboration outside KIT in internal projects:

internal collaborative project: Structuring potential and limits of the LIGA-technique, industrial partners: Arburg GmbH+Co KG, Männer GmbH, RKT GmbH, Scholz GmbH+Co KG

References

[1] J. Heneka, J. Prokop, V. Piotter, M. Guttmann, H. Hanemann and K. Plewa “Variation of the use of LIGA Mould Inserts for the Fabrication of Single Polymeric- and Metallic-Microparts”, *Proc. of euspen 12th Int. Conference, published by euspen, ISBN 13: 978-0-9566790-0-0, Vol. 2, (2012) 92-95.*

[2] E. Honza, K. Plewa and V. Piotter “A comparative study of Micro Powder Injection Moulding (MicroPIM) and simultaneous Micro Powder Injection Compression Moulding (MicroPICM)”, *Powder Injection Moulding, Vol. 6, No. 2, Inovar Communications Ltd. (2012) 67-70.*

[3] V. Piotter, E. Honza, A. Klein, T. Mueller and K. Plewa „Micro Precision Parts produced by Powder Injection Moulding“, Proc. of PM World Congress 2012, published by *Japan Society of Powder and Powder Metallurgy, ISBN: 978-4-9900214-9-8 (2012) 16B-T5-12.*

[4] E. Honza, A. Klein, K. Plewa, V. Piotter, C. Tuinea-Bobe and B. Whiteside „Micro 2C-Injection Moulding - Investigations on Interface Performance“, *Proc. of 9th International 4M Conference, Research Publishing, ISBN: 978-98107-3353-7 (2012) 250-253.*

Hot Embossing (HE)

Matthias Worgull, Alexander Kolew

EVG Nanoimprint

In 2012 a Nanoimprint system EVG510 (Figure 1) with two structuring units is implemented in the KNMF. This system allows both the structuring of thin thermoplastic films at wafer scale and the structuring of UV-curing photoresist materials. Compared to standard Nanoimprint systems the advanced technology allows the application of pressure during UV curing. This unique combination enables the filling of nanocavities with high aspect ratios (>3). In parallel the technology to use the flexible UV-transparent PDMS as mould insert is available.

a) EVG 510 Nanoimprint machine

b) open thermal unit for moulding nanostructures on the wafer scale

Fig. 1: EVG 510 Nanoimprint machine with thermal and UV Curing unit

New high temperature moulding tool for hot embossing

During 2012 the hot embossing system WUM3 has been improved by a high performance heating and cooling tool with metal bellows evacuation system. This allows for micro replication of high temperature materials like metallic glasses, low-melting glasses and metals like aluminium.

Nano and micro hot embossing and micro-thermoforming of the biodegradable and renewable resource liquid wood

Thermal nanoimprinting and structuring allows for low cost fabrication of nanostructures with highest aspect ratios on large surfaces and is commonly based on a large variety of polymers. The widespread use of nanostructured materials, however, poses environmental challenges. The new developments show that biodegradable wood from renewable resources can be structured on the nano-scale and that surface characteristics can be imprinted and three-dimensionally formed. In particular, it is shown that so-called liquid wood

made out of lignin can be structured with feature sizes down to 100-200 nm and three dimensionally shaped by micro-thermoforming (Figure 2 and Figure 3). We realized optical active surfaces by diffractive elements, the change of hydrophobic to superhydrophobic behaviour and the fabrication of super-hydrophobic microfluidic channels. Based on these results we anticipate new applications in the nano- and micro-range, particularly for use in sensitive environments without posing a risk to nature. The new compound material will allow for a substitution of conventional polymers used as material in one way applications of e.g. the consumer, the food or the disposable medical industry.

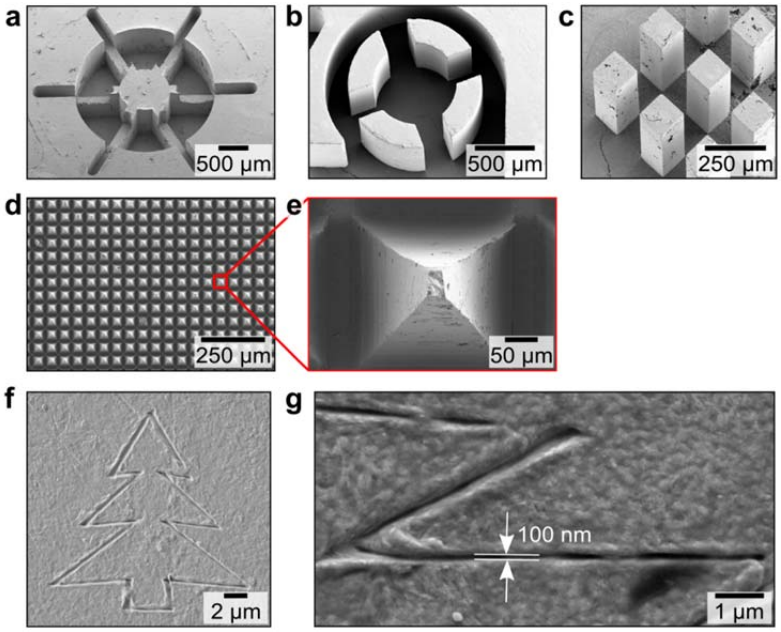

Fig. 2: a, Hot embossed microstructures with high aspect ratio. **b**, Circular structure with a height of 700 µm **c**, Free standing rectangular pillars with an aspect ratio of 4. **d**, Hot embossing of micro pyramids. **e**, Detail of one micro pyramid. **f**, A micrometer sized tree written with nanolithography using an atomic force microscope. **g**, The structure size obtained with this technique is about 100 nm

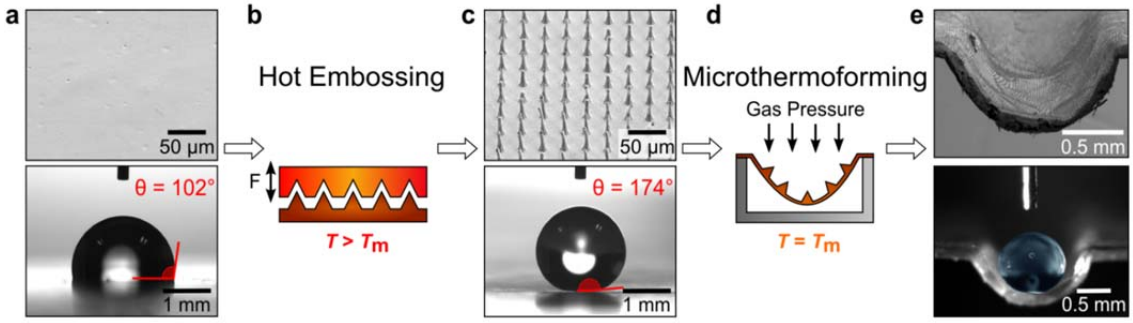

Fig. 3: Thermoforming of liquid wood: a) flat unstructured foil of liquid wood is hydrophobic with a contact angle of 102°. c) By hot embossing above the melting temperature the surface can be microstructured. d) Due to the microstructure the surface now reveals superhydrophobic properties with a contact angle of 174° that is higher than what is known from most other superhydrophobic materials

Nano-scale Hot Embossing of Bulk Metallic Glasses for Biomimetics and Microfluidics

Bulk metallic glasses (BMGs) are promising materials due to their great material properties in terms of strength, hardness, and wear resistance. Nonetheless, they face some restrictions

in terms of structuring and tooling and recent studies report that nano and micro moulding of BMGs is frequently based on dissolution of the master structure.

New development is a viable and repeatable process for nano and micro replication of BMGs with automated demoulding resulting in repeatable usage of expensive master structures. As BMGs exhibit temperature dependent ductility similar to thermoplastics they can be replicated within a narrow process window without limitations in structure size and accuracy based on micro sized grains. As BMGs start to crystallize when heated above TG commercial hot embossing systems with their maximum temperature range of 300 °C and cycle times of 30 minutes are not capable for BMG moulding at all. Our newly developed hot embossing system equipped with evacuation system and high performance electrical heating cartridges achieving heating rates of 60 K/min up to 650 °C and adjustable turbulent water cooling achieving cooling rates of 50 K/min minimizes material exposure to temperatures above TG.

With this new tool we fabricated nano and microstructures for a broad range of applications in biomimetics, microfluidics, and nanosystems. Limitations of part sizes for large area replication are solved by process integrated welding of smaller BMG parts, high precision LIGA tools and isothermal demoulding just below the solidification temperature. We have proven the capability of transfer from laboratory stage and prototypes to series production of nano and microstructures using BMG as wear resistant mould insert by thousand injection moulding cycles with highly abrasive glass fibre filled polyamide.

Advances in Material Variety For Hot Embossing

Micro structured technology offers great advances for new functions and applications based on the surface texture and micro structured geometry. Nevertheless beside micro structures a lot of important properties are still defined by the material used. Most of the actual micro systems consist of silicon based on the elaborate developments during the last decades in silicon technology or of polymers based on replication technologies like nanoimprint, hot embossing and injection moulding.

We demonstrate opportunities and limitations of micro replication by the hot embossing process for the use of a broad range of polymers like high performance polymers PEEK and LCP, biodegradable polymers like maize starch based polylactide and liquid wood, filled and reinforced polymers but also alternative materials like bulk metallic glasses, ceramics, low melting glass, and metal films. As a prerequisite to process these materials the conventional machines had to be reconstructed. The processing of low melting glass still required machine improvement with high performance heating unit to reach temperature levels up to 650 °C, bulk metallic glasses however required new tool concept for fast heating and cooling to avoid crystallization when treated several minutes at temperatures above 430 °C.

The new variety of materials has been tested in respect to the minimum feature sizes, their usage as intermediate tool for further replications, and for new combinations for multi material replications. Whereas high performance polymers have been tested already, new material classes for replication like liquid wood, ceramics or bulk metallic glasses offered the need of completely new process control and setup.

Ceramic micro parts give the opportunity for use in harsh chemical or high temperature environment and they can be used as ceramic heaters for ultrafast replication. Figure 4 shows a in ceramic feedstock hot embossed micro fluidic chip which is replicated on top of a polyethylene carrier layer. The carrier layer consists of the same material as the binder of the feedstock and allows for handling of thin parts which otherwise break during processing due to high material brittleness.

Bulk metallic glasses stand out because of their high hardness and good ductility due to the lack of grains inside the material. Whereas they can hardly be structures by conventional techniques like milling due to their hardness, they can be structured by hot embossing due to their temperature dependent viscosity. Figure 5 gives examples for palladium based bulk metallic glass replica of submicron pattern and zirconia based bulk metallic glass replica of 8 µm line and space structures. The embossing temperature used for palladium based bulk metallic glass was 310 °C and for zirconia based bulk metallic glass 450 °C. As crystallization occurs after a few minutes at temperatures above 430 °C the machine has been improved to reduce the cycle times to 4 minutes. Even further improvements are expected which allow structuring of conventional glasses. Up to now hot embossing is still limited to special low melting glasses. Figure 6 shows an array of pins of 8 µm diameters and 12 µm heights on a 70 x 70 mm² area.

Fig. 4: Microfluidic chip replicated in ceramic feedstock on a polyethylene carrier layer.

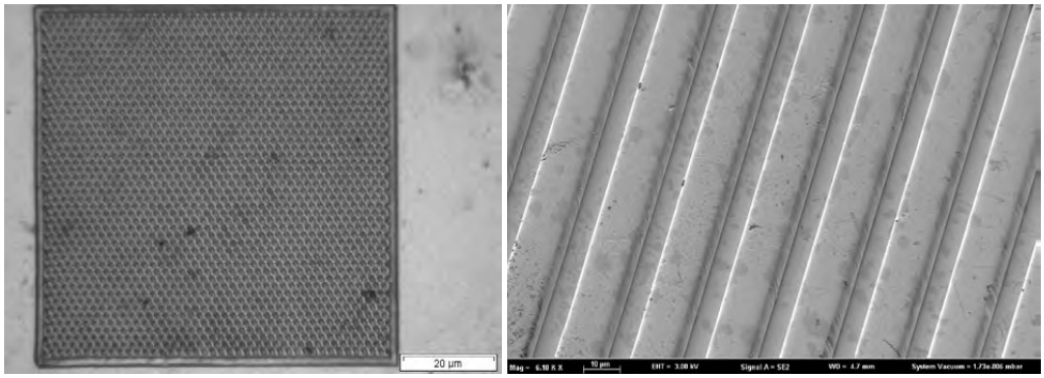

Fig. 5: Replication in bulk matellic glasses: 900 nm pattern in palladium based bulk metallic glass on the left and 8 µm lines in zirconia based bulk metallic glass on the right.

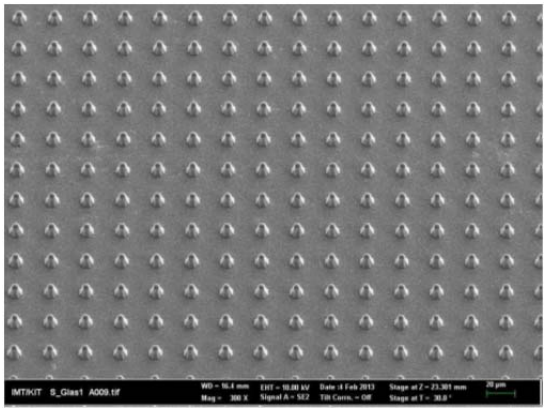

Fig. 6: Hot embossed pattern of micro pillars in low melting glass replicated at 250 °C.

Large-scale replication of biomimetic optical nanostructures inspired by blue Morpho butterflies

Large-scale replication of sophisticated 3D biomimetic nano- and microstructures faces difficulties even today. Here, we present a flexible replication process for optical active structures inspired by Morpho butterflies. This butterfly species shows a brilliant blue iridescence caused by “Christmas tree” like structures in their scales. These structures can be fabricated for example by e-beam lithography but their cost effective, large-scale manufacturing is a challenge although various technical implementations have been shown.

To overcome this problem, we developed a unique combination of hot embossing and micro-thermoforming to shape the design and features in the nano-scale. The flexibility of our method allows the easy implementation of other non-optical features like super-hydrophobicity and self-cleaning as well.

First, we use hot embossing for the imprint of the nanostructures in a polymer foil. This embossing step is followed by micro-thermoforming, in which the foil is shaped on the micro-scale. We demonstrate a successful process combination with structure sizes several orders of magnitude smaller than conventional thermoforming. As a result, we introduce a method to create low cost biomimetic surfaces unrivalled by conventional large-scale techniques (Figure 7).

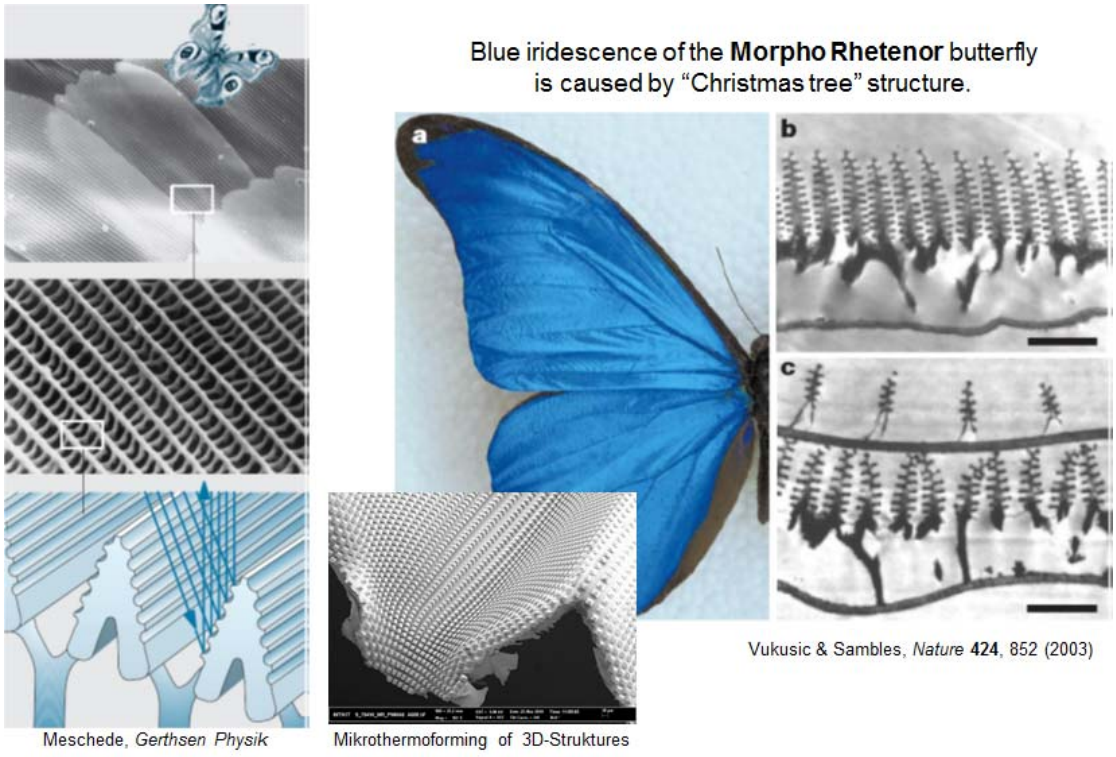

Fig. 7: Development of “Nano”thermoforming process to fabricate biomimetic surfaces like the photonic behaviour of butterfly wings (inspired by Morpho butterflies).

Fabrication of Polymeric Microfluidic Devices for BioMEMS Applications

Micro- and nanostructures on surfaces change the surface properties and enables the control of wetting behavior, friction, mixing of fluids, cell behaviour, and heat transfer. To use these effects in microfluidic devices for biomedical applications a low cost, precise fabrication of structured three dimensional shapes is needed. Within the frame of the KNMF a three step

manufacturing process was developed which is capable of fabricating three dimensional shapes with micro- and nanostructures (Figure 8).

By hot embossing micro- and nanostructures with diameters between 200 nm and 35 µm and aspect ratios of up to 9 are replicated in a first step. Using the thin carrier layer with the structures channels with an inner diameter between 200 µm and 2 mm are formed by thermoforming. The change of wetting behavior in dependency of the surface structures was demonstrated, changing the behavior from hydrophilic to hydrophobic.

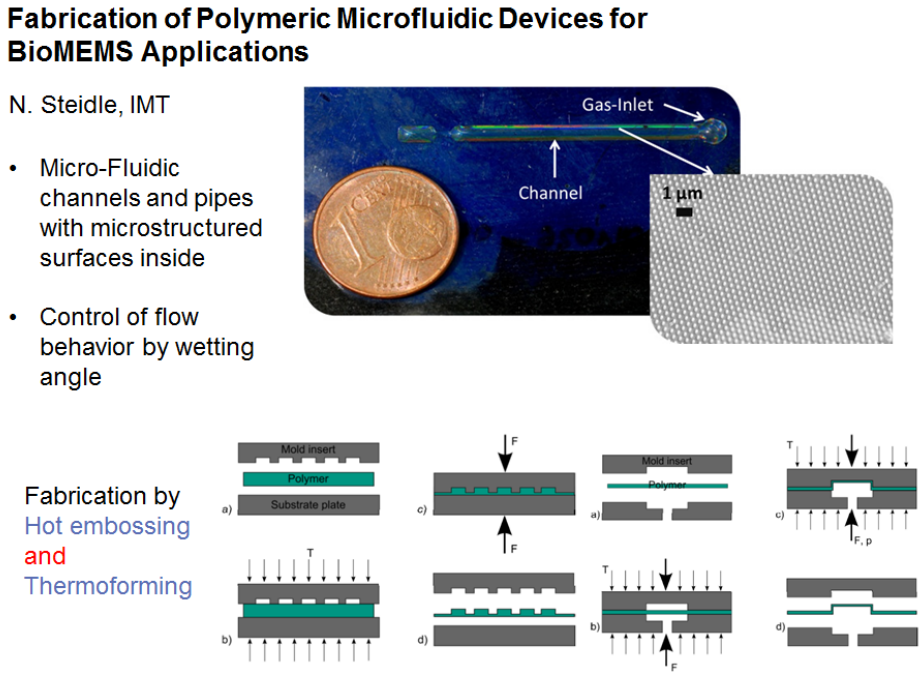

Fig. 8: Fabrication of microfluidic devices for BioMEMS applications by hot embossing and thermoforming. By this process combination the microfluidic channel is patterned by nanostructures. The process steps consist of 1) **Hot Embossing** - Structuring of 50 µm thick foils with micro- and or nanostructures. 2) **Thermoforming** - Forming of pre-structured foils into three dimensional microstructures and 3) **Bonding** - Bonding of the thermoformed foil to a base plate with all necessary fluidic connectors.

Strategic Themes

The improvement of the micro moulding equipment for hot embossing and micro-thermoforming as well as for nanoimprint offers unique technologies for a large field of applications. The installation Hot Embossing/Compression Moulding [HE] is worldwide outstanding in terms of highest moulding temperatures up to 650 °C, largest moulding area up to 250 mm in diameter, biggest moulding forces up to 1000 kN, lowest hot embossing cycle times down to a few minutes and highest flexibility with double sided moulding, through hole fabrication, multi component hot embossing, and widest process combinations of hot embossing with microthermoforming as well as thermal nanoimprint with UV-nanoimprint. This offers a great chance to close gaps between research and available facilities and is reason for further enhancement of the equipment and technologies.

References

[1] A. Kolew, M. Heilig, M. Schneider, K. Sikora, D. Münch, and M. Worgull. Hot embossing of thermoplastic multilayered stacks. Microsystem Technologies, 18:1857–1861, 2012.

[2] M. Schelb, C. Vannahme, A. Kolew, and T. Mappes. Hot embossing of photonic crystal polymer structures with a high aspect ratio. Journal of Micromechanics and Microengineering, 21:025017, 2012.

[3] Ch. Kim, K. Kreppenhofer, J. Kashef, D. Gradl, D. Herrmann, M. Schneider, R. Ahrens, A. Guber, and D. Wedlich. Diffusion- and convection-based activation of Wnt/-catenin signaling in a gradient generating microfluidicchip. Lab on a Chip, (LC-ART-02-2012-040172.R1), 2012.

[4] B. Altmann, R. Ahrens, A. Welle, H. Dinglreiter, M. Schneider, and A. Schober. Microstructuring of multiwell plates for three-dimensional cell culture applications by ultrasonic embossing. Biomed Microdevices, 14:291-301, 2012. DOI 10.1007/s10544-011-9605-8.

[5] F. Omar, A. Kolew, E. Brousseau, and H. Hirshy, Process Factors Influence on Residual Layer Uniformity in Hot Embossing, Proceedings 4M Multi Material Micro Manufacture, 9: 81-84, 2012

[6] P. Petkov and A. Kolew, Laser Drilling of Green Ceramic Tapes: Pulse Duration/shape Effects, Proceedings 4M Multi Material Micro Manufacture, 9: 207-210, 2012

[7] A. Kolew, M. Heilig, M. Schneider, D. Muench, S. Scholz, P. Petkov, and M. Worgull, Transparent High Aspect Ratio Replication Using Two-Component Hot Embossing, Proceedings 4M Multi Material Micro Manufacture, 9:254-257, 2012

[8] P. Vella, S. Dimov, A. Kolew, E. Minev, K. Popov, F. Lacan, C. Griffiths, H. Hirshy, and S. Scholz, Bulk Metallic Glass Based Tool-making Process Chain for Micro- and Nano- Replication, Proceedings 4M Multi Material Micro Manufacture, 9:309-314, 2012

[9] N.E. Steidle, A. Lepple, M. Schneider, M. Heilig, R. Ahrens, M. Worgull, and A.E. Guber. Fabrication of Polymeric Microfluidic Devices for BioMEMS Applications. In Polymer Processing Society, PPS, December 2012.

[10] K. Kreppenhofer, M. Schneider, R. Ahrens, K. Feit, R. Thelen, M.Worgull, and A. Guber. Comparative Study of Aluminum Mould Inserts for Micro Hot Embossing. In Polymer Processing Society, PPS, December 2012.

[11] M. Röhrig, M. Thiel, M. Worgull, and H. Hölscher. 3D Direct Laser Writing of Nano- and Microstructured Hierarchical Gecko-Mimicking Surfaces. SMALL 8:2918, 2012.

[12] K. Timm, C. Myant, H. Nuguid1, H.A. Spikes, M. Grunze, Investigation of friction and perceived skin feel after application of suspensions of various cosmetic powders, International Journal of Cosmetic Science, Volume 34, Issue 5, pages 458–465, October 2012

Focused Ion Beam (FIB)

Torsten Scherer, Robby Prang, Aaron Kobler, Delphine Chaissing, Kiran Chakravadhanula, Christian Kübel

A FEI Strata 400S DualBeam FIB is operated as part of the KNMF by the Institute of Nanotechnology (INT) as a universal tool for nanostructure characterization and processing. In addition to structural characterization in plane- and cross-sectional view by SEM/EDX analysis and 3D imaging using slice&view techniques, the FIB is used extensively for materials processing. Most important, high-quality TEM sample preparation, which is essential for high-end structural characterization in the TEM, but nanopatterning has also been used significantly to generate plasmonic structures. Furthermore, in-house developments focus on establishing mechanical testing of nanomaterials using various straining and bending geometries inside the FIB and on optimizing the sample preparation for in-situ mechanical and electrical testing inside the TEM. A selection of the R&D activities performed in 2012 is shown below.

Focusing and Talbot Effect of Periodic Arrays of Metallic Nanoapertures in a High-Index Medium

Three finite-sized two-dimensional (2D) periodic arrays of metallic nanoapertures with the shape of nanowaves, nanoholes, and nanodots have been developed in gold films on glass using nanopatterning by FIB (Figure. 1). Using water as an output medium, although the operating wavelengths are larger than the array period, both the focusing and far-field plasmon Talbot effect are experimentally observed (Figure. 2), showing a good agreement with the 2D finite difference time-domain (FDTD) simulation results. The focusing performance in both cases, with the output medium of air and of water, is compared. A detailed investigation of the plasmon Talbot revivals reveals that they are composed of sub wavelength hotspots with the size of $\sim 0.5\lambda$ distributed in the same array period as the original device. Three dimensional FDTD simulations prove that the existence of surface plasmons (SPs) exhibits an enhanced optical transmission at some SP resonant wavelengths dependent on the output medium. Additionally, it is demonstrated that the Talbot revivals provide a high-resolution mean to distinguish the slight geometric non-uniformity in periodic nanostructures [1].

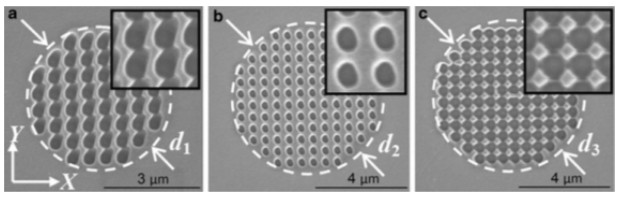

Fig. 1: Scanning electron microscopy (SEM) images of the FIB fabricated finite-sized 2D periodic arrays of metallic nanoapertures: (a) nanowaves; (b) nanoholes; and (c) nanodots.

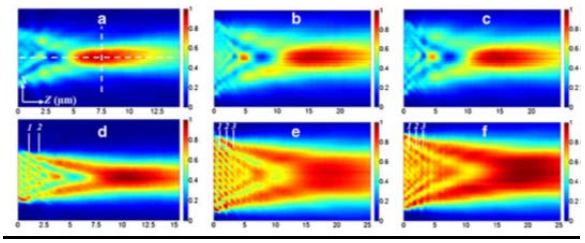

Fig. 2: Experimental results of the output optical field in X–Z plane when the devices were illuminated by an incident light of 623 nm in wavelength. The output medium is a–c air and d–f water. a and d, b and e, and c and f are for the nanowave-,nanohole-, and nanodot-arrayed devices, respectively. [1]

In-situ mechanical testing inside the FIB

Tensile (Figure 3) and bending (Figure. 4) tests have been realized inside the FIB using the micromanipulator in combination with a conventional AFM cantilever. In case of the tensile test, the cantilever was placed in an upright position without any modifications. In the case of the bending test, a gap was milled into the cantilever and the wire was placed over the gap. After milling, the cantilever was put in an upright position as for the tensile test. In both cases, the OmniProbe micromanipulator was used to apply force to the sample, while the displacement of the calibrated cantilever was used to detect the applied force. Pt deposition fixed the sample between the micromanipulator and the cantilever for tensile testing. A hock was cut into the micromanipulator to hock on the sample for bending instead of Pt deposition, to minimize Pt contamination and FIB damage. Post processing of the recorded live i-beam/e-beam images revealed a full force-displacement/stress-strain-curve using digital image correlation and tracking on both the micromanipulator (displacement) and the cantilever (force). Both methods were used on Ag wires with diameters ranging between 250-1500 nm and a length of up to several 10th of µm. First tests indicate a reduction of the E-modulus in comparison to the bulk material. The FIB-cantilever method is a cheap alternative to the expensive specialized straining devices available for the SEM [2]

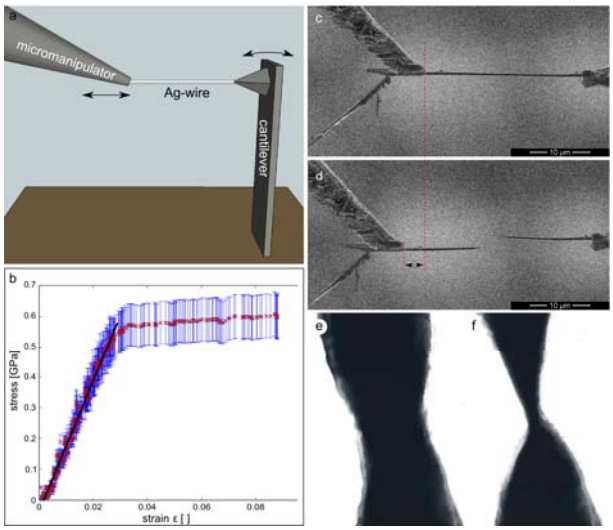

Fig. 3: Tensile test of Ag wires. (a) sketch of the tensile test inside the FIB. (b) typical strain stress curve measured by the FIB-cantilever straining method. (c,d) initial state and immediately after fracture of the Ag wire. (e,f) plastic flow of the Ag wire in tensile deformation.

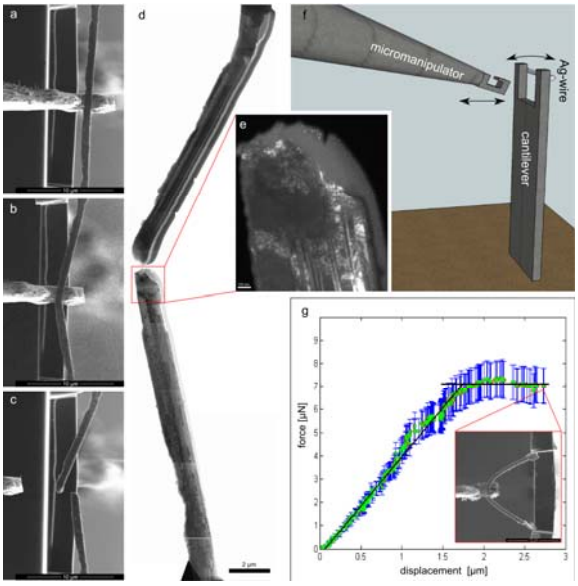

Fig. 4: Bending test of Ag wires. (a-c) Propagation of the bening test, from initial till rupture. (d,e) cross section of the wire after the bending test (BFTEM (d) and DFTEM (e)). (f) sketch of the bending test inside the FIB. (g) typical force displacement curve of the Ag wire bending test.

3D Imaging of Nanostructured Electrodes

Nanostructured electrodes made from polyaniline fibers and granular graphitic particles with distinct morphologies and aspect ratios were studied using 3D slice & viewing. The different 3D morphologies of the electrodes are expected to lead to significant differences in the I/V-characteristics and especially the reversible electrochemical cycling of the corresponding cells. Porosity, pore size distribution and connectivity can be directly examined using FIB

slice & viewing with subsequent processing of the slices into complete 3D volume of the electrode [3]

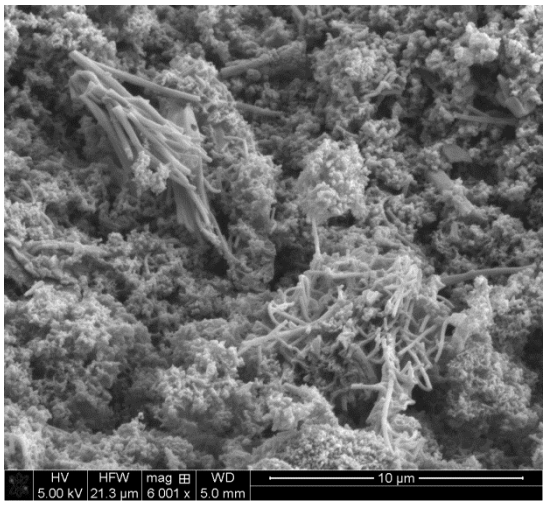

Fig. 5: SEM image of the surface of a polyaniline electrode.

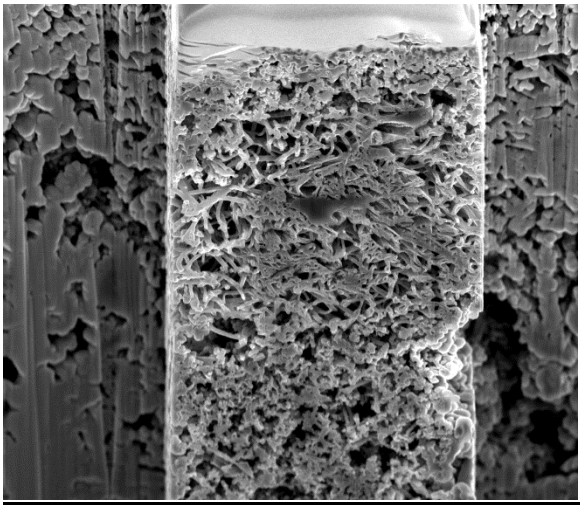

Fig. 6: Cross section of a polyaniline electrode, prepared for 3D slice & viewing.

Strategic Themes

A long-term strategic development for FIB together with TEM, HIM, XPS, ToF-SIMS, DPN and laser material processing will focus on multi-method correlative processing and characterization providing correlative analysis using reference markers and optical guidance maps as well as an inert transfer between selected installations.

Further Collaboration outside KIT in internal projects:

TU Darmstadt, Helmholtz Institute Ulm, University of Luxembourg, PTB Braunschweig

References

[1] Y. Yu, D. Chassaing, T. Scherer, B. Landenberger, H. Zappe „The Focusing and Talbot Effect of Periodic Arrays of Metallic Nanoapertures in High-Index Medium" *Plasmonics*, **2012**; DOI: 10.1007/s11468-012-9463-0

[2] A. Kobler, T. Beuth, Z. Sheng, T. Scherer, S. Wahlheim, C. Kübel, T. Schimmel to be published.

[3] B. Peter, T. Scherer, R. Prang, C. Kübel, C. Roth to be published.

Dip-Pen Nanolithography (DPN)

Michael Hirtz, Harald Fuchs

Our group, stationed at the Institute for Nanotechnology (INT), offers access to two high-end dip-pen nanolithography (DPN) platforms (DPN 5000 and NLP 2000) in the framework of KNMF. In DPN, a fine tip as also used in atomic force microscopy is coated with a chemical ink and then brought into contact with a substrate to transfer the ink onto the surface, similar to the way a quill writes, though here with the size and precision in the nanoscale. The more advanced setups developed in the last decade feature now the use of arrays of tips (instead of a single tip) which allows a bigger thru-put and large area covering by parallelization of the lithographic process. By the use of so called “inkwells” (microfluidic chips that match the feature sizes of the cantilever arrays) it is possible to deliver different inks to each particular cantilever in such an array, allowing for multiplexed writing (i.e. the integration of different inks in one process step and within the same pattern with high registry). The main strengths of DPN are the possibility of arbitrary pattern generation (maskless, direct write) in combination with high resolution (sub-micron- to nanoscale, depending on the specific ink/substrate system), mild process conditions and multiplexing. In 2012 we also began with the integration of another DPN related technique, polymer pen lithography (PPL). Here, instead of the single silicon cantilever or cantilever array as in DPN, a polymer stamp (moulded in a silicon master produced by anisotropic etching) featuring some 10.000 pyramidal tips over an area of about 1 cm². By introducing these kind of stamps into our DPN platforms that feature precise control over the stage movement in x-,y- and z-direction, we can combine the best features of microcontact printing (μCP, large area, inexpensive consumables) with that of DPN (high resolution, high spatial control, arbitrary patterns), yielding new and improved ways for advanced micro- and nanoscale surface patterning.

Click-Chemistry DPN for bioactive Surface Patterning

The application of click-chemistry DPN for patterned protein immobilization was further advanced in our installation during 2012. [1] We developed a facile modification scheme for glass and silicon oxide substrates that renders the surface susceptible for coupling of azides by the well known Huisgen 1,3-dipolar cycloaddition click reaction. In addition to writing arbitrary patterns with a flurophor coupled azide we demonstrated the large area arraying of proteins by the immobilization of streptavidin onto biotin-azide dot patterns (Figure. 1). Arbitrary biotinylated proteins can be bound onto these patterns in a sandwich approach.

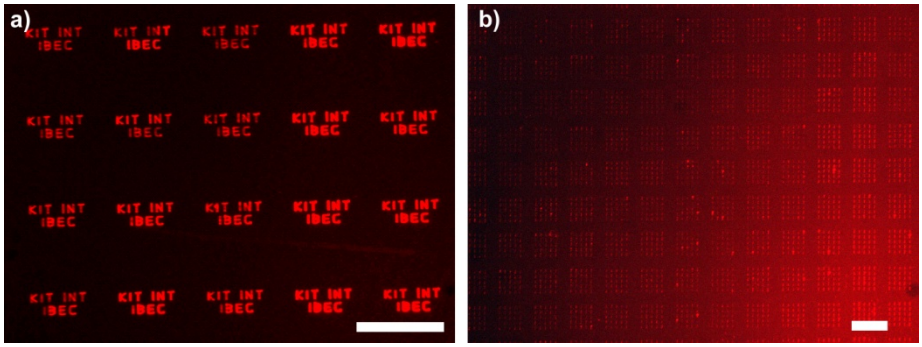

Fig. 1: Fluorescence microscope images of a) an Alexa Fluor 555 azide ink structure deposited by dip-pen nanolithography and b) fluorescent Streptavidin–Cy3 bound on a biotin azide dot pattern generated by dip-pen. The scale bars equal 35 μm.

Lipid-DPN for biosensing Applications

Striving for miniaturized immunoassays that allow for a large test area and require only a small volume of the test analyte, we demonstrated that lipid dip-pen nanolithography (L-DPN) can be used to generate large area, multi-concentration allergen arrays for the study of mast cell activation. [2] Arrays of the ligand 2,4-dinitrophenyl[1,2- dipalmitoyl-sn-glycero-3-phosphoethanolamine-N-[6-[(2,4-dinitrophenyl)amino] hexanoyl] (DNP)] were generated by L-DPN on glass surfaces as a model system for detection of allergen- specific Immunoglobin E (IgE) antibodies and for mast cell activation profiling (Figure. 2). For both cases, a dosis response curve can be obtained showing the viability of this approach to characterize the immune response to a presented allergen. In addition to the potentially application in clinical immune response profiling, we will employ this technique in the future to have a defined close-up look at the immunological synapse for in detail studies of the allergen recognition process.

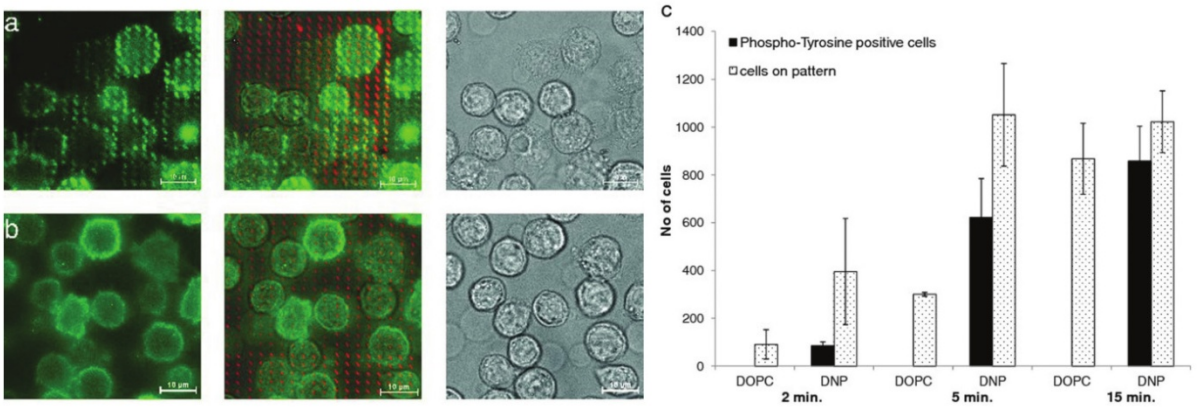

Fig. 2: Activation of mast cells on DNP arrays. RBL-2H3 mast cells, sensitized for 2 h with anti-DNP IgE antibody, were loaded onto the samples, allowed to adhere, then fixed and stained with anti-phosphotyrosine antibody. a) Concentration of phosphorylated tyrosine signal is visible on cells exposed to DNP allergen. b) No phosphorylated tyrosine signal is visible in cells adhered onto DOPC array; only homogeneous antibody staining around the cells is detected after 15min. c) Quantification of the number of activated cells on 10 mol% DNP and DOPC arrays followed over 15 min. Empty bars show the number of cells scored on the DOPC and DNP samples at the indicated time point. Filled bars show the number of activated cells where co-localization of the phosphorylated tyrosine signal over the DNP dot was detected.

Additionally, in 2012 we also saw the integration active lipids into a pre-manufactured sensor device by L-DPN for a ready-to-use biosensor with several different biomolecules. [3] As platform for the demonstrated biosensor a Surface Acoustic Wave (SAW) device integrated with a parallel-channel microfluidic module, termed as ‘‘microfluidics-on-SAW’’ (‘‘mF-on-SAW’’) was utilized. Lipids with different functionalized head groups were patterned at distinct, microfluidic-formed rectangular domains with sharp edges all located on the same sensor surface. The subsequent experiments demonstrated the efficiency of the patterning method, and the suitability of DPN for the surface modification of the acoustic device. The mF-on-SAW configuration was used to detect specific binding between the pre-patterned functionalized lipids with their corresponding biomolecules. Key achievements in this approach were improved sensitivity (5-fold compared to previous acoustic configurations) and reduced preparation time (by at least 2 h).

Template assisted assembly of tobacco mosaic virus (TMV) like particles

Many nanotechnological applications rely on the capability of some natural molecular building

blocks to self-organize into defined supramolecular architectures. The site-selective integration of such self-organized processes into a technical context, however, still poses a major challenge. Here, we introduced a new method for the site-selective RNA-directed self-assembly of tobacco mosaic virus-derived coat protein on immobilized RNA scaffolds. Isothiocyanate alkoxysilane was patterned by DPN onto oxidic surfaces in defined arrays, to prepare them for the site selective covalent immobilization of DNA oligomers, which then subsequently served as linkers for assembly-directing RNA (Figure. 3). DPN with silanes is usually difficult to achieve due to the high mobility of the silanes during patterning. Here we showed for the first time that the isothiocyanate-based chemistry combined with DPN is appropriate (1) for the site-selective immobilization of nucleic acids and, thus, (2) for the formation of viral nanoparticles by bottom-up self- assembly after adding the corresponding coat proteins. [4]

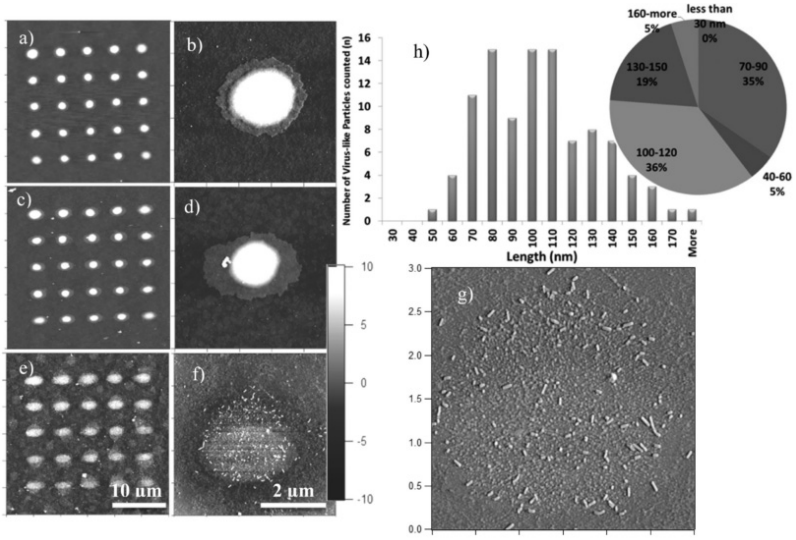

Fig. 3: AFM topography images of a) a 5 × 5 array of ITC-terminated spots after the deposition of ITCPTES by DPN on a glass slide, c) after coupling with linker DNA, and e) after TLP self-assembly. b), d), f) Magnification of individual spots in parts a), c), and e), respectively. A higher magnification of image f) and a statistical evaluation of the length distribution of TMV-like particles are shown in parts g) and h).

Strategic Themes

We strive at offering unique pattern capabilities especially for bioactive surfaces. Our installation offers great opportunities for the incorporations of diverse chemical cues onto surfaces and targeted functionalization of pre-existing surface modifications achieved by other methods. This has application in many fields, ranging from biology to optics and sensing applications. As an example for multi-step functionalization of the type we want to emphasize in future projects, we present the application of L-DPN on laser drilled and laser modified foils for application in single cell patch clamp experiments by the requesting user. After the foils were modified with laser writing (Pfleging group, IAM) to create hydrophilic areas around the laser drilled hole in the foil, L-DPN was used in our facility to further modify the surfaces by adding lipid rings around this area (Figure. 4). This proves the basic feasibility of such unique multi-process collaborations within KNMF and ongoing collaborations and will be further expanded on in different user projects and internal collaboration (e.g. Kalt group, IAP). Striving for even larger pattern areas and additional material integration, we will employ PPL in addition to DPN. Strategic targets here will be the introduction of multi-component PPL to allow for real multiplexed deposition of several inks

into one pattern and to establish this platform as robust lithographic tool for user access in the framework of KNMF.

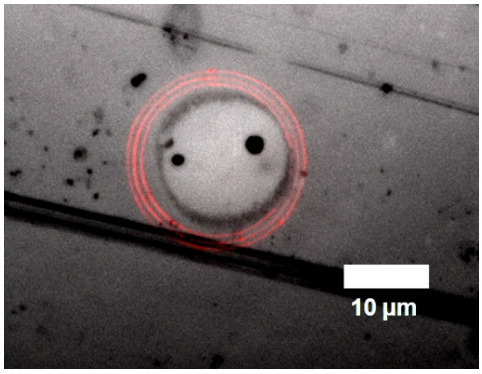

Fig. 4: Image of fluorescently labelled lipid rings (red) written by L-DPN around a laser drilled hole (black) surrounded by a hydrophilized surface area (light grey) modified by direct laser writing.

Further Collaboration outside KIT in internal projects:

Beside the user collaborations in the framework of KNMF we were also involved in additional ongoing and new collaborations inside and outside of KIT in internal projects. A technology transfer project on L-DPN with the company NanoInk Inc. was completed. Furthermore, we strengthened our ongoing collaborations on the field of biological research with the Cato (ITG) [5] and Bastmeyer group (ZOO, CS). New collaborative activities in material research were started with the Levkin (ITG) and Hahn group (INT).

References

[1] S. Oberhansl, M. Hirtz, A. Lagunas, R. Eritja, E. Martinez, H. Fuchs, J. Samitier “Facile modification of silica substrates provides a platform for direct-writing surface click chemistry”, *Small 8 (2012) 541–545, DOI:10.1002/smll.201101875*

[2] S. Sekula-Neuner, J. Maier, E. Oppong, E.; A. C. B. Cato, M. Hirtz, H. Fuchs “Allergen arrays for antibody screening and immune cell activation profiling generated by parallel lipid dip-pen nanolithography”, *Small 8 (2012) 585-591, DOI:10.1002/smll.201101694*

[3] K. Mitsakakis, S. Sekula-Neuner, S. Lenhert, H. Fuchs, E. Gizeli “Convergence of dip-pen nanolithography and acoustic biosensors towards a rapid-analysis multi-sample microsystem”, *The Analyst 137 (2012) 3076–3082, DOI:10.1039/c2an35156k*

[4] C. A. Azucena, F. J. Eber, V. Trouillet, M. Hirtz, S. Heißler, H. Fuchs, C. Wege, H. Gliemann “New approaches for bottom-up assembly of tobacco mosaic virus-derived nucleoprotein tubes on defined patterns on silica- and polymer-based substrates”, *Langmuir 28 (2012) 14867-14877, DOI:10.1021/la302774h*

[5] T. Jochum, M. E. Ritz, C. Schuster, S. F. Funderburk, K. Jehle, K. Schmitz, F. Brinkmann, M. Hirtz, D. Moss, A. C. B. Cato “Toxic and non-toxic aggregates from the SBMA and normal forms of androgen receptor have distinct oligomeric structures”, *Biochimica et Biophysica Acta 1822 (2012) 1070–1078, DOI:10.1016/j.bbadis.2012.02.006*

Thin Film Technologies (TFT)

Harald Leiste, Stefanie Spitz

For the development of new materials and the modification and enhancement of surfaces, thin films can be deposited on 2- and 3-dimensional substrates. Different facilities operate within KNMF at the Institute for Applied Materials (IAM-AWP). The PVD-processes are magnetron sputtering, arc ion plating and PVD/CVD-hybrid processes. In the scope of these facilities thin films of different compositions and properties can be developed in terms of mechanical, magnetic, electrical or optical applications. The R.F. and DC-magnetron processes in the non-reactive and reactive mode are open to users, beside other deposition methods, and allow complete new system properties. The in-house research focuses on process improvement and optimization as well as on the fabrication of new materials and concepts. The following R&D activities were performed in 2012.

Combinatorial Approach for Material Development in the System Cr-Zr-O

By means of a combinatorial approach the composition of thin films can be varied over a wide range. This method offers, as a screening method, the possibility to determine the properties and microstructure of a compound with new composition and properties for advanced applications. As a result of fast quenching of the gas phase in the PVD-process it is possible to deposit stable phases or to stabilize materials in a metastable state dependent on the composition, substrate temperature and growth rate. By the use of a segmented target which consists of two different materials, each in a geometry of two half cylindrical plates (Figure 1), the deposited thin film composition becomes dependent on the position below the target. The Cr/Zr-target with a diameter of 75 mm is shown in Figure 2, for which a partial oxidation took place during the reactive sputtering process (coloured half ring on the Zr-side).

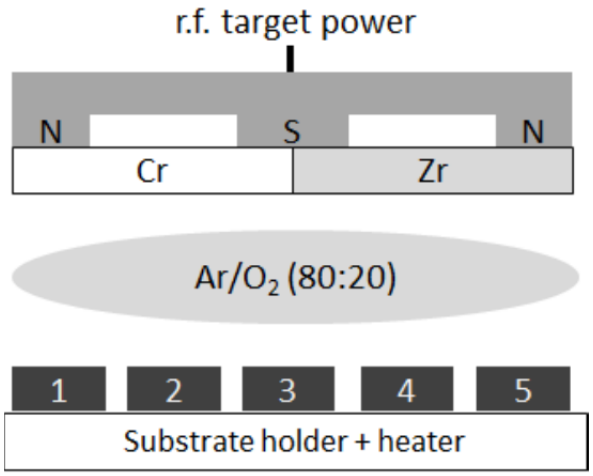

Fig. 1: Schematic combinatoric setup with different substrate positions.

Fig. 2: Symmetrically divided Cr/Zr-target for the deposition of position-dependent $Cr_xZr_yO_z$-films (diameter 75mm).

Cr-Zr-O-films were deposited by the use of this target in an Ar/O_2 gas mixture at a substrate temperature of 500°C at a gas pressure of 0.4 Pa and were characterized by electron probe

microanalysis. The films show a composition range between 3.48 for the Cr/Zr relation on the Cr-rich side and 0.26 on the Zr-rich side, as shown in Figure 3. The oxygen content remains between 60.4 at.% and 63.2 at.%.

It can be shown that the films maintain in a single phase solid solution of the corundum structure for the Cr-rich samples up to a Zr-concentration of 12 at.%. A further increase of the Zr concentration and decrease of the Cr concentration yields the ZrO_2 crystal structure and a change in the metal / oxygen relation towards 1/2 where the cubic and tetragonal structure could be identified by XRD-characterization. The fractured surface is shown in Figure 4 exhibiting a low roughness of the film surface and a good adhesion of the film on the Cr-Zr-buffer layer on the top of the cemented carbide substrate.

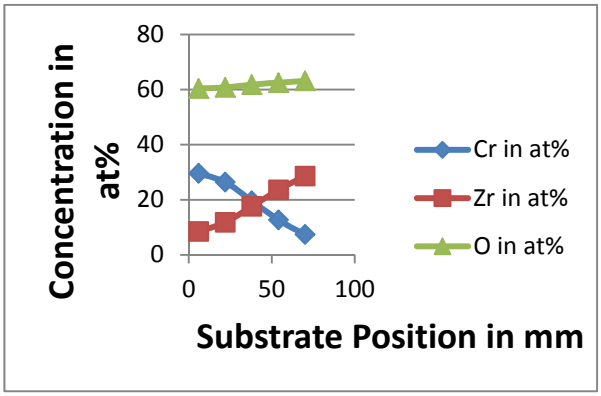

Fig. 3: Thin film composition dependent on the position below the segmented target.

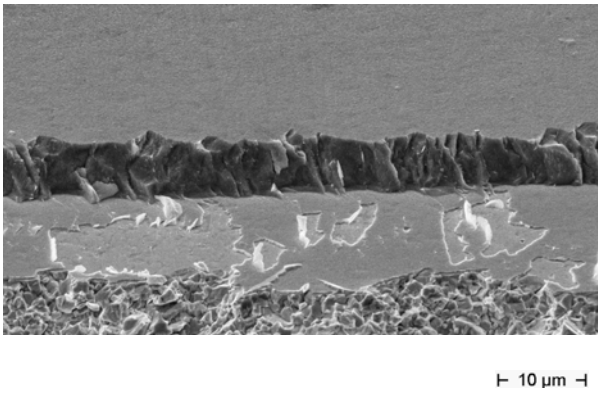

Fig. 4: Fractured surface of Cr-Zr-O film (above) and substrate (below).

Strategic Themes

The main competence of the TFT in KNMF is the development of thin film material and the optimization of the deposition parameters for tailored applications. The coatings will be realized by PVD-methods on 2- or 3-dimensional substrates e.g. as a starting material for in micro- or nanopatterned objects. Beside this single layer films complex thin film concepts can be realized like multilayer and graded coatings, nanocrystalline, metastable and solid solutions as well as superhard or multiphase coatings. The overview of the possible material starts with pure metals followed by binary carbides, nitrides, borides and oxides up to ternary and quaternary alloys for mechanic, optic, ferromagnetic or conducting applications.

Further Collaboration outside KIT in Internal Projects:

Universities of: Kassel, Kaiserslautern, Aachen, Leoben (Austria), Uppsala (Sweden), Linköping (Sweden), Coimbra (Portugal), Leeds (UK)

Companies: Walter, Gühring, Balzers, Rockwell Collins

Research Centers: FHG-IMW Freiburg, KIST (Korea), AIN Pamplona (Spanien)

References

[1] M. Stueber, D. Diechle, H. Leiste, S. Ulrich “Synthesis of Al–Cr–O–N thin films in corundum and f.c.c. structure by reactive r.f. magnetron sputtering“, Thin Solid Films 519 (2011) 4025–4031

[2] S. Weidner, S. Geburt, S. Milz, J. Ye, S. Ulrich, C. Ronning „Extension of the cubic boron nitride thin film growth phase diagram”, Diamond & Related Materials 22 (2012) 88–91

[3] K. Seemann, H. Leiste, K. Krüger „On the comparison of the polarization behavior of exchange-biased AF/F NiMn/Fe37Co48Hf15 bi-layer and multi-layer films with increased ferromagnetic cut-off frequencies”, Journal of Magnetism and Magnetic Materials 324 (2012) 1165–1171

[4] J. Pröll, R. Kohler, A. Mangang, S. Ulrich, M. Bruns, H.J. Seifert, W. Pfleging “Diode laser heat treatment of lithium manganese oxide films”, Applied Surface Science 258(2012)5146-5152

.

Dry Etching Cluster (DRIE)

Alban Muslija, Kira Köhnle, Daniel Häringer, Christian Lay and Manfred Kohl

A dry etching cluster from Oxford Instruments, having a RIE / ICP (System: Plasmalab100 with a ICP 380 source) and a RIBE (System Ionfab 300) process chamber, is operated in KNMF by the Institute of Microstructure Technology (IMT) for fabrication of Si, SiO2, SiN and Si3N4 microstructures as well as various metal (Ti, Cr) structures. A special feature of the dry etching cluster is the Ionfab 300 Plus RIBE tool (RIBE: Reactive Ion Beam Etching) used for structuring special metal alloys, in particular magnetic alloys consisting of Ni, Co, Fe, shape memory alloys (NiTi) and ferromagnetic shape memory alloys (NiMnGa). The in-house research focuses on process development and optimization as well as on the fabrication of complete nano devices.

Nano Scale Disruptive Silicon-Plasmonic Platform for Chip-to-Chip Inter-connection

The NAVOLCHI FP7 project has seven partners and is coordinated by KIT. The project explores, develops and demonstrates a novel nano-scale plasmonic chip-to-chip and system-in-package interconnection platform to overcome the bandwidth, foot-print and power consumption limitations of todays electrical and optical interconnect solutions.

The technology exploits the ultra-compact dimensions and fast electronic interaction times offered by surface plasmon polaritons to build plasmonic transceivers with a few square-micron footprints and speeds only limited by the RC constants. Key elements developed in this project are monolithically integrated plasmonic lasers, modulators, amplifiers and detectors on a CMOS platform. [1]

For test purposes as well as for the fabrication of deliverables, different waveguides in the nm-range were fabricated on SOI substrates. The thickness of the silicon device varies between 220 nm and 340 nm, the structure width ranges between 190 and 300 nm. Thus, aspect ratios up to 1,5 were realized in these critical lateral dimensions.

A representative waveguide design is shown in the following Figures 1 and 2:

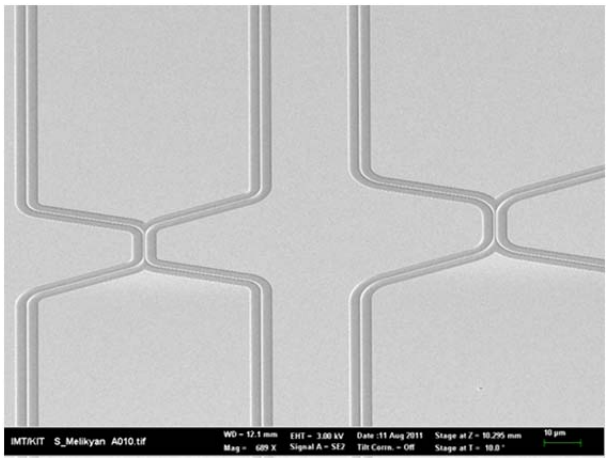

Fig. 1: Plasmonic waveguides – overview

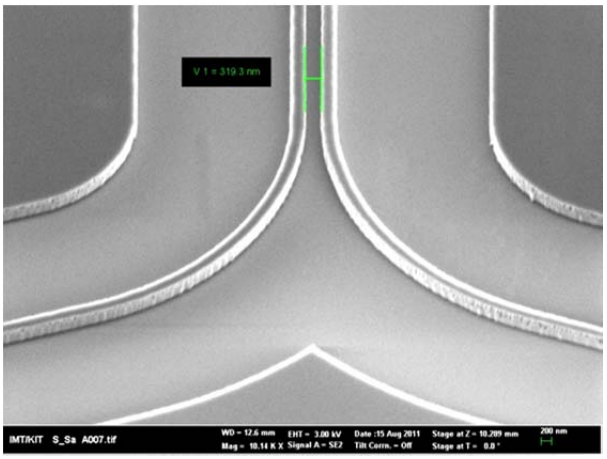

Fig. 2: Detail – width ~250nm, hight ~ 340 nm

Auxetic structures fabricated in Silicon

When a material is stretched there is normally an accompanying reduction in width. A measure of this dimensional change can be defined by Poisson ratio (PR). For most materials this value is positive and reflects a need to conserve volume.

Auxetic materials (or metamaterials) are those with a negative Poisson ratio (NPR) and display the unexpected property of lateral expansion when stretched, as well as an equal and opposing densification when compressed. Natural (some minerals, skins) and man-made (foams, Gore-Tex®, polymeric foams) auxetics have been described and very special attention is being paid to the development of auxetic structures designed and controlled on a molecular scale. [2]

Using the Cryo Dry Etching Process for Silicon, auxetic structures has been fabricated in the µm range, based on a SOI substrate with a silicon device thickness of 1,0 µm and a 4,0 µm thick BOX layer. The typical auxetic layout was written into a photoresist using laserlithography and the etched into the device layer using the standard Cryo Process. Finally, the etched silicon structures were underetched, removing the oxide layer with HF (wet etching).

The results are shown in the following Figures 3 and 4:

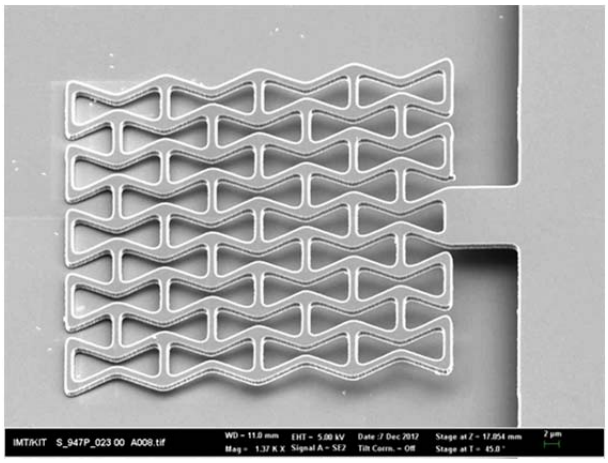

Fig. 3: Auxetic structure – overview

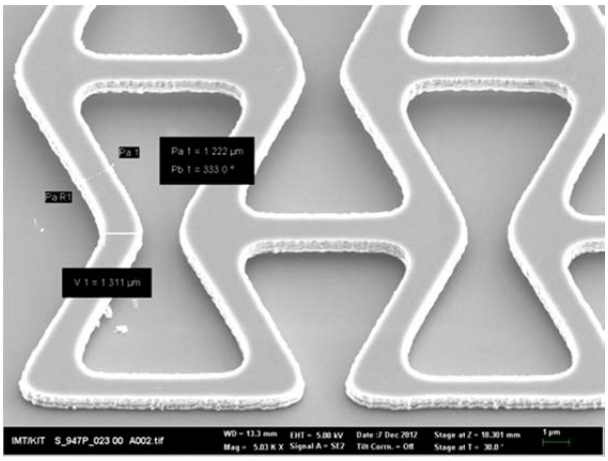

Fig. 4: Detail – ligament width ~ 1,3 µm

The structures are intended to be tested in further force measurements, thus analizing the relation between the auxetic geometry and the specific properties of the processed silicon material.

Silicon-rich Silicon-nitride Ring Resonators

In this project the following KMNF tools are used:

- Electron Beam Writer: VISTEC VB6
- Dry Etching Tool: Oxford Plasmalab System 100 with ICP 380 source

This project aims to fabricate very high quality ring resonators in silicon-rich silicon nitride. With these ring resonators it will be possible to achieve the high photon density needed to create frequency combs by four-wave mixing. These frequency combs are a requirement for optical data transmission with data rates in the range of Tbit/s [3, 4].

To achieve a high photon density in the ring, losses should be kept to a minimum. Therefore the ring resonators need to have an absolutely flat surface and no defects. The advantage of the KMNF electron beam writing tool is the large main field which allows for rings with a diameter up to 1000 µm without main field stitching errors.

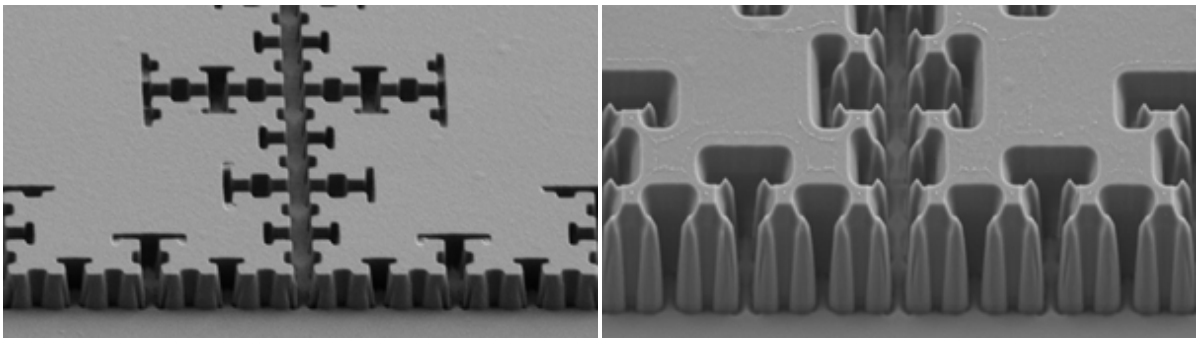

a b

Fig. 5: CHF_3/SF_6 etch process for silicon nitride etching with an etch duration of (a) 2 minutes and (b) 3.5 min. The smallest features are around 200 nm.

The transfer of the resist into the silicon-rich silicon nitride requires an etch process which doesn't introduce sidewall roughness and at the same time produces sidewalls which are as vertical as possible. In the last year a suitable process using CHF_3/SF_6 could be developed successfully (see Figure 5.a). As can be seen in Figure 5.b the mask from the electron beam lithography step is not high enough to sustain the etch process leading to etched silicon nitride where small resist structures have been. In the next iteration the resist height of the electron beam lithography step will be increased.

Sub-wavelength Grating Waveguides

In this project the following KMNF tools are used:

- Electron Beam Writer: VISTEC VB6
- Dry Etching Tool: Oxford Plasmalab System 100 with ICP 380 source

This project tries to show a Chi(2) effect by functionalizing sub-wavelength grating waveguides with electro-optic material. Until now this non-linear effect could only be shown for other types of waveguides (e.g. slot waveguides or photonic crystals) [1-3]. Electro-optic material can be put directly in the path of light leading to an increased interaction between light and material compared to the use as cladding material in a standard strip waveguide.

To reach this goal, a gold layer and a waveguide layer have to be exposed aligned to each other. Markers which are partially etched into the top silicon layer of the SOI chip have to be detected in the following electron beam exposure steps in a reproducible way and with very high precision.

Multiple etch depths into the top silicon layer to create more complex waveguide structures are targeted. In combination with doping layers multiple etch depths enable the fabrication of slot waveguides at the KIT and though an integration of slot waveguides and sub-wavelength grating waveguides.

This requires a silicon etch process which can be etched within 10 nm of the target etch depth. The current cryogenic etch process with SF_6 at a temperature of -126 °C is not suited for that. The new etch process with HBr which will be introduced after the extension of the tool should be able to fulfill this task.

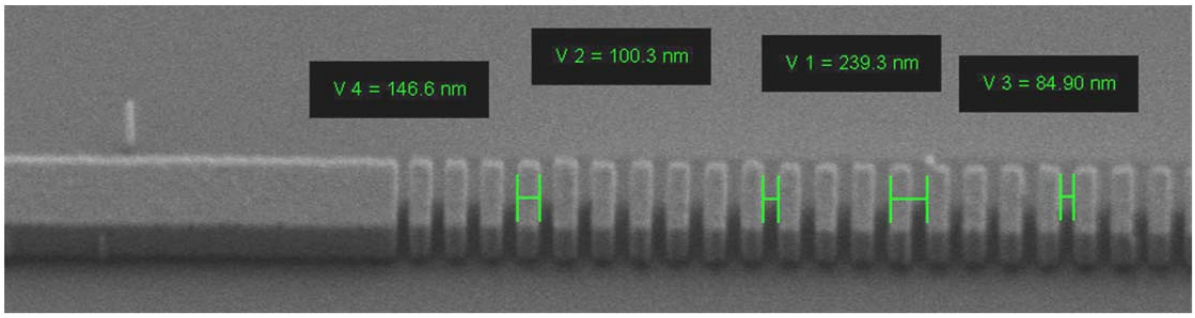

Fig. 6: Sub-wavelength Grating Waveguides - etched in silicon by SF_6 cryo process

As can be seen in figure 6 the single waveguide pieces fit well to the design dimensions of 150 nm by 450 nm.

Gold nano structures by RIBE technology

Dry etching of metals is more sophisticated compared to silicon dry etching. This is the case for gold as well because of its chemical inertness. On the other hand gold is frequently used for nano devices because of its stability on ambient conditions and optical properties. Therefore fabrication routes are needed. In this example we demonstrate the fabrication of gold cantilevers using Reactive Ion Beam Etching (RIBE). First a PMMA mask for a 30 nm thick gold layer was structured by e-beam lithography. Then the dry etching of gold was performed within 40 seconds, resulting in arrays of cantilevers of different dimensions and alignments (see Figures 7 and 8).

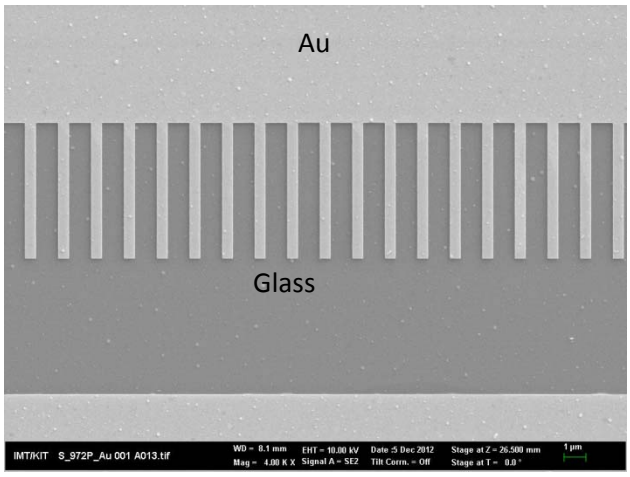

Fig. 7: Array of gold cantilevers on a glass substrate, produces by RIBE technology. Cantilevers width: 500 nm, etch time: 40 sec.

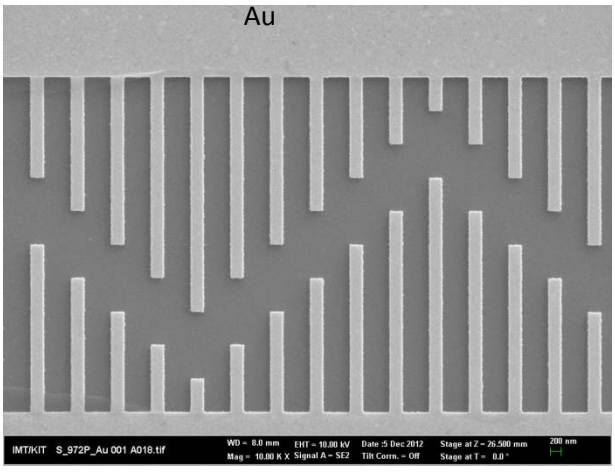

Fig. 8: Array of gold cantilevers on a glass substrate, produces by RIBE technology. Cantilevers width: 250 nm, etch time: 40 sec.

Nanoimprint Silicon Stamps

Nanoimprint technology allows the parallel production of nanoscale structures at high speed. However, the fabrication of nanoimprinted structures requires the development of high precision stamps with low surface roughness for low demoulding forces.

Electron beam lithography is essential to create structures with feature sizes down to 100 nm. We use PMMA positive resist as well as AR-N 7520 negative resist on silicon

wafers to create silicon stamps for nanoimprinting. An example of developed resist structures can be seen in figures 9 and 10.

The challenge in creating these imprint stamps are the different demands of electron beam exposure and imprinting. For the latter, large filling structures have to be adjacent to the desired nanostructures to achieve a homogeneous distribution of polymer in the stamp's trenches and a low residual polymer height under the stamp's elevated structures. However, when large structures are exposed with the electron beam, nearby small structures recieve part of the dose. This proximity effect has to be mitigated by careful layout design as well as adjusting the dose according to results of a proximity effect simulation. After development of the resist, the pattern is transfered to the silicon with reactive ion etching in the Oxford Plasma Lab 100 RIE chamber.

To achieve rectangular as well as smooth sidewalls, we use a cryogenic silicon etch process with a very low etch rate to improve control of the profile depth. Figure 11 shows an etched silicon stamp with structure sizes down to 280 nm. The result of an imprint process with a silicon stamp is shown in figure 12. While it was possible to reproduce the structures, the residual resist height was still too high. Thus, further optimization of filling factor and profile depth are required.

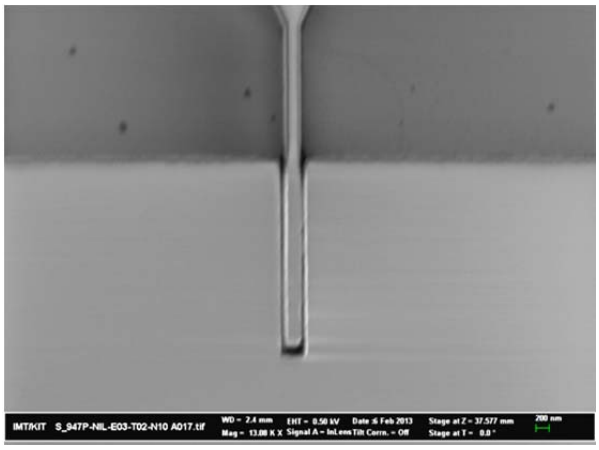

Fig. 9: SEM image of negative resist after exposure and development.

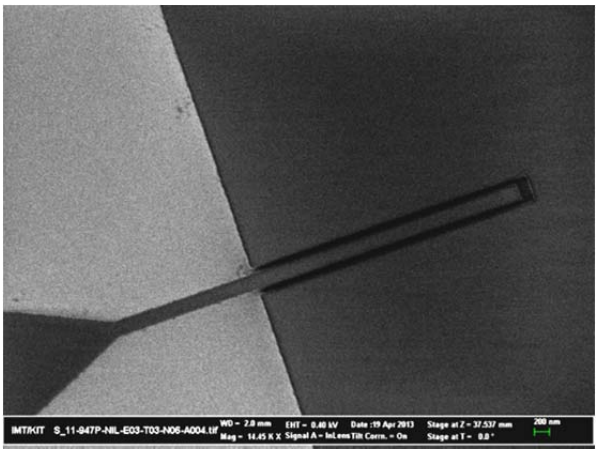

Fig. 10: SEM image of positive resist after exposure and development.

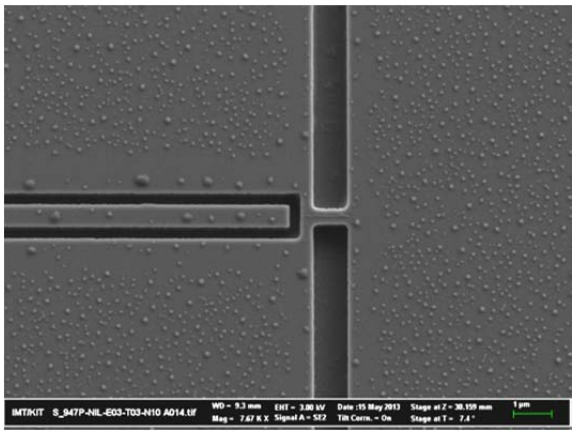

Fig. 11: The stamp after silicon etching. The surface is contaminated with resist residue, which can be removed by oxygen plasma.

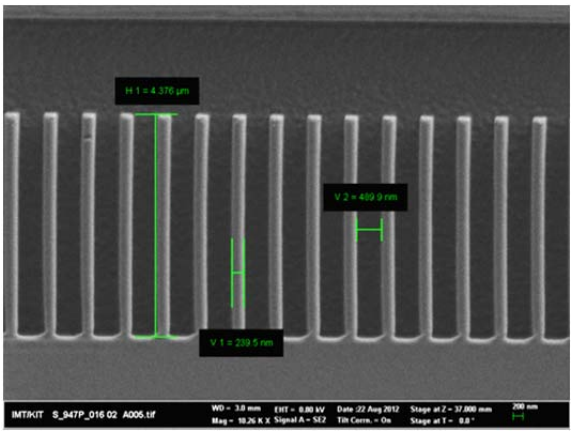

Fig. 12: Imprinted resist structures. The beams have a height of 4.4 µm and a width of 240 nm.

References

[1] www.navolchi.eu: Project website, © - Institute of Microstructure Technologies, Karlsruher Institute of Technology (KIT) - all rights reserved.

[2] Juan Carlos Álvarez Elipe and Andrés Díaz Lantada: Comparative study of auxetic geometries by means of computer-aided design and engineering. 2012 *Smart Mater. Struct. 21 105004 doi:10.1088/0964-1726/21/10/105004*

[3] D. Hillerkuss, R. Schmogrow, M. Meyer, S. Wolf, M. Jordan, P. Kleinow, N. Lindenmann, Philipp C. Schindler, A. Melikyan, X. Yang, S. Ben-Ezra, B. Nebendahl, M. Dreschmann, J. Meyer, F. Parmigiani, P. Petropoulos, B. Resan, A. Oehler, K. Weingarten, L. Altenhain, T. Ellermeyer, M. Moeller, M. Huebner, J. Becker, C. Koos, W. Freude, and J. Leuthold, "Single-Laser 32.5 Tbit/s Nyquist WDM Transmission," *J. Opt. Commun. Netw.,* vol. 4, pp. 715-723, 2012.

[4] C. Koos, J. Leuthold, W. Freude, T. J. Kippenberg, J. Pfeifle, C. Weimann, K. Hartinger, V. Brasch, T. Herr, R. Holzwarth, D. Hillerkuss, and R. Schmogrow, "Terabit/s data transmission using optical frequency combs," pp. 860009-860009, 2013.

[5] R. Palmer, A. Luca, D. Korn, P. Schindler, M. Baier, J. Bolten, T. Wahlbrink, M. Waldow, R. Dinu, W. Freude, C. Koos, and J. Leuthold, "Low Power Mach-Zehnder Modulator in Silicon-Organic Hybrid Technology," *Photonics Technology Letters, IEEE,* vol. PP, pp. 1-1, 2013.

[6] D. Korn, M. Lauermann, P. Appel, L. Alloatti, R. Palmer, W. Freude, J. Leuthold, and C. Koos, "First Silicon-Organic Hybrid Laser at Telecommunication Wavelength," in *CLEO: Science and Innovations*, 2012.

[7] W. Freude, J. Brosi, C. Koos, P. Vorreau, L. C. Andreani, P. Dumon, R. Baets, B. Esembeson, I. Biaggio, T. Michinobu, F. Diederich, and J. Leuthold, "Silicon-Organic Hybrid (SOH) devices for nonlinear optical signal processing," in *Transparent Optical Networks, 2008. ICTON 2008. 10th Anniversary International Conference on*, 2008, pp. 84-87.

Transmission Electron Microscopy (TEM)

Christian Kübel, Di Wang, Kiran Chakravadhanula, Eglantine Courtois, Aaron Kobler, Torsten Scherer, Robby Prang, Delphine Chassaing, Emma Tröster

An image corrected FEI Titan 80-300 Transmission Electron Microscope (TEM) is operated within the KNMF by the Institute of Nanotechnology (INT) for high-end structural characterization in materials sciences using a combination of atomic resolution imaging, nanoscale compositional analysis and nanoscale 3D imaging. The TEM work is supported by Focused Ion Beam (FIB) and classical polishing techniques for preparation of high-quality samples. In-house research focuses on optimizing the performance of the existing microscopy techniques as well as developing new techniques for nanoscale crystallographic analysis (ACOM-TEM) and in-situ mechanical and electrical characterization of materials inside the TEM. In addition, in-house research is used for high-end characterization of a range of nanomaterials for HGF and KIT internal partners. A selection of the R&D activities performed in 2012 is shown below.

Combination of *in-situ* straining and ACOM TEM: A novel method for analysis of plastic deformation of nanocrystalline metals

Nanocrystalline metals are expected to exhibit different deformation mechanisms when compared to their coarse grained counterparts because the dislocation storage capacity decreases and the grain boundary mediated processes become increasingly pronounced with decreasing grain size. However, imaging the structure and structural changes of these materials directly is very challenging as classical imaging techniques such as BF/DF-TEM only provide limited information and are often difficult to interpret for nanocrystalline metals. As a new approach to characterize these nanocrystalline metals, we have established automated crystal orientation mapping (ACOM) in TEM providing full orientation maps with nanometer resolution to close the gap between EBSD and BF/DF-TEM. Their global quantitative analysis in terms of texture and grain size is in very good agreement with X-ray diffraction based analysis of bulk materials as was shown for electrodeposited nanocrystalline Nickel before and after compression (Figure 1).

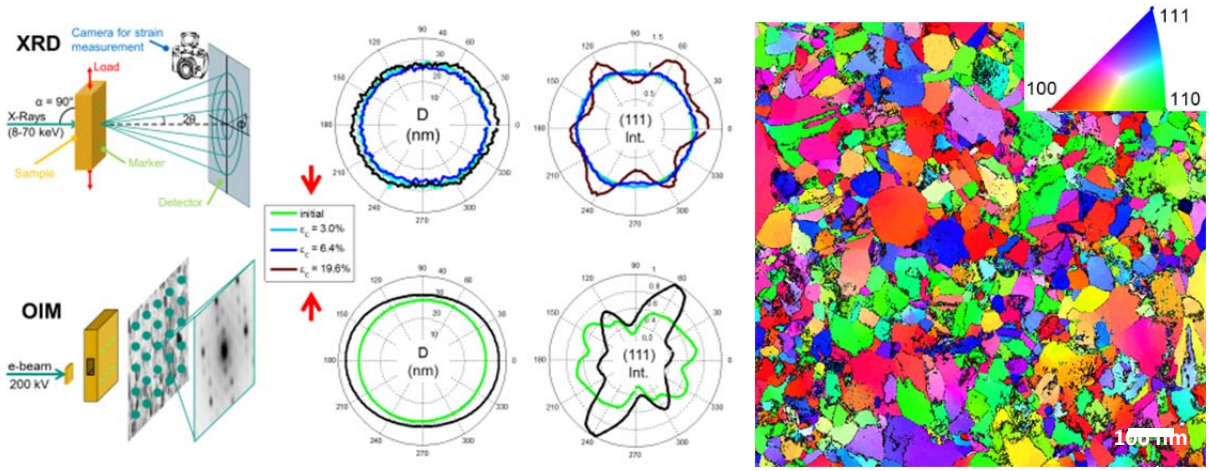

Fig. 1: Comparison of the grain size/anisotropy and texture development during compression of nanocrystalline Nickel measured by synchrotron based X-ray analysis (top) and ACOM-TEM (bottom). The graphs show the grain size anisotropy before and after compression and the anisotropy of the (111) reflection as a measure for the texture development. Reproduced with permission from C. Kübel et al., Microscopy & Microanalysis (2013), Cambridge University Press; in press.

As a new approach to directly image and quantify the local plastic deformation processes in nanocrystalline thin films during mechanical deformation, a combination of automated crystal orientation mapping in microprobe STEM mode with in situ straining inside a TEM (Figure 2) has been developed. It was used to characterize the metallographic changes during tensile deformation of a nanocrystalline Au thin film with an average grain size around 37 nm prepared by magnetron sputtering. The investigation of the grain size, grain orientation and twinning on a global (grain average over a micron sized area) and local (assembly of selected grains) scale allowed for the development of an in depth picture of the deformation processes.

We were able to clearly distinguish between an initial unbending and a sample loading regime. During the unbending and the early stages of sample loading, we observed a micro-plastic behaviour that showed no significant global grain growth, grain rotation and twin density variations. However, localized plastic deformation was observed with small grains shrinking to the advantage of neighbouring larger grains leading to anomalous grain growth (Figure 3) as well as local twinning/detwinning and grain rotation. At higher strain levels, a significant macroscopic increase in grain size was observed globally, which was locally accompanied by further twinning/detwinning and grain rotation as two deformation mechanisms active in nc Au to dissipate the applied strain.

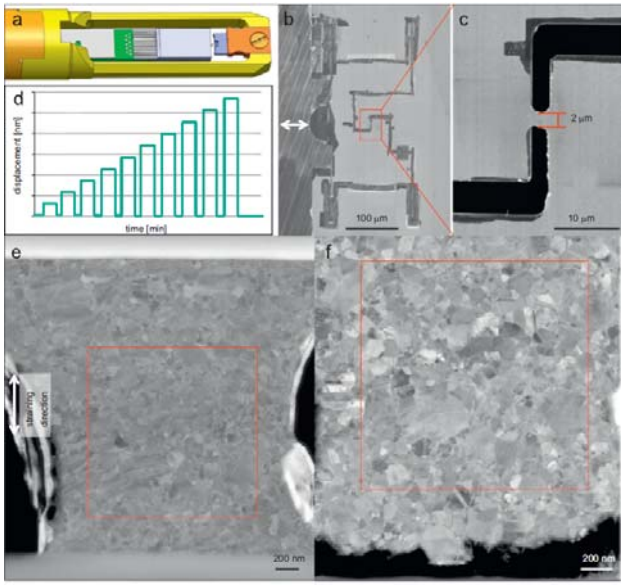

Fig. 2: (a) Tip of the TEM PicoIndenter holder for FEI from Hysitron with PTP (purple), and (b) PTP with the Au thin film on top. The spring system of the PTP has been cut free by FIB. (c) Magnified image of the straining zone with a specimen width of ~2 µm. (d) Schematic load versus time diagram for the preformed mechanical test. (e) µp-STEM image of the specimen in the initial state. The red box indicates the area where the ACOM maps are acquired. (f) µp-STEM image of the specimen after rupture of the film.

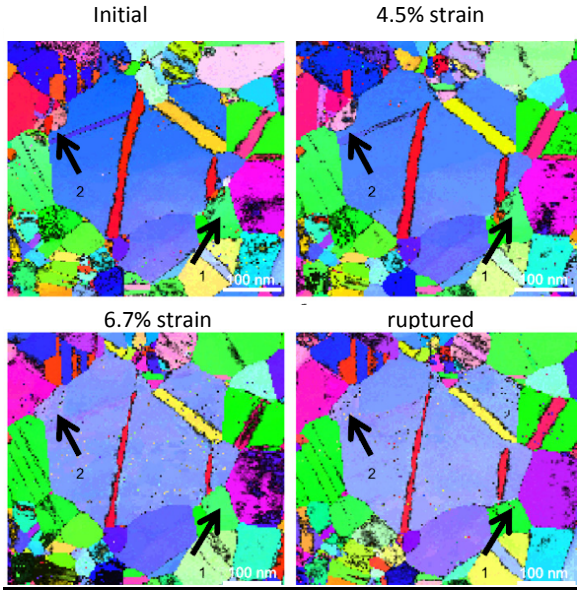

Fig. 3: Orientation maps overlaid with the reliability at different straining states of a nanocrystalline Pd thin film. The ACOM maps show two different types of grain growth during straining. The large central grain is growing by continuously 'eating' from grain 1 while extending the twin boundary initially present at the grain boundary. In contrast, grain 2 is first detwinning and suddenly merging with the large grain from one straining state to the next.

Morphological and Compositional Analysis of Organic LEDs with Silicon QDs as Active Layer (SiLEDs)

Quantum dot light emitting diodes (QD-LEDs) feature great scientific and economic potential. Compared to their purely organic counterparts, the organic emissive layer of these devices is replaced by solution-processable functionalized quantum dots (QDs). QDs and QD-LEDs feature a wide spectral tunability and high colour purity. Furthermore, as the efficiency of these devices is not intrinsically limited by spin statistics as in case of purely organic LEDs, they have the potential to reach much higher efficiencies. This, together with recently reported all-inorganic QD-LEDs without need for encapsulation, shows the great potential of this novel generation of LEDs in terms of efficiency and stability of the devices.

In this study, we have performed a detailed morphological and compositional study of SiLEDs using an image corrected FEI Titan 80-300 operated at 300kV. Initial BF-TEM and HAADF-STEM imaging was performed under strict low-dose conditions (dose <100 e/nm²), but as the morphology of the organic multilayers is stable even at significantly higher doses, a more detailed compositional analysis by EFTEM and STEM-EDX mapping could be performed for the various 2.5-35 nm thick organic layers. The resulting elemental distribution for C, N, O, S, Si and F is in very good agreement with the nominal composition of the different layers (Figures 4 and 5).

A comparison of as fabricated and electrically driven SiLEDs as well as SiLEDs prepared using monodisperse and polydisperse SiQDs [3] has been carried out to correlate morphological and compositional features with the degradation behaviour and was combined with electroluminescence and photoluminescence life time studies. This analysis showed that the morphology and composition of the SiLED is very well preserved during normal operation of the devices even though the electroluminescence is reduced to 20% during this operation, which is attributed to atomic scale processes within the SiQDs themselves. In contrast, at high voltage/current, significant electromigration of SiQDs into the hole blocking layer TPBi is observed, whereas no change for the other organic layers is observed. For non-size separated SiQDs, device life times are significantly reduced compared to SiLEDs build from monodisperse SiQDs. This seems to be related to both percolating path of larger nanoparticles inside the SiQD layer as well as diffusion/electromigration of extremely small nanoparticles into the hole blocking layer. We expect that these results are not only valid for SiLEDs but also transferable to other QD-based LEDs.

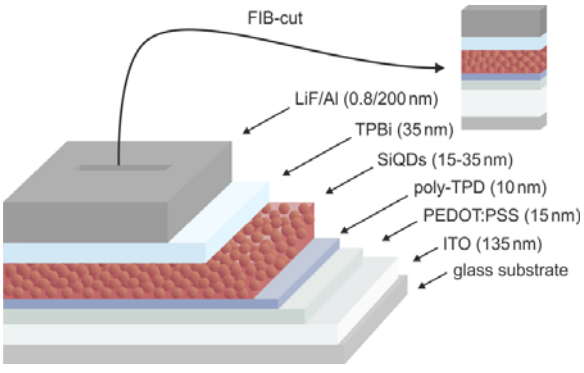

Fig. 4: Schematic representation of the SiLED stack. Reproduced with permission from C. Kübel et al., Microscopy & Microanalysis (2013), Cambridge University Press; in press.

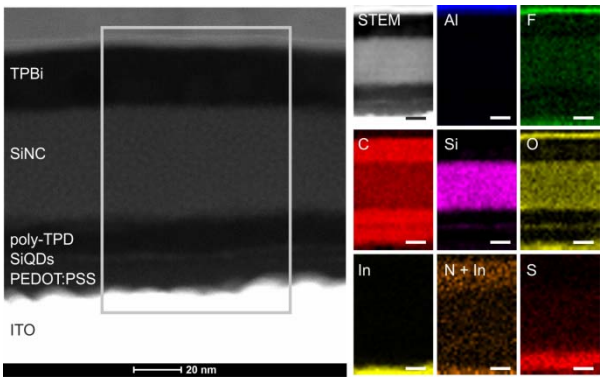

Fig. 5: HAADF-STEM cross-section image with corresponding EDX maps (scale bars 20 nm) showing the compositional differences between the various organic layers and the active Si nanocrystal layer. Reproduced with permission from C. Kübel et al., Microscopy & Microanalysis (2013), Cambridge University Press; in press.

Non-aqueous Synthesis of Isotropic and Anisotropic Actinide Oxide Nanocrystals

Transition metal and main-group based nano-objects have been extensively studied for their magnetic, optical or catalytic properties. However, our knowledge is still considerably limited when dealing with actinide elements. The synthesis of actinide-based nano-objects offers a unique opportunity to study size and shape effects on the properties of 5f electrons and is of interest both for fundamental and applied research. Whereas several groups developed the synthesis of actinide containing molecular clusters that have dimensions extending into the nanoscale, less is known about actinide-based nanocrystals (NCs). In this project, well-defined thorium- and uranium oxide nanocrystals have been synthesized by a non-aqueous approach and characterized by TEM and STEM techniques to correlate synthesis conditions and morphology.

It could be shown that the experimental conditions well suited for the formation of uranium oxide NCs do not allow the formation of thorium oxide NCs. For a given organic medium, the nature of the actinide precursor and/or the nature of the actinide centre drastically influence the reactivity and hence the characteristics of the final actinide oxide NCs [4]. It contributes to our understanding of the controlled synthesis of actinide oxide NCs and prepares the ground for the synthesis of trans uranium-based (particularly Np and Pu) nano-objects.

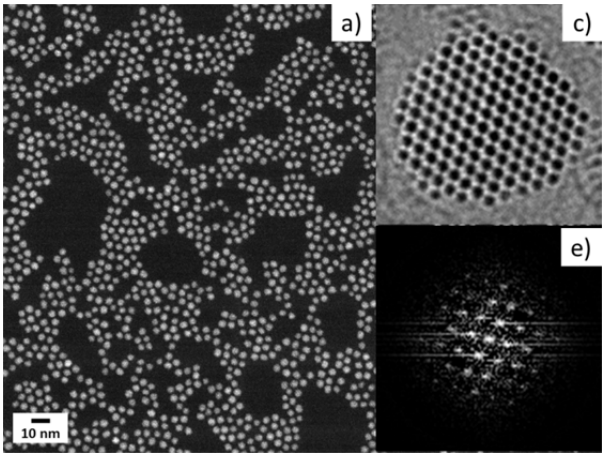

Fig. 6: HAADF-STEM and HRTEM images of close to hexagonal UO_2 nanodots 3-4 nm in diameter.

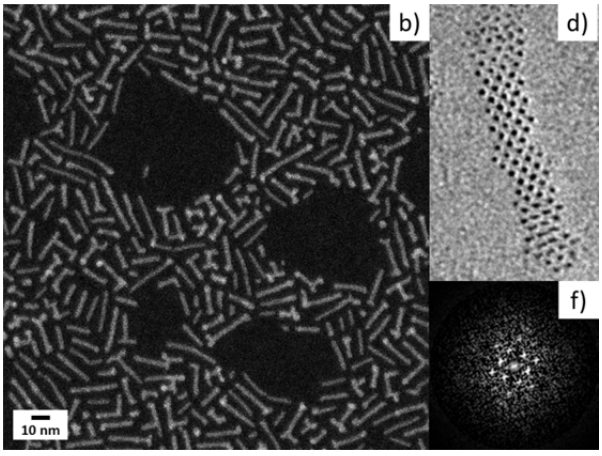

Fig. 7: HAADF-STEM and HRTEM images of rod-like ThO_2 nanocrystals ~1 nm in diameter and 3-20 nm long.

Macroscopic 3D Nanographene

Surface-dominated bulk materials provide the unique opportunity to dynamically control their physical bulk properties by modification of their surfaces through interfacial phenomena. Generating a sizable effect, however, requires that surface atoms constitute a large fraction of the total number of atoms. This requirement limits the technical potential of surface-dominated bulk materials, as structures with more than 10% surface atoms are typically not very stable and tend to reduce their surface energy by coarsening. Here, graphene is an exception — it combines a very high surface area of up to 2630 $m^2\ g^{-1}$ with the chemical and thermal stability intrinsic to the two-dimensional (2D) structure of sp^2-bonded carbon. This makes graphene an interesting building block for realization of stable ultra-high surface area bulk materials.

In this project, a “top down” strategy has been developed to fabricate mass-producible graphene-based bulk materials from low-cost polymer-derived carbon foams through the controlled removal of carbon atoms from a network composed of both amorphous carbon and graphite nanoplatelets (Figure 8 a). This approach yields mechanically robust, centimeter-sized monolithic samples (Figure 8 b) that are composed almost entirely of interconnected networks of single layer graphene nanoplatelets. Structural characterization by HRTEM revealed that the material consists mostly of short curved and intertwined graphene monolayers, whereas only few domains with stacks of graphitic layers could be observed.

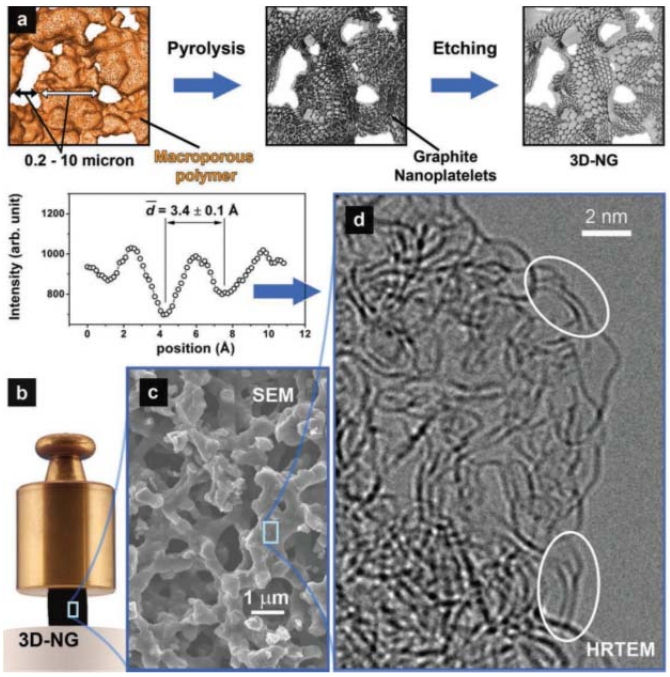

Fig 8: Processing and architecture of 3D-NG. a) Schematic of the polymer-based top-down approach. b) Illustration of the mechanical robustness of a centimeter-sized 3D-NG sample. c) Open macroporous network architecture composed of micrometer-sized pores and ligaments. d) Internal structure of ligaments composed of curved and intertwined graphene sheets. Selected double-layer regions are marked by ovals, and a typical intensity profi le across such a double-layer region is shown on the left.

High-resolution transmission electron microscope observations of multiwalled carbon nanotube microstructures grown by plasma enhanced chemical vapor deposition

Among the different techniques available to obtain thin films of densely packed vertically aligned carbon nanotubes (CNTs), plasma-enhanced chemical vapor deposition (PECVD) is especially useful because of its ability to significantly reduce the growth temperature. This is particularly important for the integration of CNTs in microelectronics, optoelectronic components, and micromechanical structures. However, PECVD requires the deposition of a catalyst to trigger the growth mechanisms, which increases the process complexity. Numerous studies have been dedicated to the growth mechanisms present during the PECVD process and to understanding the influence of different experimental parameters on the resulting CNTs. It is well-known that the supported catalyst has a much more active CNT growth when it has a nanoparticle (NP) shape. The growth results are influenced e.g. by the catalyst type and composition, as well as by the NP size, pattern geometry, density, and crystallographic orientation. The experimental conditions under which the NP catalysts are produced also influence the CNT structure and growth. Here we report on a high resolution TEM study of vertically aligned CNTs where we focus on the catalyst nanoparticle shape and localization within the CNTs with respect to the support layer and growth temperature to better understand the influence of the catalyst on the CNT growth.

For the Fe/Si_3N_4 system, CNT growth with a well-defined wall structure typically consisting of 3-10 graphene layers is observed. Both, CNTs where the top end is filled with catalyst nanoparticles (Figure 9a/d) as well as CNTs where the top end is empty (Figure 9c) are seen commenly indicating that tip and base growth modes are possible simultaneously. Under the conditions used in this study, CNT growth was only observed for the Fe/Si_3N_4 system and the Ni/TiN system, whereas very limited growth was achieved for the Ni/Si_3N_4 and the Fe/TiN system. However, when using a bimetallic catalyst Fe:Ni with a nominal atomic ratio of 2:1, CNT growth was observed on both substrates. EFTEM studies (Figure 10) of the particles present inside and at the CNT tip always shows bimetallic particles present, although the atomic ratio is varying between particles.

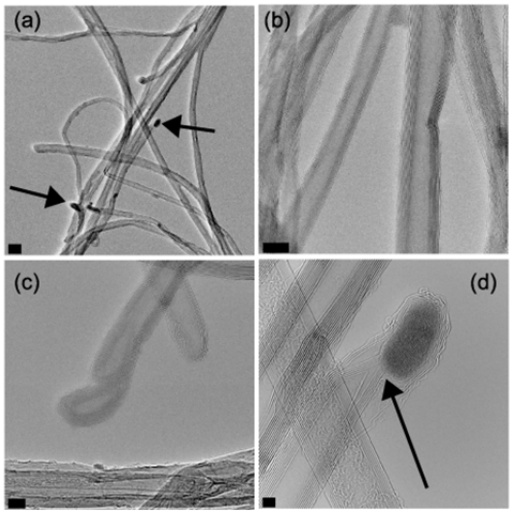

Fig. 9 shows typical TEM images of CNTs grown from a Fe/Si_3N_4 system with a well-defined wall structure typically consisting of 3-10 graphene layers (scale bars 20 nm (a), 10 nm (b), 5 nm (c), and 2 nm (d)). The graphene layers are typically growing perpendicular to the inner catalyst particle surface [6]]

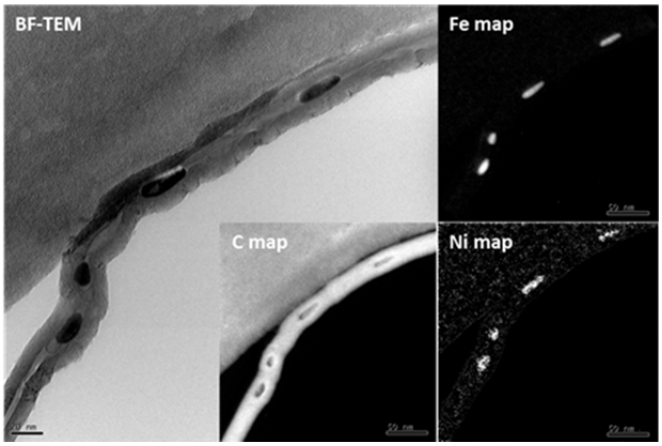

Fig. 10: BF-TEM image and corresponding elemental maps for carbon, iron and nickel of a MWCNT grown from the Fe_2Ni/Si_3N_4 system showing that the catalyst particles inside the CNTs are always bimetallic.[6]

Strategic Themes

For a close correlation between structure and materials properties, *in-situ* TEM techniques provide an essential link at the nano scale. Over the last two years, we have successfully developed in-situ mechanical testing and have the world wide unique ability to follow structural changes during plastic deformation by orientation mapping with nanometer resolution. We will continue to develop this approach, especially working on data analysis and interpretation. In addition, we are also developing other in-situ TEM techniques to follow structural changes during cooling, heating, electrical testing and electrochemical reactions to extend our characterization portfolio. On-going strategic collaborations in this area include

Prof. Edgar Rauch, CNRS Grenoble / NanoMegas;
Dr. Harald Rösner, Universität Münster;
Prof. Wolfram Jägermann, TU Darmstadt;
Prof. Jürgen Janik, Universität Gießen

A long-term strategic development for TEM together with FIB, HIM, XPS, ToF-SIMS, DPN and laser material processing will focus on multi-method correlative processing and characterization providing correlative analysis using reference markers and optical guidance maps as well as an inert transfer between selected installations.

Further Collaboration outside KIT in internal projects:

TU Darmstadt, Helmholtz Institute Ulm, European Institute for Transuranium Elements, Grenoble Institute of Technology, University Leiden, University of Luxembourg, Universität Hannover, PTB Braunschweig

References

[1] C. Kübel, A. Kobler, P.A. Gruber, J. Lohmiller, O. Kraft, C. Braun, M. Grewer, R. Birringer, H. Hahn „Analysis of Deformation Induced Grain Growth and Texture Development in electrodeposited Nickel– a Quantitative Comparison between ACOM-STEM and in-situ X-ray Diffraction" Microscopy & Microanalysis (2013) in press.

[2] A. Kobler, A. Kashiwar, H. Hahn, C. Kübel "Combination of in-situ straining and ACOM TEM: a novel method for analysis of plastic deformation of nanocrystalline metals" *Ultramicroscpoy*, Volume 128 (2013) 68-81*;* DOI: 10.1016/j.ultramic.2012.12.019.

[3] F. Maier-Flaig, M. Stephan, T. Bocksrocker, M. Bruns, C. Kübel, J. Rinck, A.K. Powell, G.A. Ozin, U. Lemmer "Multicolour Silicon Light Emitting Diodes (SiLEDs)" *Nano Letters*, Volume 13 (2013) 475-480; DOI: 10.1021/nl3038689*.*

[4] D. Hudry, C. Apostolidis, T. Gouder, E. Courtois, C. Kübel, O. Walter "Non-Hydrolytic Synthesis of Isotropic and Anisotropic Actinide Oxides Nanocrystals", *Chem. Eur. J.*, Volume 18, Issue 27 (2012) 8283-8287; DOI: 10.1002/chem.201200513.

[5] J. Biener, S. Dasgupta, L Shao, D. Wang, M. Worsley, A. Wittstock, J.R. Lee, M. Biener, C. Orme, S.O. Kucheyev, B.C. Wood, T.M. Willey, A.V. Hamza, J. Weissmüller, H. Hahn, T. Baumann „Macroscopic 3D Nanographene with Dynamically Tunable Bulk Properties" *Adv. Mat.*, Volume 24 (2012**)** 5083-5087, DOI: 10.1002/adma.201202289.

[6] M. Gaillard, C. Kübel, C. Boulmer-Leborgne, D. Wang,N. Semmar, A. Petit, E. Millon, "High-resolution transmission electron microscope observations of multi-walled carbon nanotube microstructures grown by plasma enhanced chemical vapor deposition", *JVST B*, Volume 31, Issue 3 (2013) 031805; DOI: 10.1116/1.4804543*.*

Atomic Force Microscopy (AFM)

Tobias Meier, Zhenhao Zhang, Richard Thelen, Hendrik Hölscher

Since the invention of atomic force microscopy (AFM) in the 1980s it has become a versatile tool used in, e.g., nanoscale metrology, biosensing, maskless lithography and high density data-storage. The experimental set-up of an AFM is based on a simple idea. It detects forces acting between a sample surface and a sharp tip that is mounted on a soft leaf spring (the cantilever). A feedback system, which controls the vertical z-position of the tip on the sample surface, keeps the deflection of the cantilever (and thus the force between tip and sample) constant. Moving the tip relative to the sample of the surface by means of piezoelectric drives, the actual z -position of the tip is recorded as a function of the lateral position with very high precision. The obtained data represent a map of equal forces which can be interpreted as the surface topography.

Self-sensing AFM Cantilevers Based on Tunnel Magnetoresistance Sensors

Most AFM setups rely on micro-machined cantilevers with an optical readout. Micro-machined AFM cantilevers are mass fabricated but the optical readout which is needed to focus the laser onto the backside of the cantilever and to move the position-sensitive photo-detector or a mirror (a challenge for vacuum conditions)contains bulky mechanical parts . Furthermore, the optical readout has to be readjusted not only after every change of the sensor but also after larger drifts of the environmental conditions like temperature. Self-sensing tuning forks on the other hand suffer from the limited capability of mass-production and a reduced number of operation modes compared to micro-machined cantilevers made from silicon or silicon nitride. Therefore, an ideal AFM sensor should allow various operation modes, have the capability being mass produced, and be self-sensing to eliminate the mechanical parts of the readout. Previous attempts to tackle this problem mostly used integrated piezoresistive and piezoelectric sensors on micro-machined cantilevers to measure either the strain in the lever or its displacement.

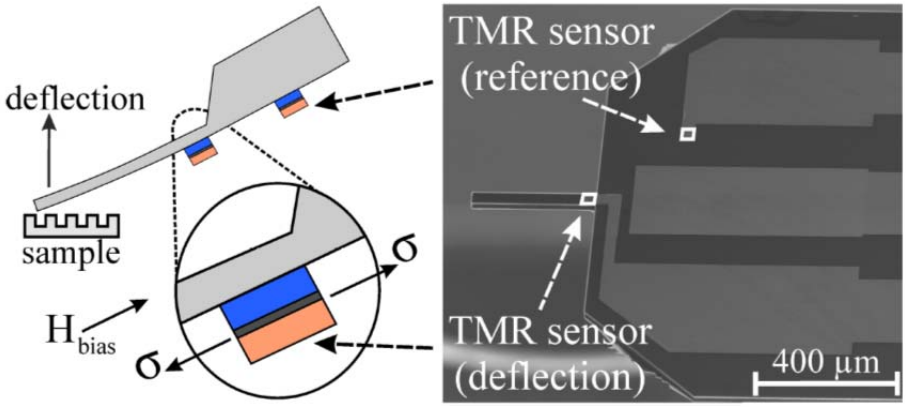

Fig. 1: A schematic of a self-sensing AFM cantilever based on magnetostrictive TMR sensors. Upward deflection causes tensile stress on the bottom side of the cantilever. This is detected by a resistance change of the deflection TMR sensor. The TMR sensor on the cantilever chip is not subjected to stress and can be used as a reference. A scanning electron microscopy image (bottom view) of a self-sensing AFM cantilever shows the two TMR sensors on the cantilever and its chip, respectively.

In a joint research project with the group of Dirk Meyners and Eckhard Quandt from the Christian-Albrechts University of Kiel we demonstrated the integration of magnetostrictive tunnel magnetoresistance (TMR) sensors for self-sensing cantilevers. A magnetostrictive TMR sensor consists of two ferromagnetic layers, the so-called reference and sensing layers, separated by an insulating tunnelling barrier. The reference layer is magnetically pinned in an artificial antiferromagnet sandwich by exchange bias effect to a natural antiferromagnet. The magnetostrictive sensing layer is free to rotate. As the TMR effect is a spin-dependent electron tunnelling phenomenon, tunnel resistance depends on the angle between the magnetizations of these two ferromagnetic layers. Due to the inverse magnetostrictive effect, induced strain rotates the easy axis of the positive magnetostrictive sensing layer to be in the direction of the applied tensile stress, thereby varying the tunnel resistance value.

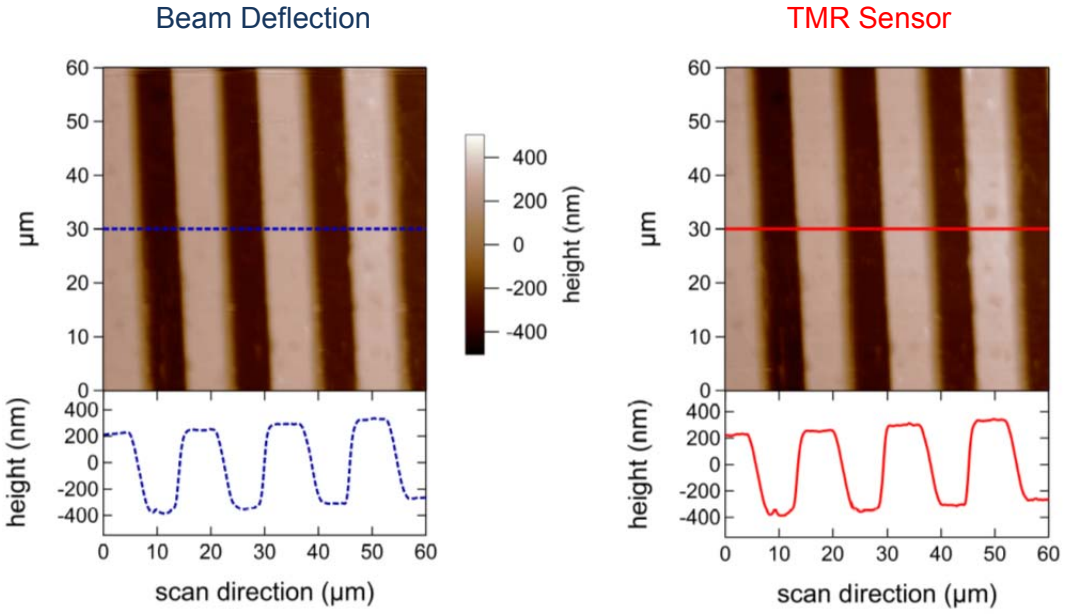

Fig. 2: Comparison of the AFM results obtained in tapping mode with beam deflection readout (left) and TMR sensor (right). The topography images of an optical grating are displayed at the bottom and were subsequently recorded at the same sample position using the conventional beam deflection and the TMR sensor signal as feedback, respectively. Line sections taken from the same positions are shown at the bottom of the two AFM images and reveal that the data quality obtained with both sensors is the same.

As depicted in Figure 1 this detection principle of a magnetostrictive TMR sensor can be easily applied to measure the bending of a AFM cantilever. In order to use the cantilevers with integrated TMR sensors as self-sensing sensors we modified a home-built AFM with optical beam-deflection readout. The system allows the application of a magnetic bias in arbitrary directions within the cantilever plane. To keep the bias field homogeneous, the system was entirely built out of non-magnetic materials. The measurement of the relative resistance change of the TMR sensor was realized by its integration into a Wheatstone bridge configuration. For the measurements shown in the following a bias field was applied perpendicular to the magnetization of the reference layer and the readout of the TMR sensor was recorded in parallel to the conventional optical beam-deflection signal. The scanning of sample surfaces is possible in contact (not shown) as well as in dynamic mode operation. Figure 2 shows a comparison of the results obtained in dynamic mode (tapping) with the TMR and optical readout. As our cantilevers have no integrated tips up to now, we used one of the cantilever apexes for scanning. During scanning the cantilever was mechanically oscillated at its mechanical fundamental resonance f_d = 123.5 kHz. Topography images of an optical grating were subsequently recorded at the same sample position with a feedback on

the conventional beam deflection and TMR sensor, respectively. The data quality observed in the topography of an optical phase grating imaged in tapping mode is the same. The measured height and width of the grating are identical and the same tiny details can be found in both images.

In summary, self-sensing AFM cantilevers with TMR sensors offer high strain sensitivity and remarkable miniaturization possibilities. The deflection signal can be easily detected as a resistance signal since the electrical resistance of a magnetostrictive TMR sensor is a function of the strain occurring at the bended cantilever surface. The successful recording of topography images demonstrates that the classical optical beam deflection method can be replaced by this type of cantilever. Especially, for tip-scanning AFMs as well as for compact and low-cost probe microscopes, TMR sensors are a valuable alternative to bulky optical deflection sensors. Permanent magnets or other magnetic biasing schemes might be integrated into new designs in order to avoid the application of the external magnetic field by coils. On-going studies have to extend the application of TMR-based self-sensing cantilevers to other environments (liquids and vacuum). Furthermore, the TMR stacks might be improved for even higher sensitivity.

Analysis of CIGS Solar Cells under White Light Illumination

Thin-film solar cells based on polycrystalline Cu(In,Ga)Se_2 (CIGSe) achieved high attention due to their extremely good power conversion efficiency in all kinds of thin film solar cells. Therefore, numerous measurement techniques were applied to investigate the electrical and opto-electrical properties of CIGSe solar cells in the last decades. A very high spatial resolution within nanometers is achieved with an extension of the AFM the Kelvin probe force microscope (KPFM) enabling simultaneous imaging of topography and contact potential difference (CPD). Particularly for solar cells, KPFM is an outstanding tool for two-dimensional potential imaging on cross sections of solar cells. In a recent project together with the Light Technical Institute of the KIT and the “Zentrum für Sonnenenergie- und Wasserstoff-Forschung Baden-Württemberg” (ZSW) we examined their performance under illumination with white light.

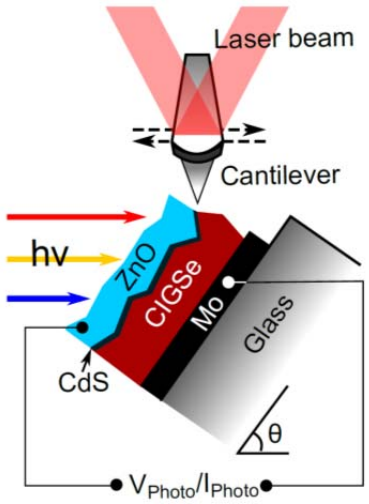

Fig. 3: Schematic illustration of the experimental setup used in our KPFM experiments. The sample is tilted relative to the cantilever. The orientation of the cantilever axis is perpendicular to the image plane. For the analysis of the cantilever oscillation, a laser beam is reflected on the back side of the cantilever and detected by a four-quadrant photo-detector. For measurements under illumination, the sample is illuminated through the ZnO transparent layer from the left. Photo-voltage V_{Photo} and photocurrent I_{Photo} between the electrodes ZnO and Mo are recorded by a multi-meter.

KPFM measurements were performed at the same position in darkness, under illumination, and in darkness again. The second measurement in darkness was carried out to examine

possible impacts of the illumination on the surface conditions of the cross sections. The results for different measurement conditions are shown in Fig. 4. The different layers of the CIGS solar cell are clearly distinguishable in the topography images. As shown in Fig. 4a), there is a large contrast between the layers in the CPD image in darkness. A line section from the position marked by a dashed line in this CPD image reveals the potential distribution through the ZnO/CdS/CIGSe-heterojunction. As indicated by the arrow, the potential drop through the heterojunction is 440 mV in darkness. Subsequently, the sample was illuminated with increasing intensity. It is observed that the CPD signal decreases with increasing illumination intensity up to flat-band conditions for intensities over 107 mW/cm^2. This light intensity is similar to the standard test conditions for solar cells.

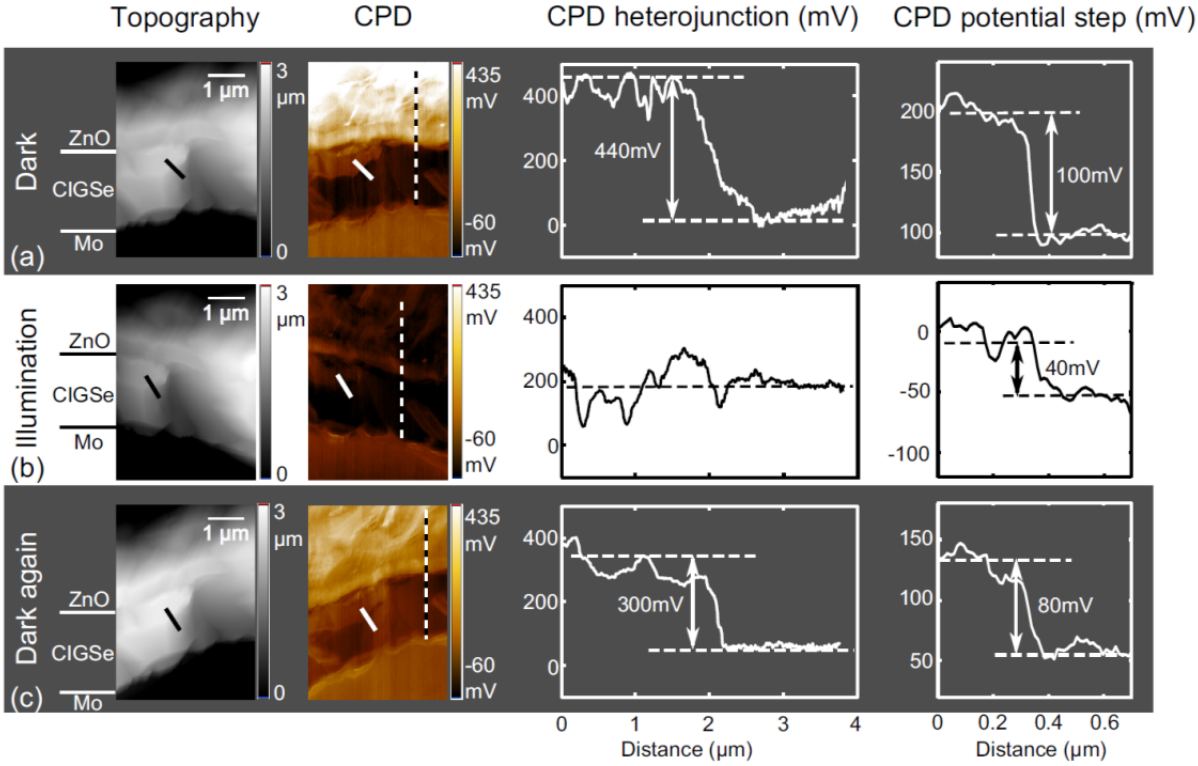

Fig. 4: KPFM measurements of topography and contact potential difference (CPD) images are carried out (a) in darkness, (b) under illumination with an intensity of 134 mW/cm^2 and (c) in darkness again. The scan lines in the third column show the potential drop through the heterojunction (extracted from the position marked by the dashed lines). The potential steps in the CIGSe absorber (extracted from the positions marked by the solid lines) are displayed on the right.

After the illumination experiments, we switched off the white light and subsequently the contrast of the CPD image recovers as shown in Fig. 4c). The height of the potential drop and the potential step rise to 300 mV and 80 mV, respectively. Typically, these values are 20-30% smaller as the original ones at the beginning of the dark-light-dark cycle displayed in Figure 4a). This effect is most likely evoked by the heat generated in the solar cell.

In summary, we analyzed the potential distributions on cleaved cross sections of operating CIGSe thin-film solar cells under defined illumination intensities. In a detailed study we observed that the potential drop through the solar cell hetero-junction decreases with increasing illumination intensity and the magnitude of its decrease correlates with the increase of the photovoltage induced by illumination.

Strategic Themes

Atomic force microscopy enables the imaging of surface properties down to the atomic scale. The imaging of single atoms, molecules, and defects is possible using the so-called non-contact atomic force microscopy technique (NC-AFM) in ultra-high vacuum (UHV) at low temperatures. Recent studies showed that this high resolution is also possible in liquids. The main requirement for successful atomic-scale imaging is the ability to acquire images of surfaces with extremely low noise and defined conditions over extended periods of time. Key to success is the signal-to-noise ratio and the preparation of clean samples as well as sharp and well defined tips. Therefore, our current research focusses on the improvement these issues together with the development of new imaging modes [4].

Further Collaboration outside KIT in internal projects:

Dr. Dirk Meyners and Prof. Dr. Eckhard Quandt, Christian-Albrechts University of Kiel

Dr. Andreas Günther and Prof. Dr. József Fortágh, University of Tübingen

Dr. Daniel Ebeling and Prof. Dr. Santiago Solares, University of Maryland

Dr. Bernd Gotsmann, IBM Zürich

Prof. Dr. Udo D. Schwarz, Yale University

References

[1] H. Hölscher, “Atomic Force Microscopy and Spectroscopy”. In: *Dynamical Force Spectroscopy and Recognition (ed. by A. R. Bizzari and S. Cannistraro), Taylor & Francis, pp. 51-91 (2012)*

[2] Ali Tavassolizadeh, Tobias Meier, Karsten Rott, Günter Reiss, Eckhard Quandt, Hendrik Hölscher, and Dirk Meyners. Self-sensing atomic force microscopy cantilevers based on tunnel magnetoresistance sensors. *Applied Physics Letters **102**, 153104 (2013)*

[3] *Zhenhao Zhang, Michael Hetterich, Uli Lemmer, Michael Powalla, Hendrik Hölscher. Cross Sections of Operating Cu(In,Ga)Se2 Thin-film Solar Cells Under Defined White Light Illumination Analyzed by Kelvin Probe Force Microscopy*. *Applied Physics Letters **102**, 023903 (2013)*

[4] Hendrik Hölscher, Cold Atoms Feel the Force (News & Views article). *Nature Nanotechnology **7**, 484 (2012)*

X-ray Photoelectron Spectroscopy (XPS)

Michael Bruns (Surface Analysis Group)

X-ray photoelectron spectroscopy (XPS) is the most widely used surface analysis technique to provide both quantitative atomic concentration and chemical state information of the detected elements. X-ray irradiation of surfaces results in the emission of photoelectrons whose energies are characteristic of its constituting elements. The information depth is approximately 5–7 nm. Angle-resolved XPS offers non-destructive resolution of structures within the XPS sampling depth, e.g. layer ordering, composition and thickness can be determined. Moreover, XPS can be utilized for sputter depth profiling to characterize thin films and multilayer systems by quantifying matrix-level elements as a function of depth.

In 2012 the ESCA/Alpha 110 spectrometer was equipped with a new digital dual anode X-ray source (MgKα/AlKα) to improve angle resolved XPS regarding non-destructive depth profiles within the XPS sampling depth. In May 2013 a glove-box was attached to the K-Alpha XP spectrometer to allow for atmosphere-contact-free sample transport and load into the spectrometer.

The in-house research focuses on surface analytical characterization of (polymer)modified surfaces based on a number of cutting-edge projects within the Barner-Kowollik group, on energy storage materials in collaboration with the Pfleging, Ulrich, and Indris teams, and on sputtered barium strontium titanate thin films for tunable passive microwave applications in collaboration with the Binder group. In all cases XPS was used as one of the few characterization methods which give precise information of the molecular composition of the modified surfaces.

(Bio)molecular surface patterning by phototriggered oxime ligation

A very promising approach for (bio)molecular surface patterning is the photoinduced oxime ligation via shadow-mask techniques. Here a quantitative, low-energy photodeprotection generates aldehyde, which subsequently reacts with aminooxy moieties.

XPS is the method of choice to prove the successful silanization of silicon surfaces using a 2-[(4,5-dimethoxy-2-nitrobenzyl)oxy]tetrahydro-2H-pyranyl (NOTP)-functionalized silane (Figure 1). The N 1s spectrum of such surfaces in Figure 2a (bottom) shows clearly the expected NO_2 and NH components at 406.6 eV and 399.8 eV, respectively. The subsequent spatially controlled surface functionalization with O-((perfluorophenyl)methyl)hydroxylamine is substantiated by the drastically increased intensity of F 1s peak at 688.4 eV assigned to C-F groups (Figure. 2b), and is corroborated by the disappearance of the NO_2 peak after irradiation of the NOTP-silanized sample (Figure 2a, top). Thus, N 1s and F 1s spectra together prove the successful complete photodeprotection of the surface and the successful coupling. [1]

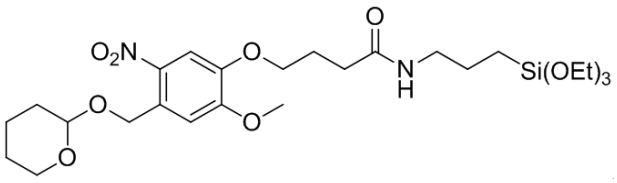

Fig. 1: NOTP-functionalized silane.

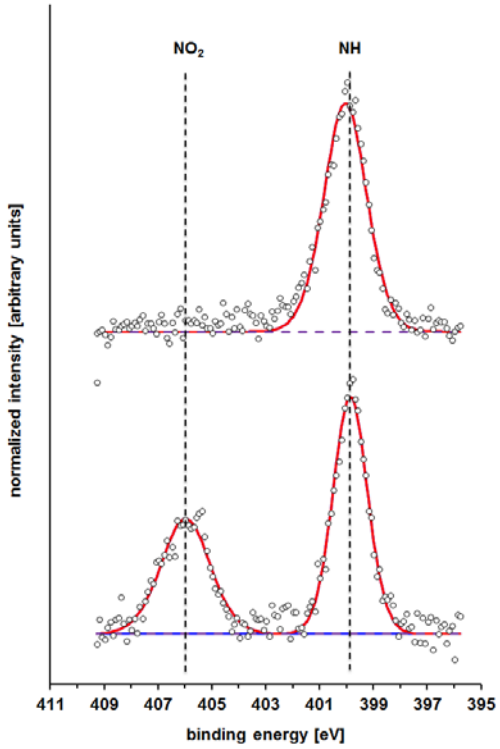

Fig 2a: Comparison of NO_2 and NH spectra of Si-substrates after NOTP silanization (bottom). The NO_2 moiety fully disappeared after irradiation (top). Peak heights have been normalized to maximum intensity.

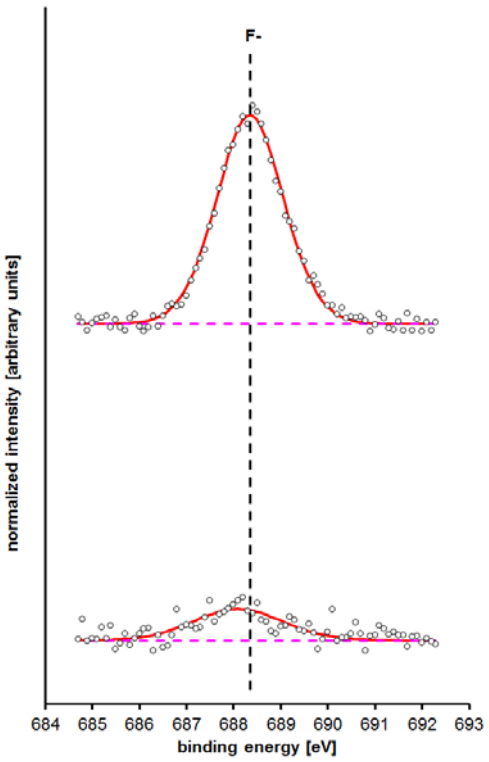

Fig 2b: Comparison of F 1s of Si-substrates after NOTP silanization (bottom) and after performing the photo-triggered oxime ligation strategy with O-((perfluorophenyl) methyl) hydroxylamine hydrochloride (top). Peak heights have been normalized to the N1s peak intensity of the NH component

Diode laser heat treatment of lithium manganese oxide films

Spinel lithium manganese oxide ($LiMn_2O_4$) is a promising candidate for lithium-ion batteries (LIB) using intercalation compounds as cathode materials and has the advantages of non-toxicity, cost-efficiency and a high operating voltage in the 4 V region. In the present study Li–Mn–O thin films were deposited on stainless steel substrates via R.F. magnetron sputtering under an argon atmosphere. In order to obtain well-crystallized electrochemical active cathode material, subsequent laser annealing had to be applied for t = 2000 s at a temperature of T = 600 ◦C.

The chemical composition of the surface before and after laser annealing of the sputtered films was investigated using XPS sputter depth profiling (Fig. 3a-c). Aside weak Carbon contamination at the topmost layers all profiles show a homogeneous in-depth distribution of the layer constituents. Li increases by a factor of 2 after annealing, which is an impressive result showing that diffusion kinetics take place at this temperature and Li^+ ions may diffuse to surface near regions and could cause bulk homogenization of the film elements. The XPS sputter depth profile of the SEI-like coating on top of the cycled Li–Mn–O surfaces prove an enrichment of lithium within the first 20 nm and fluorine within the first 5 nm, which is in a good agreement with former findings, while the carbon signal drops down just below the surface within the first 5 nm (Figure 2d). [2]

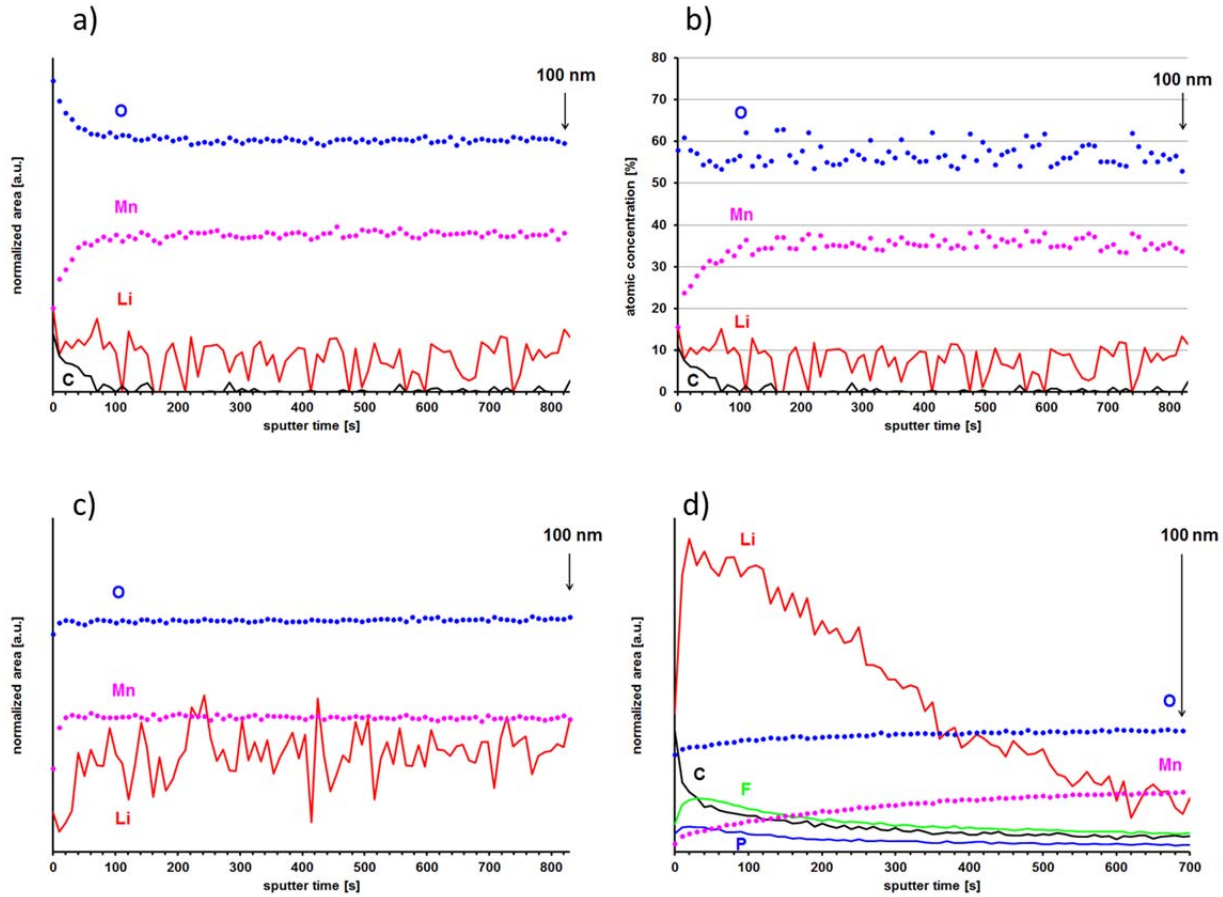

Fig. 3: XPS sputter depth profiles of a laser annealed Li–Mn–O film in the as prepared status (a, b), after subsequent laser annealing (c) and after electrochemically cycling (d). Due to the insufficient Li sensitivity atomic concentration profiles are very noisy (b) and, therefore, normalized area profiles are shown in a, c, d.

Fabrication and characterization of iron and fluorine co-doped BST thin films for microwave applications

Bariumstrontiumtitanate ($Ba_{1-x}Sr_xTiO_3$, BST) is a promising material for tunable passive microwave applications due to the wide range of the dielectric constant dependency on the electric field strength. This characteristic dielectric behaviour allows its use for phase shifters, filters, and matching networks. This contribution focuses on XPS characterization of novel iron and fluorine co-doped thin films prepared by means of r. f. magnetron Fe co-sputtering and a subsequent annealing step in fluorine atmosphere. In particular, XPS prove the achieved elemental composition in a non-destructive manner (cf. Figure 4) and, via sputter depth profiles (not shown), the homogeneous iron and fluorine dopant distribution throughout the films. The main components for Ba^{2+} (Ba $4d_{5/2}$ = 88.3 eV), Sr^{2+} (Sr $3d_{5/2}$ = 133.1 eV), Ti^{4+} (Ti $2p_{3/2}$ = 458.4 eV), and O^{2-} (O 1s = 529.7 eV) are attributed to Me-O bonds in bariumstrontiumtitanate and are in a good agreement with literature. The two Fe $2p_{3/2}$ components at 709.9 eV and 711.9 eV binding energy in the case of pure iron doped BST can be attributed to Fe^{2+} and Fe^{3+}, respectively. The 1 eV high energy shift of the iron binding energies gives evidence of a strong influence of the fluorine co-dopant on the iron acceptor dopant on the B-site of the perovskite structure. [3]

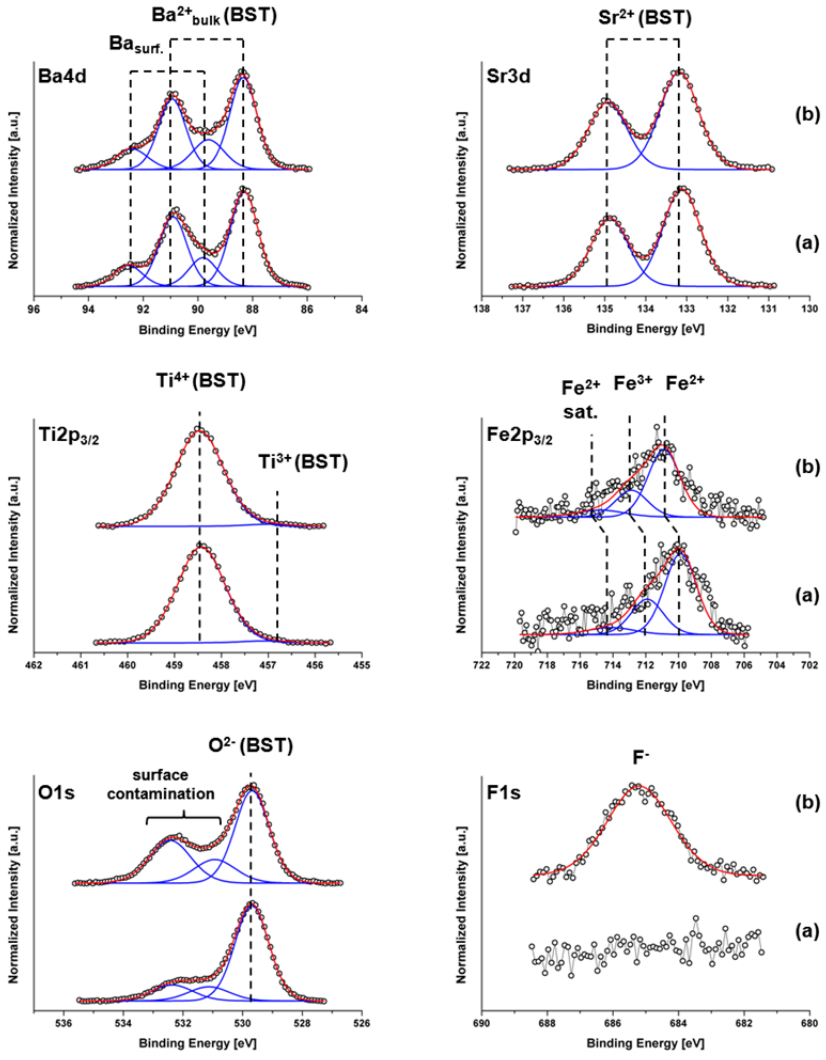

Fig. 4: Ba 4d, Sr 3d, Ti $2p_{3/2}$, Fe $2p_{3/2}$, O 1s, and F 1s XPS spectra of non-fluorinated (a) and fluorinated (b) iron

doped BST thin films. Spectra are normalized to maximum intensity.

Strategic Themes

For the *KNMF Call 11* we will open time-of-flight secondary ion mass spectrometry (ToF-SIMS) as new technology complementary to XPS. In the frame of strategic method development both XPS and ToF-SIMS together with TEM, FIB, HIM, LMP and DPN will represent a unique multi-method correlative processing and characterization lab, providing inert transfer between selected installations as well as correlative analysis using reference markers and optical guidance maps.

Subsidiary, we have scientific based collaborations with the Thermo Fisher Scientific Application Lab, East Grinstead, UK, [4] and since 2009 we are K-Alpha Demo-Lab for Thermo Fisher Scientific.

Further Collaboration outside KIT in internal projects:

B. Holländer, Peter Grünberg Institute (PGI-9), Forschungszentrum Jülich: Rutherford Backscattering Spectrometry (RBS)

F. Stemme, Institute for Energy and Climate Research (IEK-1), Forschungszentrum Jülich, PVD Coatings

References

[1] T. Pauloehrl, G. Delaittre, M. Bruns, M. Meißler, H. G. Börner, M Bastmeyer, and C. Barner-Kowollik, (Bio)Molecular Surface Patterning by Phototriggered Oxime Ligation, Angew. Chem. Int. Ed., 51 (2012) 9181 –9184.

[2] J. Pröll, R. Kohler, A. Mangang, S. Ulrich, M. Bruns, H.J. Seifert, W. Pfleging, Diode laser heat treatment of lithium manganese oxide films, Applied Surface Science 258 (2012) 5146– 5152.

[3] F. Stemme, M. Bruns, H. Geßwein, M. Schroeder, M. Sazegar, M. D. Drahus, R.-A. Eichel, F. Paul, C. Azucena, and J. R. Binder, Fabrication and characterization of iron and fluorine co-doped BST thin films for microwave applications, J. Mater. Sci. 48 (2013) 3586-3596.

[4] M. Bruns, C. Barth, P. Brüner, S. Engin, T. Grehl, C. Howell, P. Koelsch, P. Mack, P. Nagel, V. Trouillet, D. Wedlich, R. G. White, Structure and Chemical Composition of Mixed Benzylguanine and Methoxy Terminated SAMs for Immobilization of Biomolecules, Surf. Interface Anal. 44 (2012) 909–913.

Auger Electron Spectroscopy (AES)

Tobias Weingärtner, Thomas Bergfeldt

An Auger electron spectrometer (Physical Electronics 680 Auger Nanoprobe) is operated in KNMF by the analytical group of the Institute of Applied Materials - Applied Material Physics (IAM-AWP).

Design Parameters of our equipment

Auger electron spectroscopy (AES) provides information about composition and to some extends chemical state, within nanometer size of solid and vacuum stable, not insulating materials. In combination with Ar ion sputtering and Zalar rotation depth profiles to 1000 nm are available.

Semi-quantitative analysis of Li to U is possible by including sensitivity factors and quantitative analysis standards in the calculation. The practical detection limit ranges from 0.5 to 5 at%. The element distribution is shown by point and area analysis, linescans, depth profiles and element mappings. The practical lateral resolution begins at 24 nm and the depth resolution varies between 0.5 to 5 nm depending on the energy of the Auger electrons. The spot of the low energy ion gun has a size of about 0.5 mm. in situ fracture of samples with liquid N2 cooling can be used for grain boundary analysis.

In 2013 the instrument will be upgraded with a High Energy Resolution Optic (HERO) and a new SE-Detector. The HERO will improve the Auger-electron energy resolution from the AES. So for example it will be possible to differ between Al-metal and Al-oxide. The new SE-Detector will improve the sensitivity, the contrast and the S/N ratio of the SE image.

History of AES at KIT

Long before KNMF was founded, AES was involved in co-operations with internal (KIT) and external scientific as well as with industrial partners. From 2009 to mid-2011 external commercial customers order AES investigations in direct contact to IAM-AWP and since the 7th call (2011) via KNMF. “User access to the KNMF installation Auger electron spectroscopy“ means that we give advice about the best strategy of analytical investigation, and that we perform, summarize and evaluate the AES analysis and the results. Since the 4th call in 2010 the number of accepted standard proposals rises gradually but has not yet reached the number of commercial proposals.

Measurement possibilities overview

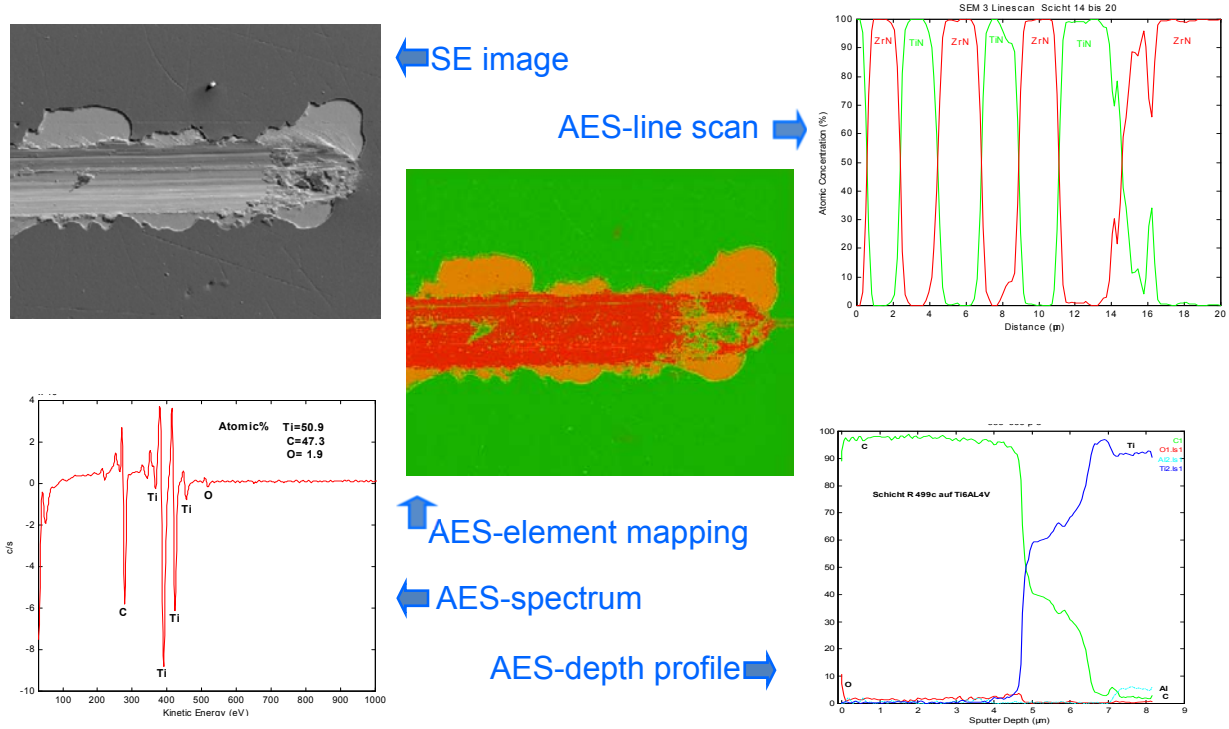

The Following examples point out the capability of the AES investigations.

Depth profile

At the department of “thin film technology” of IAM-AWP FeCoHfN/TiN (53/67 nm) multilayers for high frequency sensor applications are developed. Auger electron spectroscopy is the most suitable analytical tool to determine the elemental composition of the Nano layers and the interfaces. Figure 1 shows the depth profile of the first two double-layers and Figure 2 gives an overview of the multilayer.

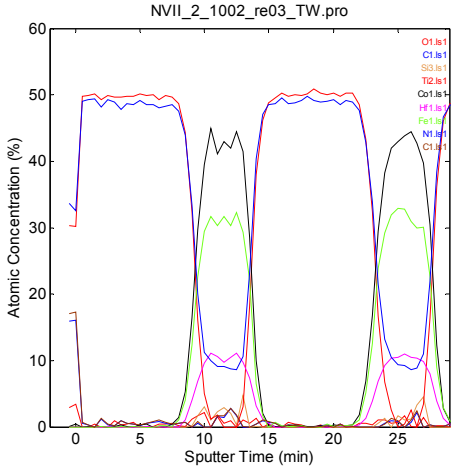

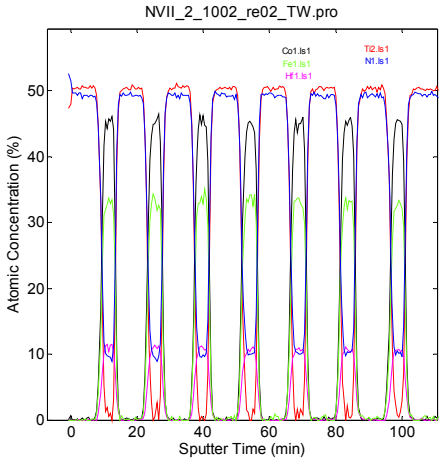

Fig. 1: FeCoHfN/TiN element profile, first two double layers Fig. 2: sequence of 15 layers

The FeCoHfN- and TiN-layers are detectable as separate layers.

Spectrum (semi quantitative analysis)

At the group “Thermophysics and Thermodynamics” of IAM-AWP the modeling of Phase diagrams of ternary systems is one part of interests. To proof theoretic modeled 3D phase diagrams it is necessary to determine the different phases in a material at specific points of the phase diagram. The following sample is a heat treated AlTiCr material. After the heat treatment it was cooled down fast and then it was polished for the analysis. In Figure 3 and 4 you can see the SE images and a spectrum of the specimen’s polished surface.

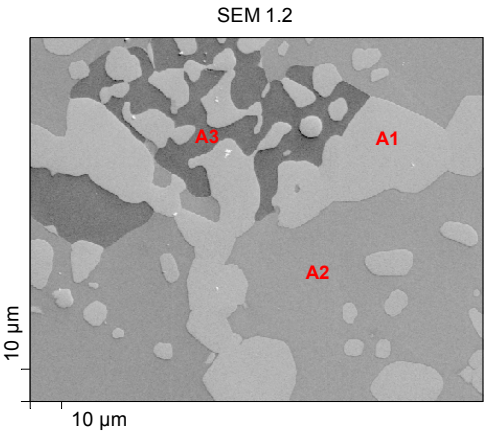

Fig. 3: SEM of a corroded area on steel

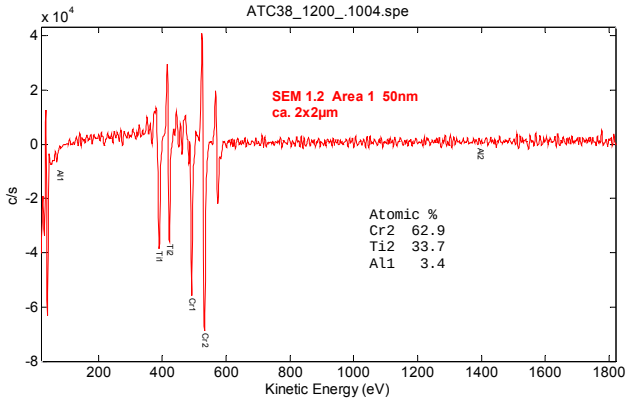

Fig. 4: RGB element mapping overlay

Element mapping at grain boundaries

One group at IAM-WPT is focused on the design and development of divertor-parts for future fusion power plants. Therefor tungsten with its physical properties is a very interesting material to be used for Plasma Facing Components. To determine the quality of the designed and machined tungsten components one of the methods which are used is to fracture a specimen in the ultra-high vacuum chamber of the AES. The fresh fracture surface can then be measured immediately without the influences of normal atmosphere. In the following pictures you can see a fracture surface of a tungsten specimen.

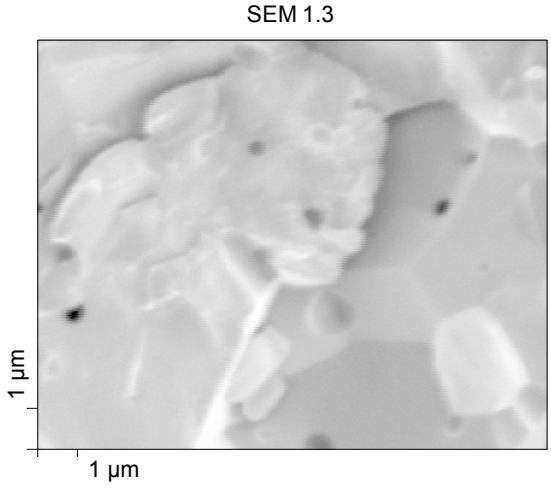

Fig. 5: SEM of a tungsten fracture surface

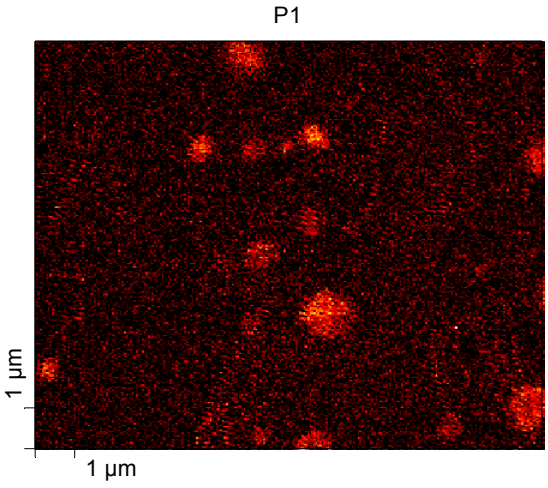

Fig. 6: P in pores of the fracture surface

References

[1] Antusch, S.; Müller, M.; Norajitra, P.; Pintsuk, G.; Piotter, V.; Ritzhaupt-Kleissl, H.; Weingärtner, T.; Two component tungsten powder injection moulding for mass production of the He-cooled DEMO divertor parts., *Fusion Sience and Technology, Vol. 62 July/Aug. 2012, 110-115*

[2] Krüger, K.; Seemann, K.; Leiste, H.; Stüber, M.; Ulrich, S.; High-frequency magnetoelastic measurements on Fe–Co–Hf–N/Ti–N multilayer coatings, *Journal of Magnetism and Magnetic Materials 343 (2013) 42–48*

[3] Lemberg, J.A.; Middlemas, M.R.; Weingärtner, T.; Gludovatz, B.; Cochran, J.K.; Ritchie, R.O., On the fracture toughness of fine-grained Mo-3Si-1B (wt.%) alloys at ambient to elevated (1300^0C) temperatures*, Intermetallics, 20(2012) S.141-154*

[4] Kriegel, M. J.; Pavlyuchkov, D.; Cupid, D. M.; Fabrichnaya, O.; Heger, D.; Rafaja, D.; Seifert, H.-J.; Phase equilibria at 1473 K in the ternary Al–Cr–Ti system, *Journal of Alloys and Compounds 550 (2013) 519–525*

Bulk and Trace Analysis (BTA)

Christel Adelhelm, Thomas Bergfeldt

For the chemical characterization of materials five different analytical instruments are operated for the KNMF by the analytical group of the Institute of Applied Materials - Applied Material Physics (IAM-AWP).

X-Ray Fluorescence Spectrometry, XRF (S4 Pioneer, Bruker-AXS) is a non-destructive method for quick qualitative and semi-quantitative analysis. In combination with reference materials it is also a precise quantitative element determination. In samples like powders, solids, paste, films and liquids with sizes of 10 to 50000 µm elements from F to U can be analyzed in the concentration range from ppm to 100 % depending on the atomic mass.

Atomic or Optical Emission Spectrometry by Inductively Coupled Plasma, ICP-AES or ICP-OES (OPTIMA 4300 DV, Perkin-Elmer) is widely used in inorganic analysis of aqueous solutions and metals, oxides, nitrides, carbides etc. dissolved by acids. Simultaneous measurement of all elements except noble gas, halogens, hydrogen, oxygen and nitrogen can be conducted. The element concentrations range from below 1 µg/g to 50 % in solids and < 0.001 to 100 mg/L in liquids. Reference or matrix matched standard solutions enable precise element determinations.

Mass Spectrometry by Inductively Coupled Plasma, ICP-MS (7500ce, Agilent) is the preferred analytical method for isotope and Ultra trace analysis of aqueous and acid solutions. The quadrupole mass spectrometer equipped with off-axis Omega lenses and an octopole Reaction System (ORS) to eliminate polyatomic interferences covers the mass range from 6 to 260 u, Li to U. Depending on sensitivity and number of isotopes the quantification limits vary from 1 ng/g to 1000 µg/g in dissolved solids or < 0,001 to 1000 µg/L in aqueous solutions.

Carrier Gas Heat Extraction, CGHE (TC600, LECO) is one of few reference methods to determine Oxygen and Nitrogen. Solid samples are heated in a graphite crucible in a metal bath up to 2600°C with He as carrier gas. Released CO and CO_2 are detected by IR and N_2 by thermal conductivity. The concentrations range from < 0.1 µg/g to 50 %.

In a **Carbon-Sulfur-Analyzer** (CS600, LECO) solid samples are combusted in a high frequency furnace under oxygen flow and the formed CO_2 and SO_2 are detected by IR-cells. C and S concentrations range from 5 µg/g to 100 %.

In 2012 a lot of different research issues for KNMF and the HGF programme STN had taken place. One important task was the investigation of different Nano powders such as SiO_2, ZnO, CeO_2, TiO_2, PS etc. in regard to impurities. New methods for the chemical digestion had to be found and it was a great challenge handling the different matrices with high concentration of one element to get very low quantification limits (< 0,01 µg/g – 20 µg/g) for more than sixty elements with the ICP-MS and ICP-OES.

One other topic was the stoichiometric analysis of different powders with ICP-OES and CGHE for the development of new battery materials. For this purpose a new method has been established in our lab for the analysis of fluoride with an Ion selective electrode (ISE). Providing the material is soluble, it is now possible to analyze the fluoride content with even less sample material.

A new aim in the future (2013) will be the chemical analysis of different electrolytes which are used in batteries. In this context the usually very small quantity of solution for analysis in small batteries will be difficult to handle.

Further Collaboration outside KIT in internal projects / Collaboration in in-house research

The Bulk and Trace Analysis group is not only part of KNMF. There are many other activities and co-operations with other research groups in the KIT and abroad. The following will give a short overview about topics and co-operations in 2012.

HGF program Fusion:
Determination of main compounds and impurities in ceramic breeding blanket
Chemical analysis of ODS alloys
Impurities in PbLi in the liquid metal corrosion loop PICOLLO

HGF program Nuclear:
Chemical analysis of SiC

HGF program REUN and EE:
Determination of elements from filters deposits of an experiment by REGA (Research Entrained-flow GAsifier). This is part of a Humboldt stipendium research in the institute of ITC
Chemical analysis of raw material for Celitement a new hydraulic binder. Celitement is a foundation of the Schwenk group, Karlsruhe Institute of Technology (KIT), and scientists of KIT

Co-operation with other institutes in KIT:
Chemical analysis of material from a catalytic converter (ITCP)
Stoichiometric of Ti and Au in TiO_2 and Au Nano particles in buffer solution (DFG-Centre for Functional Nanostructures).

Project with BMU:
Chemical analysis of Ba in different solutions from test stations by the institute of IKET (KIT). This is part of the project “Scaling and outgassing in geothermal sites – influence factors, kinetic, inhibitors and technical actions”

References

[1] Fischer, J.; Adelhelm, C.; Bergfeldt, T.; Chang, K.; Ziebert, C.; Leiste, H.; Stüber, M.; Ulrich, S.; Music, D.; Hallstedt, B.; Seifert, H.J. Development of thin film cathodes for lithium-ion batteries in the material system Li-Mn-O by r.f. magnetron sputtering. *39th Inernat.Conf.on Metallurgical Coatings and Thin Films (ICMCTF 2012), San Diego, Calif., April 23-27, 2012*

[2] Issac, I.; Heinzmann, R.; Becker, S.M.; Bräunigner, T.; Zhao-Karger, Z.; Adelhelm, C.; Chakravadhanula, V.S.K.; Kübel, C.; Ulrich, A.S.; Indris, S**.** Synthesis of nanocrystalline solid solutions AlySn1-yO2-y/2 (y = 0.57, 0.4) investigated by XRD, 27Al/119Sn MAS NMR, and Mössbauer spectroscopy. *RSC Advances, 2(2012) S.10700-10707*

[3] Klix, A.; Adelhelm, Ch.; Fischer, U.; Gehre, D.; Kaiser, T. Determination of the 6Li content in the LiPb of a neutronics mock-up of the European HCLL TBM. *Fusion Science and Technology, 62(2012) S.196-203*

[4] Canic, T.; Baur, S.; Adelhelm, C.; Seibt, A.; Müller, K. Geschwindigkeit von Barytausfällungen aus Geothermalwasser - Einfluss der Scherung. *Geothermische Energie, 73(2012) S.28-31*

Thin Film Characterisation (TFC) Methods

Harald Leiste, Klaus Seemann, Kathrin Krüger

For thin film characterisation different measurement setups are operated within KNMF at the Institute for Applied Materials (IAM-AWP). The composition, structure, properties and behaviour of thin films can be measured. The focus of characterisation is on the microstructure (by XRD and Raman spectroscopy), the mechanical and the magnetic property.

The in-house research aims at the process improvement and optimization of the characterisation methods, *i.e.*, to establish new possibilities for the measurement of the ferromagnetic properties of soft magnetic materials. The following R&D activities have been performed in 2012.

High frequency permeameter

In order to determine the frequency dependent complex permeability of ferromagnetic thin films, a short-circuited strip-line is used as a measuring head. The strip-line is adjusted to a characteristic impedance of 50 Ω and permits a frequency measurement range from 50MHz up to 5GHz. It is connected to a vector network analyser in a one-port measurement arrangement. The complex permeability can be analytically calculated from the reflection coefficient S_{11}. The schematic setup is shown in Figure 1. A typical frequency-dependent permeability of a Fe-Co-Hf-N thin film with its real and imaginary part is presented in Figure 2. It shows the ferromagnetic resonance at around 2.4 GHz. The solid lines represent the Landau-Lifshitz-Gilbert theory.

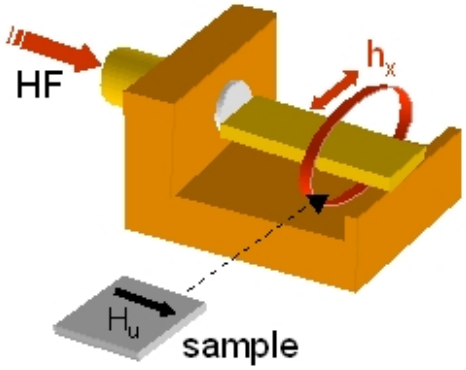

Fig. 1: 5 GHz strip-line permeameter (Z_0= 50 Ω) connected to a network analyser

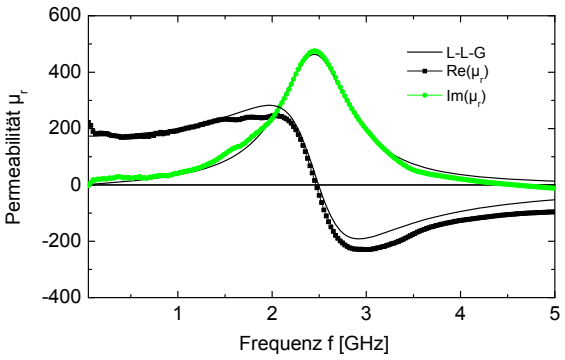

Fig. 2: Frequency-dependent permeability of a FeCoHfN thin film and comparison with LLG

For the characterisation of the influence of additional mechanical load on the magnetoelastic properties of thin ferromagnetic films a comparable strip-line setup was designed and built for sample bending and tensile tests (Figure 3). As substrates for the thin film deposition borosilicate glass or silicon wafers (dimensions 5 mm x 45 mm) can be used with a coated area of 5 mm x 5 mm. After the film deposition the samples were post annealed at 400°C – 600°C in a static magnetic field of 50mT to induce a uniaxial anisotropy. Due to substrate bending, the film is strained which causes variations in the resonance frequency by changing the magnetoelastic anisotropy field. Correlated with the sign of the applied stress it results in

a decrease (tensile stress) or increase (compressive stress) of the resonance frequency values. The used films show a resolution of the applied stress of at least 1.5 MPa.

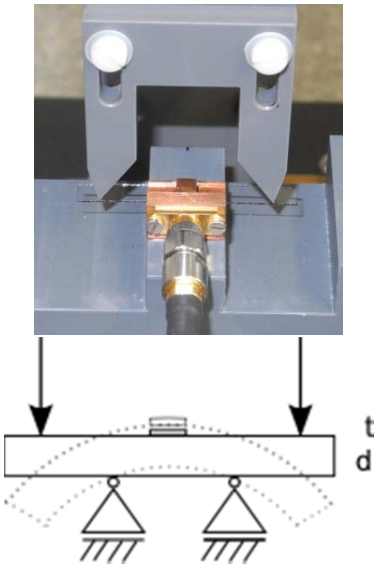

Fig. 3: Scheme and experimental setup for magnetoelastic measurements

Fig. 4: Frequency dependent real part of scattering parameter S_{11} of a multilayer film consisting of 7 layers of FeCoHfN and TiN . Above: tensile, Below: compressive stress

Strategic Themes

The main competence of the TFC in KNMF is the characterisation of the constitution and properties thin films. KNMF offers different X-ray diffraction methods (Bragg-Brentano, Rocking, Texture, x-ray-reflection or reciprocal space mapping) to determine the crystal structure and growth behaviour, the Raman Spectroscopy for the chemical bonding state and microstructure with different excitation wavelength, as well as the characterisation of mechanical properties (hardness and adhesion, by nano- and microindentation). It also offers ferromagnetic characterisation techniques for measuring the magnetisation and coercive field strength and for measuring the high frequency permeability.

Further Collaboration outside KIT in Internal Projects:

Universities of: Bochum, Kiel, Kaiserslautern, Aachen, Uppsala (Sweden), Linköping (Sweden), Coimbra (Portugal)

Companies: Walter, Gühring, Balzers, Rockwell Collins

Research Centers: FHG-IMW Freiburg, KIST (Korea), AIN Pamplona (Spain)

References

[1] K. Krüger, K. Seemann, H. Leiste, M. Stüber, S. Ulrich “High-frequency magnetoelastic measurements on Fe-Co-Hf-N/TiN multilayer coatings“, Journal of Magnetism and Magnetic Materials 343 (2013) 42–48

[2] K. Seemann, H. Leiste, K. Krüger „On the comparison of the polarization behavior of exchange-biased AF/F NiMn/Fe37Co48Hf15 bi-layer and multi-layer films with increased ferromagnetic cut-off frequencies”, Journal of Magnetism and Magnetic Materials 324 (2012) 1165–1171

KNMF Laboratory for Synchrotron Characterisation

The national German synchrotron radiation facility ANKA at KIT is engaged in the KNMF activities of its Laboratory for Synchrotron Characterisation. Within these labs, ANKA's beamlines provide dedicated user service for the Nanoscience and Microtechnology user communities. It provides the exceptional possibility of combining well-known micro/nano fabrication and characterisation methods with synchrotron-based methods at a single site. The combination of the complementary characterisation techniques allows to obtain a more comprehensive picture of the materials structure and properties. The synergistic overlap between the two Helmholtz Research Infrastructures – ANKA and KNMF - is a strong and unique benefit to the MNT user community. The beamtime is accessible via the portals for scientific proposal of both ANKA and the KNMF, and is based on a peer-review process. In 2012, 16 % of the available synchrotron beamtime distributed by the proposal review committee was assigned to the field of Nanoscience and Microtechnology.

Soft X-ray Spectroscopy, Microscopy, and Spectromicroscopy (WERA)

P. Nagel, M. Merz, D. Fuchs, Th. Wolf, A. Assmann, S. Uebe, H. v. Löhneysen, and S. Schuppler

Karlsruhe Institute of Technology (KIT), Institut für Festkörperphysik (IFP)

The Institute for Solid-State Physics (IFP), KIT, owns and operates the soft x-ray facility WERA at the Karlsruhe synchrotron radiation source ANKA. WERA is designed for facilitating combinatory studies of the electronic and magnetic structure and microstructure, which have particular promise for strongly correlated, thin-film, and nanoscale materials. This is both at the heart of IFP's own activities within the HGF Programme "Science and Technology of Nanosystems" (STN) and those of the external user communities, which can access WERA via peer review through the ANKA and KNMF portals and also through the EU programme Qualitynano.

The soft x-ray analytics facility WERA takes a fully combinatory and integrative approach to studying the microscopic electronic and magnetic structure – (i) by coherently combining important electron spectroscopies (PES, NEXAFS, XMCD; all in a number of variants; XMCD is supplied through a long-term cooperation with the MPI-IS Stuttgart) mutually and also with laterally resolved spectromicroscopy in PEEM (μ-NEXAFS, μ-PES, μ-XMCD); (ii) by organically tying in quasi-*in-situ* sample synthesis in currently 4 preparation chambers, all dedicated to specific techniques including pulsed-laser deposition (PLD), and with UHV sample transfer between endstations and chambers; and (iii) also by combining radiation sources: bending magnet for more "standard" experiments and covering the full photon-energy range 100 – 1500 eV; undulator for experiments demanding considerably enhanced sensitivity (higher photon flux / flux density) and ultimately also with full polarization control. The resulting cluster of methods and possibilities is unique, and users increasingly appreciate the further insights that this approach and these combinations offer for their experiments.

Within the general thrust of IFP's activities in STN to understand strong electron-electron correlations and related phenomena in condensed matter, current in-house research at WERA concentrates on 3*d* transition-metal (TM) compounds where electron correlation competes with other interactions on similar energy scales to create phases with novel

properties, and on iron-based pnictides whose superconducting properties have posed important challenges in condensed-matter physics as well. The element-specific electronic and magnetic structure of many of these materials has been studied by performing electron spectroscopies like NEXAFS, PES, and XMCD and spectromicroscopy (PEEM), and also taking full advantage of IFP's successful sample synthesis program (single crystals as well as epitaxial thin films – the latter giving the opportunity to apply tunable epitaxial strain) and additional characterization. In the following, we briefly touch upon a selection of recent results.

Cobaltates are a prime example for the near-equivalency of several energy scales in some TM oxides: the values for crystal field and Hund's exchange energy are so similar that tipping the balance in one or the other direction – in the present work by applying epitaxial strain – allows one to actively realize different spin states of the Co ion. The spin-state structure of the undoped but strained "(113)" cobaltate $LaCoO_3$ as found in XMCD and NEXAFS at the Co $L_{2,3}$ and the O K edge shows that configuration-fluctuation superexchange between Co^{3+} high-spin (HS) and low-spin (LS) states is responsible for the strain-enabled ferromagnetism in this compound. No evidence for the often-discussed intermediate-spin (IS) state was found. In addition, epitaxial strain allows electron doping in significant levels. For electron-doped $La_{0.7}Ce_{0.3}CoO_3$, the Co^{3+} ions are in an LS state and the spin and orbital moments are predominantly determined by Co^{2+} HS. A spin blockade between these neighboring configurations naturally explains the low transition temperature and the insulating characteristics of $La_{0.7}Ce_{0.3}CoO_3$ [1].

A related evolution of interaction with doping, yet with its own distinct "twist", could be unraveled in the single-layered "(214)" cobaltates of the family $La_{2-x}Ca_xCoO_4$ (x = 0, 0.5, 1, and 1.5): Co L-edge and O K-edge NEXAFS shows that starting from x = 0, superexchange between neighboring Co^{2+} HS states is responsible for the strong antiferromagnetism, but that for x = 0.5, the Co^{3+} LS content is already so high as to form a checkerboard arrangement with the remaining Co^{2+} HS – an arrangement that results in a spin blockade and directly leads to the high resistivity and the low Néel temperature observed. For x = 1, the Co^{2+} component is gone and a mixture of Co^{3+} LS and HS occurs. Superexchange via configuration fluctuation seems to induce long-range ferromagnetism while the superexchange between adjacent Co^{3+} HS neighbors may lead to a competing antiferromagnetic exchange. For x > 1, Co^{4+} HS is introduced to the system at the expense of Co^{3+} LS, and t_{2g} double exchange between Co^{3+} and Co^{4+} HS further enhances ferromagnetism and reduces resistivity [2].

Epitaxial strain was also used to tune the electronic and magnetic structure of thin $Sr_{0.7}Ca_{0.3}RuO_3$ films. Despite great fundamental difficulties in this type of 4d TM system, it was possible to gain direct spectroscopic evidence in O K and Ru M XMCD for a strain-dependent Jahn-Teller distortion in these films. In turn, this also showcases the very high quality of XMCD possible at WERA.

For the novel iron-based pnictide superconductors, it turns out in our experiments that they exhibit a highly peculiar "doping" behavior. Starting with partial substitution of Fe by Co in $Sr(Fe_{1-x}Co_x)_2As_2$ (x = 0 – 0.38) and studying valence and spin state with NEXAFS at the $L_{2,3}$ edges of Fe, Co, and As, we find effectively isovalent substitution of Fe^{2+} by Co^{2+}, which is in contrast to the widely assumed Co-induced electron-doping effect [3]. Theoretical work by Sawatzky and others[1] indicates that the extra positive charge of the Co "impurity" may be screened by all d electrons on such a short length scale that Co may appear isovalent to Fe.

User projects performed at WERA cover a large variety of interesting subjects and range, for instance, from a study of extraterrestrial nanodiamonds [4] in PEEM to organic solar-cell materials [5] in PES and NEXAFS, as well as to XMCD studies such as one on the magnetic proximity effect (MPE) in superlattices composed of superconducting $YBa_2Cu_3O_7$ and ferromagnetic (113) manganites [6]. In all cases, the overlap and interaction between WERA

[1] H. Wadati *et al*., Phys. Rev. Lett. **105**, 157004 (2010); T. Berlijn *et al*., Phys. Rev. Lett. **108**, 207003 (2012).

and the user groups has been mutually beneficial and fruitful, and the sheer range of systems and effects in fundamental and applied condensed-matter physics covered illustrates well the wide applicability of WERA's portfolio of methods and capabilities.

Most fruitful has been the cooperation with the Max-Planck Institute for Intelligent Systems (MPI-IS) Stuttgart (Prof. G. Schütz, PD E. Goering) – the excellent XMCD setup at WERA is theirs. Very importantly, they have recently upgraded it with a fast-ramp 7 T magnet, making the setup almost peerless worldwide. We are grateful to everyone involved for this truly exciting "advancement of science".

[1] M. Merz et al., Phys. Rev. B **82**, 174416 (2010).

[2] M. Merz et al., Phys. Rev. B **84**, 014436 (2011).

[3] M. Merz et al., Phys. Rev. B **86**, 104503 (2012).

[4] A. Shiryaev et al., Geochim Cosmochim Acta **75**, 3155 (2011).

[5] H. Hintz et al., Chem. Phys. Chem. **11**, 269 (2010).

[6] D. K. Satapathy et al., Phys. Rev. Lett. **108**, 197201 (2012); R. Werner et al., Phys. Rev. B **82**, 224509 (2010).

IR1, PDIFF, and XAS Beamlines:
Infrared/THz Spectroscopy and Ellipsometry (IR/THz)
Polycrystalline/Powder Diffraction (PDIFF)
X-ray Absorption Spectroscopy (XAS)

T. Baumbach, S. Doyle, B. Gasharova, M. Hagelstein, J. Heinrich, C. Heske, B. Krause, S. Mangold, Y.-L. Mathis, D. Moss, and A.-S. Müller

In the summer of 2012, three additional ANKA beamlines became accessible via the KNMF proposal portal. These beamlines focus on Infrared/THz spectroscopy and ellipsometry (IR1 beamline), polycrystalline/powder X-ray diffraction (PDIFF beamline), and X-ray absorption spectroscopy (XAS beamline).

The IR1 beamline features classical synchrotron radiation and edge radiation from a bending magnet and offers infrared/THz spectroscopy and ellipsometry. The spectroscopy station is based on an FTIR spectrophotometer (Bruker IFS 66v/S), covering a spectral range from 4 to 10,000 cm^{-1} with a resolution down to 0.1 cm^{-1}, and is equipped with high sensitivity detectors and appropriate beamsplitters. The ellipsometry set-up at IR1 is operated by MPI-FKF Stuttgart and the University of Fribourg, Switzerland, runs under vacuum, and features an optimized bolometer detector and a liquid He cryostat. Coherent THz emission can be exploited when the ANKA accelerator is operated in low-α mode, resulting in an extremely intense beam in the 5 – 50 cm^{-1} spectral range. In 2013, the IR2 beamline will see a completion of its front-end optimization and commissioning phase. It is envisioned to offer IR microscopy capabilities at IR2 as part of the KNMF Laboratory for Synchrotron Radiation in 2014.

The XAS-beamline features X-ray absorption spectroscopy (XAS) on a dipole magnet source. Besides standard XAS measured in transmission (detection limit ~5%) and fluorescence (detection limit 1 mmol/L) modes, the beamline offers a “Quick XAS” mode, allowing scans as fast as 30 seconds. Grazing incidence XAS provides surface sensitivity in the 50 nm range. The XAS beamline spans the energy range from 2.4 to 27 keV, covering the K-edges from S to Cd, and up to the L-edge of U. Upgrades performed in 2012 focused on enhanced automation and faster data acquisition. Further ongoing upgrades will allow the use of heavier and larger experimental set-ups.

The PDIFF beamline allows hard X-ray diffraction investigations of bulk polycrystalline materials under varying *in-situ* conditions and for high-resolution powder diffraction, residual-stress, and texture measurements. It is also equipped to perform scattering studies on thin-films and epitaxial layers, and consists of two experimental stations, a heavy-duty 3-circle powder diffractometer and a 4-circle Kappa diffractometer carrying up to approx. 5 kg loads. The major upgrade efforts focus on the facilities for *in-situ* experiments on the heavy-duty powder diffractometer, including an implementation of an XYZ-stage for the positioning of various sample chambers and construction of a motorized linear stage for the large CCD detector, as well as the development of macros for automated measurements.

As an example of research conducted within the framework of the KNMF Laboratory for Synchrotron Radiation (in combination with other KNMF facilities), we report on a study of a class of complex materials used as hard coating materials. This class is based on transition-metal carbides and nitrides and is used, e.g., as protective layers for cutting tools. For the design of new coatings, controlling the phase and texture formation is essential. In the case

of multi-element materials, this is not trivial and influences strongly the mechanical properties of the coating. With measurements at the PDIFF and XAS beamlines, combined with XPS measurements, we were able to identify the composition-dependent phases of V-Al-C-N [Krause et al., J. Appl. Cryst. (2013), in print]. The structure formation of V-C was furthermore monitored *in-situ* by XRD [Fig. 1; Krause et al., J. Synchr. Rad. 19 (2012) 216]. In combination with AFM, TEM, and nano-indentation measurements, these results will help to understand the interplay between structure formation and coating properties of complex hard coating materials.

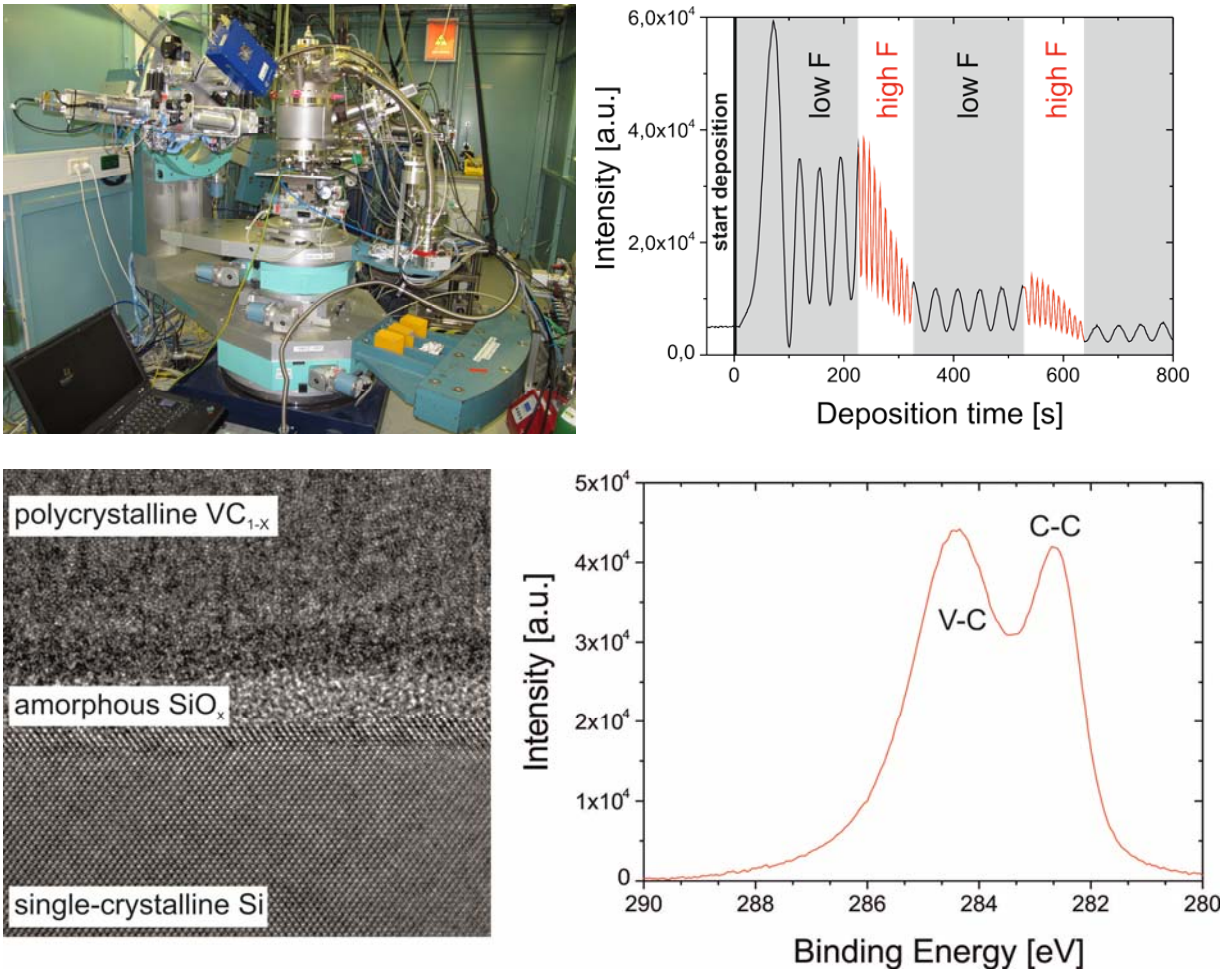

Fig. 1: Top left: Experimental setup for *in-situ* sputter deposition. Top right: *In-situ* X-ray reflectivity measurements of VC as a function of deposition rate F. The power applied to the sputter target was varied periodically, resulting in a periodic change of the deposition rate. Bottom left: TEM cross section, and, bottom right, C 1s XPS spectrum of a polycrystalline VC_{1-x} film on a single-crystalline Si substrate with an amorphous SiO_x interlayer.

Publication List

The following list gives details of publications which have resulted from KNMF user projects.

(published in 2012, reported to KNMF by 1st October 2013)

Citation	Published in	Impact Factor
J. Biener, S. Dasgupta, L Shao, D. Wang, M. Worsley, A. Wittstock, J.R. Lee, M. Biener, C. Orme, S.O. Kucheyev, B.C. Wood, T.M. Willey, A.V. Hamza, J. Weissmüller, H. Hahn, T. Baumann: Macroscopic 3D Nanographene with Dynamically Tunable Bulk Properties	Adv. Mat.	13.877
T. Pauloehrl, G. Delaittre, M. Bruns, M. Meißler, H. G. Börner, M Bastmeyer, and C. Barner-Kowollik: (Bio)Molecular Surface Patterning by Phototriggered Oxime Ligation	Angew. Chem. Int. Ed.	13.455
J. X. Fang, U. Vainio, W. Puff, R. Würschum, X. L. Wang, D. Wang, M. Ghafari, F. Jiang, J. Sun, H. Hahn, H. Gleiter: Atomic Structure and Structural Stability of Sc75Fe25 Nanoglasses	Nano Lett	13.198
M. Mastronardi, F. Maier-Flaig, D. Faulkner, E. Henderson, C. Kübel, U. Lemmer, G.A. Ozin : Size-Dependent Absolute Quantum Yields for Size-Separated Colloidally-Stable Silicon Nanocrystals	Nano Lett	12.219
M.A. Reddy, B. Breitung, V.S.K. Chakravadhanula, C. Wall, M. Engel, C. Kübel, A.K. Powell, H. Hahn, M. Fichtner: CFx Derived Carbon-FeF2 Nanocomposites for Reversible Lithium Storage	Adv. Energy Mater.	10.043
I. Zanette, M. Bech, A. Rack, G. Le Duc, P. Tafforeau, C. David, J. Mohr, F. Pfeiffer, and T. Weitkamp: Trimodal low-dose X-ray tomography	PNAS	9.681
Arne Tapfer, Martin Bech, Astrid Velroyen, Jan Meiser, Jürgen Mohr, Marco Walter, Joachim Schulz, Bart Pauwels, Peter Bruyndonckx, Xuan Liu, Alexander Sasov, and Franz Pfeiffer: Experimental results from a preclinical X-ray phase-contrast CT scanner	PNAS	9.681
M. Guan, W. Wang, E.J. Henderson, Ö. Dag, C. Kübel, I.L. Moudrakovski, J. Thomson, J. McDowell, H. Zhang, G.A. Ozin : Photoluminescent Nanocrystal-Silicon-Embedded Periodic Mesoporous Organosilica	J. Am. Chem. Soc.	9.023
F. Hübler, M.J. Wolf, T. Scherer, D. Wang, D. Beckmann, H.v.Löhneysen: Observation of Andreev Bound States at Spin-active Interfaces	Phys. Rev. Lett.	7.370
Sekula-Neuner, Sylwia; Maier, Jana; Oppong, Emmanuel: Cato, Andrew C. B.; Hirtz, Michael; Fuchs, Harald: Allergen Arrays for Antibody Screening and Immune Cell Activation Profiling Generated by Parallel Lipid Dip-Pen Nanolithography	Small	7.336
Oberhansl, Sabine; Hirtz, Michael; Lagunas, Anna; Eritja, Ramon; Martinez, Elena; Fuchs, Harald; Samitier, Josep: Facile Modification of Silica Substrates Provides a Platform for Direct-Writing Surface Click Chemistry	Small	7.336
S. Ren, R. Prakash, D. Wang, V.S.K. Chakravadhanula, M. Fichtner: Fe3O4-anchored helical carbon nanofibers as high performance anode in lithium ion batteries	ChemSusChem	6.827
D. Hudry, C. Apostolidis, T. Gouder, E. Courtois, C. Kübel, O. Walter: Non-Hydrolytic Synthesis of Isotropic and Anisotropic Actinide Oxides Nanocrystals	Chem. Eur. J.	5.925
Kim, C.; Kreppenhofer, K.; Kashef, J.; Gradl, D.; Herrmann, D.; Schneider, M.; Ahrens, A.; Guber, A.; Wedlich; D.: Diffusion- and convection-based activation of a Wnt/ß-catenin signaling in a gradient generating microfludic chip	Lab on a Chip	5.670

Citation	Published in	Impact Factor
G. Delaittre, M. Dietrich, J. P. Blinco, A. Hirschbiel, M. Bruns, L. Barner and C. Barner-Kowollik: Photo-Induced Macromolecular Functionalization of Cellulose via Nitroxide Spin Trapping	Biomacromolecules	5.479
N. Zydziak, C. Hübner, M. Bruns, A. P. Vogt, C. Barner-Kowollik: Modular Ambient Temperature Functionalization of Carbon Nanotubes with Stimuli-Responsive Polymer Strands	Polymer Chemistry	5.321
Tobias Jochum, Manuela E. Ritz, Christoph Schuster, Sarah F. Funderburk, Katja Jehle, Katja Schmitz, Falko Brinkmann, Michael Hirtz, David Moss, Andrew C.B. Cato: Toxic and non-toxic aggregates from the SBMA and normal forms of androgen receptor have distinct oligomeric structures	Biochimica et Biophysica Acta (BBA) - Molecular Basis of Disease	5.211
V. Šepelák, S.M. Becker, I. Bergmann, S. Indris, M. Scheuermann, A. Feldhoff, C. Kübel, H.M. Bruns, N. Stürzl, P.J. Sideris, M. Kappes, A.S. Ulrich, M. Ghafari, H. Hahn, C.P. Grey, K.D. Becker, P. Heitjans: Non-equilibrium structure of Zn2SnO4 spinel nanoparticles	J. Mat. Chem	5.101
N. Boucharat, D. Wang, E.G. Bardaji, M. Fichtner, W. Lohstroh : Effect of a Ti-Based Additive on the Desorption in Isotope-Labeled LiB(H,D)(4)-Mg(H,D)(2) Nanocomposites	J Phys Chem. C	4.805
Anne Neumeister, Daniel Bartke, Niko Bärsch, Tobias Weingärtner, Laure Guetaz, Alexandre Montani, Giuseppe Compagnini, and Stephan Barcikowski: Interface of Nanoparticle-Coated Electropolished Stents	Langmuir	4.186
Carlos Azucena, Fabian J. Eber, Vanessa Trouillet, Michael Hirtz, Stefan Heissler, Matthias Franzreb, Harald Fuchs, Christina Wege, and Hartmut Gliemann: New Approaches for Bottom-Up Assembly of Tobacco Mosaic Virus-Derived Nucleoprotein Tubes on Defined Patterns on Silica- and Polymer-Based Substrates	Langmuir	4.186
Venkata Sai Kiran Chakravadhanula, Christian Kübel, Tomislav Hrkac, Vladimir Zaporojtchenko, Thomas Strunskus, Franz Faupel and Lorenz Kienle: Surface segregation in TiO2-based nanocomposite thin films	Nanotechnology	3.979
Mitsakakis, Konstantinos; Sekula-Neuner, Sylwia; Lenhert, Steven; Fuchs, Harald; Gizeli, Electra: Convergence of Dip-Pen Nanolithography and acoustic biosensors towards a rapid-analysis multi-sample microsystem.	The Analyst	3.913
H. Soeriyadi, V. Trouillet, F. Bennet, M. Bruns, M. R. Whittaker,C. Boyer, P. J. Barker, T. P. Davis, and C. Barner-Kowollik: A Detailed Surface Analytical Study of Degradation Processes in (Meth)Acrylic Polymers	Journal of Polymer Science Part A: Polymer Chemistry	3.894
A.M. Hartel, S. Gutsch, D. Hiller, C. Kübel, N. Zakharov, P. Werner, and M. Zacharias: Silicon Nanocrystals prepared by PECVD: Importance of parasitic oxidation for third generation photovoltaic applications	Appl. Phys. Lett.	3.844
M. Pouryazdan, D. Schwen, D. Wang, T. Scherer, H. Hahn, R. S. Averback, P. Bellon: Forced chemical mixing of the immiscible Ag-Cu hetero-interfaces using high pressure torsion	Phys. Rev. B	3.691
Pfeifle, J.; Alloatti, L.; Freude, W.; Leuthold, J.; Koos, C.: Silicon-organic hybrid phase shifter based on a slot waveguide with a liquid-crystal cladding	Optics Express	3.587
Christian Kluge, Michael Rädler, Arfat Pradana, Matthias Bremer, Peter-Jürgen Jakobs, Nicole Barié, Markus Guttmann, Martina Gerken: Extraction of guided modes from organic emission layers by compound binary gratings	Optics Letters	3.399

Citation	Published in	Impact Factor
G. Potdevin, A. Malecki, Th. Biernath, M. Bech, T. H. Jensen, R. Feidenhans'l, I. Zanette, T. Weitkamp, J. Kenntner, J. Mohr, P. Roschger, M. Kerschnitzki, W. Wagermaier, K. Klaushofer, P. Fratzl and F. Pfeiffer: X-ray vector radiography for bone micro-architecture diagnostics	Physics in Medicine and Biology	3.057
H.T. Beyene, V.S.K. Chakravadhanula, C. Hanisch, T. Strunskus, V. Zaporojtchenko, M. Elbahri, F. Faupel: Vapor phase deposition, structure, and plasmonic properties of polymer-based composites containing Ag-Cu bimetallic nanoparticles	Plasmonics	2.989
S.R. Yeduru, A. Backen, C. Kübel, D. Wang, T. Scherer, S. Fähler, L. Schultz, M. Kohl: Microstructure of free-standing epitaxial Ni-Mn-Ga films before and after variant reorientation	Scripta Materialia	2.820
Devin E. Burns, Yong Zhang, Michael Teutsch, Klaus Bade, Jarir Aktaa and Kevin J. Hemker: Development of Ni-based superalloys for microelectromechanical systems	Scripta Materialia	2.699
Dieter Hahn, Pierre Thibault, Martin Bech, Marco Stockmar, Simone Schleede, Irene Zanette, Alexander Rack, Timm Weitkamp, Aniko Sztrókay, Thomas Schlossbauer, Fabian Bamberg, Maximilian Reiser, and Franz Pfeiffer: Numerical comparison of X-ray differential phase contrast and attenuation contrast	Biomedical Optics Express	2.333
C. Wall, R. Prakash, C. Kübel, H. Hahn, M. Fichtner: Synthesis of [Co/LiF/C] nanocomposite and its application as cathode in lithium-ion batteries	J. Alloys Comp	2.138
A. Rashidian, D. M. Klymyshyn, M. T. Aligodarz, M. Börner, J. Mohr: Microwave Performance of Photoresist-Alumina Microcomposites for Batch Fabrication of Thick Polymer-Based Dielectric Structures	J. Micromech. Microeng.	2.105
J. Pröll, R. Kohler, A. Mangang, S. Ulrich, M. Bruns, H.J. Seifert, W. Pfleging: Diode laser heat treatment of lithium manganese oxide films	Applied Surface Science	2.112
Mireille Gaillard, Chantal Boulmer-Leborgne, , Nadjib Semmar, Éric Millon, Agnès Petit: Carbon nanotube growth from metallic nanoparticles deposited by pulsed-laser deposition on different substrates	Applied Surface Science	2.112
J. Pröll, R. Kohler, A. Mangang, S. Ulrich, M. Bruns, H.J. Seifert, W. Pfleging: Diode laser heat treatment of lithium manganese oxide films	Applied Surface Science	2.112
T. Roelandts, K.J. Batenburg, E. Biermans, C. Kübel, S. Bals, J. Sijbers: Partially Discrete Tomography for Dense Particle Segmentation	Ultramicroscopy	2.063
F. Stemme, M. Bruns, H. Geßwein, M. Schroeder, M. Sazegar,M. D. Drahus, R.-A. Eichel, F. Paul, J. Haußelt, and J. R. Binder: Effects of thermal processing and iron doping in co-sputtered barium strontium titanate thin films	Journal of Materials Science	2.015
Florian Maier-Flaig, Eric J. Henderson, Sebastian Valouch, Sönke Klinkhammer, Christian Kübel, Geoffrey A. Ozin, Uli Lemmer: Photophysics of organically-capped silicon nanocrystals - A closer look into silicon nanocrystal luminescence using low temperature transient spectroscopy	Chemical Physics	1.896
P.M. Leufke, A.K. Mishra, A. Beck, D. Wang, C. Kübel, R. Kruk, H. Hahn: Large-distance rf- and dc-sputtering of epitaxial La1-xSrxMnO3 thin films	Thin Solid Films	1.890
Michael Bohling, Thomas Seiler, Boguslaw Wdowiak, Jürgen Jahns, Jürgen Mohr, and Martin Börner: Highly precise micro-retroreflector array fabricated by the LIGA process and its application as tapped delay line filter	Applied Optics	1.748
Anja Backen, Srinivasa Reddy Yeduru, Anett Diestel, Ludwig Schultz, Manfred Kohl, Sebastian Fähler: Epitaxial Ni-Mn-Ga Films for Magnetic Shape Memory Alloy Microactuators	Advanced Engineering Materials	1.746

Citation	Published in	Impact Factor
I. Ennen, S. Löer, C. Kübel, D. Wang, A. Auge, A. Hütten, P. Schattschneider: Site-specific chirality in magnetic transitions	J. Magn. Mag. Mat.	1.690
R. Kohler, J. Proell, M. Bruns, S. Ulrich, H.J. Seifert, W. Pfleging: Conical surface structures on model thin-film electrodes and tape-cast electrode materials for lithium-ion batteries	Applied Physics A Materials Science & Processing	1.630
S. Dengler, C. Kuebel, A. Schwenke, G. Ritt, B. Eberle: Optical Limiting Properties of Laser Ablated Gold, Silver and Gold Silver Alloy Nanoparticles	Journal of Optics	1.573
M. Bruns, C. Barth, P. Brüner, S. Engin, T. Grehl, C. Howell, P. Koelsch, P. Mack, P. Nagel, V. Trouillet, D. Wedlich, R. G. White: Structure and Chemical Composition of Mixed Benzylguanine and Methoxy Terminated SAMs for Immobilization of Biomolecules	Surf. Interface Anal.	1.249
Jian Fu, Simone Schleede, Renbo Tan, Liyuan Chen, Martin Bech, Klaus Achterhold, Martin Gifford, Rod Loewen, Ronald Ruth, Franz Pfeiffer: An algebraic iterative reconstruction technique for differential x-ray phase-contrast computed tomography	Zeitschrift für Medizinische Physik	1.212
Schwab F, Schleede S, Hahn D, Bech M, Herzen J, Auweter S, Bamberg F, Achterhold K, Yildirim AO, Bohla A, Eickelberg O, Loewen R, Gifford M, Ruth R, Reiser MF, Nikolaou K, Pfeiffer F, Meinel FG: Comparison of Contrast-to-Noise Ratios of Transmission and Dark-Field Signal in Grating-Based x-ray Imaging for Healthy Murine Lung Tissue	Z Med Phys	1.212
M. Fuchs, A. Zaenal, C. Kübel, P. Weidler, T. Henmi, R. Köster, H. Gliemann: Patterned Deposition of Allophane Nanoparticles on Silicon Substrates	Clays and Clay Minerals	1.162
Akanksha Singh, Wilhelm Pfleging, Markus Beiser, Chantal Khan Malek: Transparent thin thermoplastic biochip by injection-moulding and laser transmission welding	Microsystem Technologies	0.827
Pascal Meyer, James D. Claverley, Richard K. Leach: Quality control for deep x-ray lithography (LIGA): a preliminary metrology study	Microsystem Technologies	0.827
Johannes PROELL, Robert KOHLER, Alexander MANGANG, Sven ULRICH, Carlos ZIEBERT, Wilhelm PFLEGING: 3D Structures in Battery Materials	JLMN-Journal of Laser Micro Nanoengineering	1.024
A. Rashidian, D.M. Klymyshyn, M. Tayfeh Aligodarz, M. Boerner and J. Mohr: Photoresist-based polymer resonator antennas with permanent frame	Electronics Letters	0.965
F. Greiner and H. Schlaak: High aspect ratio metal micro and nano pillars for minimal footprint MEMS suspension	Microsystem Technologies	0.931
Heungsoo KIM, Johannes PROELL, Robert KOHLER, Wilhelm PFLEGING, Alberto PIQUE: Laser-Printed and Processed LiCoO2 CathodeThick Films for Li-Ion Microbatteries	Journal of Laser Micro/Nanoengineering	0.556
Cato, Andrew C. B.; Oppong, Emmanuel; Sekula-Neuner, Sylwia: Micropatterned Surfaces as Tools for the Study of the Rapid Non-Genomic Actions of Steroid Receptors	Advances in Rapid Sex-Steroid Action	
P.M. Leufke, R. Kruk, D. Wang, C. Kübel, H. Hahn: Ferroelectric vs. structural properties of large-distance sputtered epitaxial LSMO/PZT heterostructures	AIP Avances	
Martin Bech, Arne Tapfer, Astrid Velroyen, Andre Yaroshenko, Bart Pauwels, Peter Bruyndonckx, Xuan Liu, Alexander Sasov, Jürgen Mohr, Marco Walter and Franz Pfeiffer: Results from the first preclinical CT scanner with grating based phase contrast and a rotating gantry	AIP Conference Proceedings	
Christian David, Simon Rutishauser, Michael Sprung, Irene Zanette, and Timm Weitkamp: X-ray grating interferometry - Applications in metrology and wave front sensing	AIP Conference Proceedings	

Citation	Published in	Impact Factor
I. Zanette, S. Rutishauser, C. David, F. Pfeiffer, J. Mohr, and T. Weitkamp : Multidirectional X-ray dark-field imaging with two-dimensional gratings	AIP conference proceedings	
Kenntner, J.; Altapova, V.; Grund, T., Pantenburg; F. J.; Meiser, J.; Baumbach, T.; Mohr, J.: Fabrication and Characterization of Analyzer Gratings with High Aspect Ratios for Phase Contrast Imaging Using a Talbot Interferometer	AIP Conference Proceedings	
Mohr, J.; Grund, T.; Kunka, D.; Kenntner, J.; Leuthold, J.; Meiser, J.; Schulz, J.; Walter, M.: High Aspect Ratio Gratings for X-Ray Phase Contrast Imaging	AIP Conference Proceedings	
Th. Grund, J. Kenntner, A. Last, J. Mohr, V. Nazmov, M. Simon: Reiststruktur zur Herstellung einer röntgenoptischen Gitterstruktur	Deutsches Patent DE 10 2010 049 994 B3	

User Reports

Following the completion of a user project users are encouraged to publish the results in high ranking scientific journals and to disseminate them at the most relevant conferences with acknowledgement to KNMF. In addition users are expected to submit a report on their work to the KNMF user office. Reports received for work completed in 2012 are given below.

List of contributors

(Reports received by 18th October 2013)

Proposal ID	Proposal Title	Name	Organisation	Country
2010-003-000182	Hybrid organic photodetector mediated by optical antennas	Katja Dopf	Karlsruhe Institute of Technology (KIT)	Germany
2010-004-000301	Optically Responsive Nanostructures for the Label-Free Readout of Biospecific Interactions in High-Density Peptide Arrays	Reiner Dahint	Ruprecht-Karls-Universität Heidelberg	Germany
2011-007-000621	Analysis of Interferometric phase contrast imaging for dental imaging and comparison with simulation results	Ciamak Abkai	Sirona Dental Systems GmbH	Germany
2012-009-001153	3D forming of laser patterned foils by micro thermoforming	Alexander Kolew	Cardiff University	United Kingdom
2012-009-001154	Nanosphere lithography for micro tooling in bulk metallic glass	Nicolas Blondiaux	CSEM SA - Centre Suisse d'Electronique et Microtechnique SA	Switzerland

Final Reports as submitted by the Users

Proposal 2010-003-000182

Hybrid organic photodetector mediated by optical antennas

Katja Dopf

Karlsruhe Institute of Technology (KIT)

Germany

Summary Report

1. **Project goals**:
   We envision in this project to build a novel photodetection device, containing optical nanoantennas, electrical contacts and organic photosensitive materials (see Fig. 1)

   Optical antennas are metallic nanoobjects that efficiently confine light into a tiny volume resulting in high electric. They show a high potential to improve photodetectors in many respects and to use them for special photodetection applications.

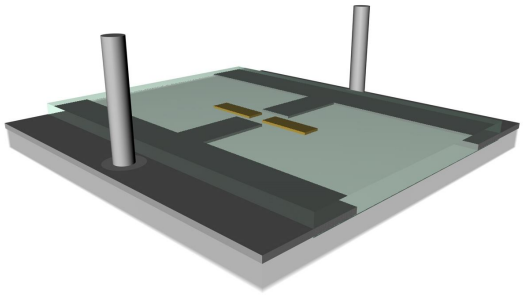

Fig. 1: Organic photodetector containing an optical gold nanoantenna.

The aim of the proposal is to develop the fabrication processes that are necessary to build optical antennas and contact pads. The method of choice is e-beam lithography and a metal lift-off process.

2. **Project results**:

   In the KNMF project the main focus is on developing a fabrication protocol to fabricate both gold nanoantennas and pads for electrical contacts of the device. The main challenges are the fabrication of the nanostructures by e-beam lithography, gold deposition and a lift-off which are not the standard dimensions for that the e-beam system at IMT is usually used for. And secondly the combination of nanometer scale antennas with micrometer scale contact pads onto the same substrate with a high precision and not short-circuited is challenging as well. That means, as for standard e-beam lithography an electrically conducting substrate is necessary, the conducting ITO layer used in our case needs to be patterned as well. Therefore multiple e-beam lithography steps are necessary to reach the final goal.

Karlsruhe Nano Micro Facility (KNMF)
Karlsruhe Institut of Technology (KIT)
Hermann-von-Helmholtz-Platz 1
76344 Eggenstein-Leopoldshafen
Germany

User Office
Phone: +49 (0)7247 82-3123
Fax: +49 (0)7247 82-7273
Email: knmf-useroffice@kit.edu
Web: www.kit.edu/knmf

Or a different approach as e.g. writing the structures onto a glass surface where parts of the ITO are removed before will be necessary.

In accordance with the technicians we decided to realise the aim by two steps as the fabrication is very complex. In a first series of tests the goal was to develop a single step reproducible fabrication protocol for nanoantennas on a 170 µm thin glass cover slip that is covered with approximately 30 nm conducting ITO (indium tin oxide) layer.

As resist we used PMMA 950 k (Allresist) that was spincoated for 60 s with 7000 rpm onto the substrate and baked out according to the specifications of the manufacturer. The PMMA layers are 65-70 nm thick. The thickness was measured by using a Dektak profilometer.

E-beam lithography was then performed with a Vistec e-beam system by the technicians of the IMT. The structures were repeated several times with dose variations. The layout of the structures covers a huge range of different nanoantenna geometries and contact pads in rectangular and in trapezoid shape. A 30 nm layer of gold was evaporated onto the structured e-beam resist and a lift-off in Acetone was performed. The nanostructures were characterized with a dark-field microscopy setup.

The first test run resulted in nearly empty substrates. Possible reasons are choosing an inapplicable dose range during the e-beam process or problems with the lift-off. Therefore, in the second run the dose of the e-beam process was varied over a much bigger range and the lift-off was performed without using ultrasound as this maybe separated all gold structures from the substrate.

With this adaptations we could successfully fabricate some nanoantenna arrays and contact pads (see Fig. 2). But still most of the gold could not be removed during the lift-off process (see Fig. 3).

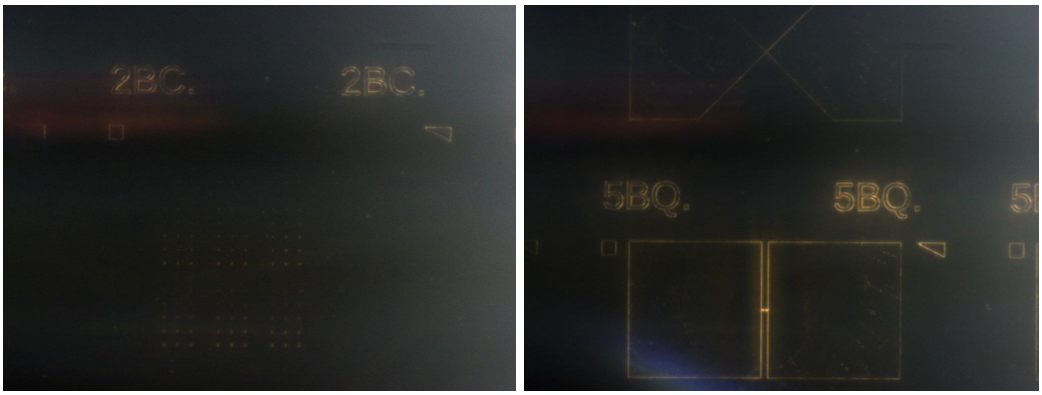

Fig. 2: Dark-field microscopy images (in reflection) of a nanoantenna array (left) and contact pad structures (right) consisting of a 30 nm gold layer.

Karlsruhe Nano Micro Facility (KNMF)
Karlsruhe Institut of Technology (KIT)
Hermann-von-Helmholtz-Platz 1
76344 Eggenstein-Leopoldshafen
Germany

User Office
Phone: +49 (0)7247 82-3123
Fax: +49 (0)7247 82-7273
Email: knmf-useroffice@kit.edu
Web: www.kit.edu/knmf

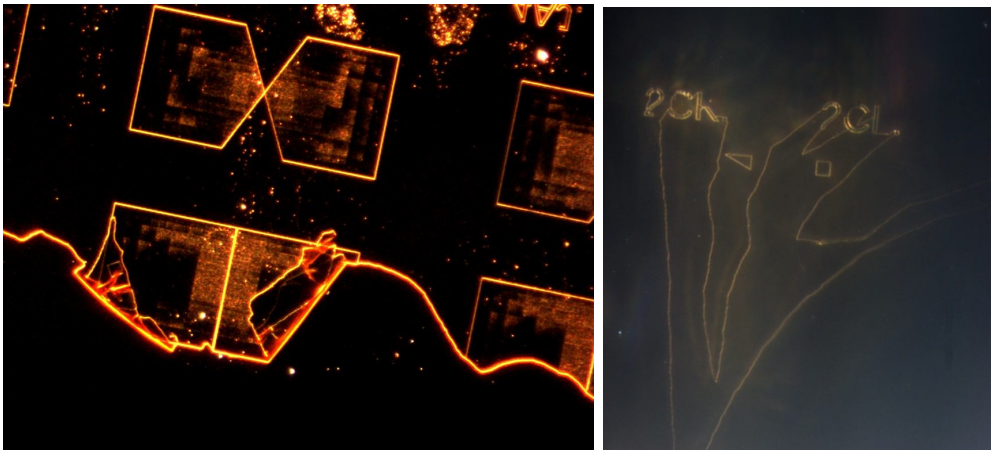

Fig. 3: Dark-field microscopy images (left: in transmission, right: in reflection) of lift-off problems. During the lift-off process parts that should not be removed were separated from the substrate others could not be removed at all.

For a next and last e-beam run we envision the use of a finer dose variation around the optimum dose from the second run. The e-beam run is not planned before January 2012 because of malfunction of the e-beam system in the second half of 2011.

Parameters as resist thickness, e-beam lithography dose and lift-off parameters could successfully optimized for the single-step process. Nevertheless the main goal we envisioned in the proposal is not yet reached due to the complexity of the final structures and the time limitations within KNMF proposal. Therefore we apply for a continuation of the proposal.

3. **Publications** (please stick to the user guidelines for publications & acknowledgements on www.kit.edu/knmf):

   not yet (project is not yet finished)

4. **Comments**:

   Please note that the project is not yet completed, and consequently this is only a preliminary summary report.

   There are two reasons for the unusual long period of this KNMF project. The project start was shifted due to the pregnancy leave of the proposer and afterwards the e-beam system was out of order for several months. Until now two e-beam time slots were assigned, the third and last will presumably be in January 2012.

Proposal 2010-004-000301

Optically Responsive Nanostructures for the Label-Free Readout of Biospecific Interactions in High-Density Peptide Arrays

Reiner Dahint

Ruprecht-Karls-Universität Heidelberg

Germany

Final Report

1. Project goals (max. 1.800 characters):

In recent years, array concepts have become popular and powerful tools to facilitate highly parallel, rapid identification of binding events for applications in biomedical sciences, biotechnology and pharmacology. Interaction analysis is usually facilitated by labelling the potential binding partners with additional markers. To overcome the associated obstacles, strong efforts are being made to establish label-free detection schemes.

For this purpose, we have developed a new optically responsive, nanocomposite material. It is formed by self-assembly of (sub)monolayers of dielectric nanoparticles on a metal-coated substrate followed by metallization of the dielectric cores.[1,2] Upon reflection of white light, the layer exhibits a pronounced plasmonic extinction spectrum, which shifts to higher wavelengths upon molecule adsorption, thus, providing a label-free sensing mechanism (Fig. 1).

A major problem of the detection system stems from the fact that the particles are deposited by self-assembly, resulting in not strictly regular films. As the optical properties of the layers depend on packing density, local changes in optical properties may occur which deteriorate the detection of binding events in high-density arrays and reduce sensitivity. Moreover, the diversity of accessible patterns is limited, and theoretical modelling of the optical properties to provide guidelines for improved sensor design is complicated by the non-regular structure.

The goal of the project is, therefore, a systematic study aiming at the generation of strictly regular, optically responsive nanostructures with different internal structure to optimize biosensor response. As structural elements ranging from 50 to 900 nm in size are in the focus of our interest, Electron Beam Lithography (EBL) has been chosen for the fabrication process.

2. Project results (max. 7.000 characters + figures):

As an alternative to nanoparticle monolayers, nanostructures have been fabricated at KNMF (Fig. 2). Starting point was a so-called *reference structure* which employs a silicon substrate coated with a 5 nm adhesion layer of chromium followed by a gold film of 15 nm thickness. The nanostructures were formed from PMMA and coated with 30 nm of gold by thermal evaporation. They consist of interconnected cubes of 300 nm in size, with connecting units of the same height and length, but a width of only 100 nm. In addition, variants of this reference structure have been investigated as described in the following. The total size of each nanopattern was 2.5 x 2.5 mm.

First experiments show that even without further optimization the reference structure exhibits practically the same sensitivity towards protein adsorption as the nanoparticle films (Fig. 3). However, it provides a better lateral homogeneity and additional options to tune the sensor response. For example, the extinction spectrum can be deliberately altered if the angle between the incident beam and the main axes of the nanostructure is varied. Such option does not exist in case of the quasi-isotropic structure of the nanoparticle films.

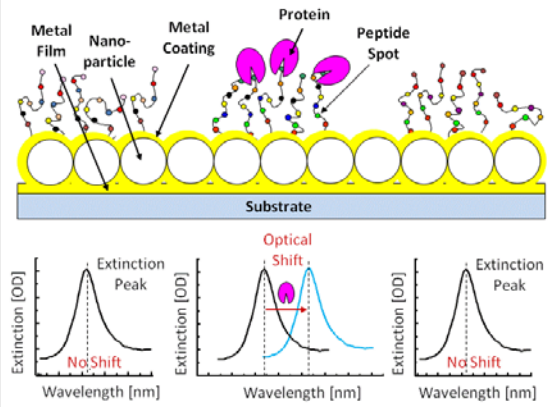

Figure 1: *Label-free detection of biospecific binding events in peptide arrays (schematic). The extinction spectrum is shifted to longer wavelengths at the locations where proteins bind to their specific probes (here: specific peptide sequences).*

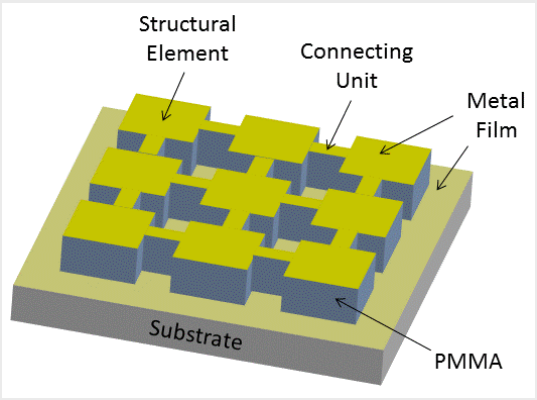

Figure 2: *Nanostructures fabricated by Electron Beam Lithography at KNMF (schematic). A silicon wafer coated with a 5 nm adhesion layer of chromium and a 15 nm gold film serves as the substrate. The PMMA structure is covered with 30 nm of gold.*

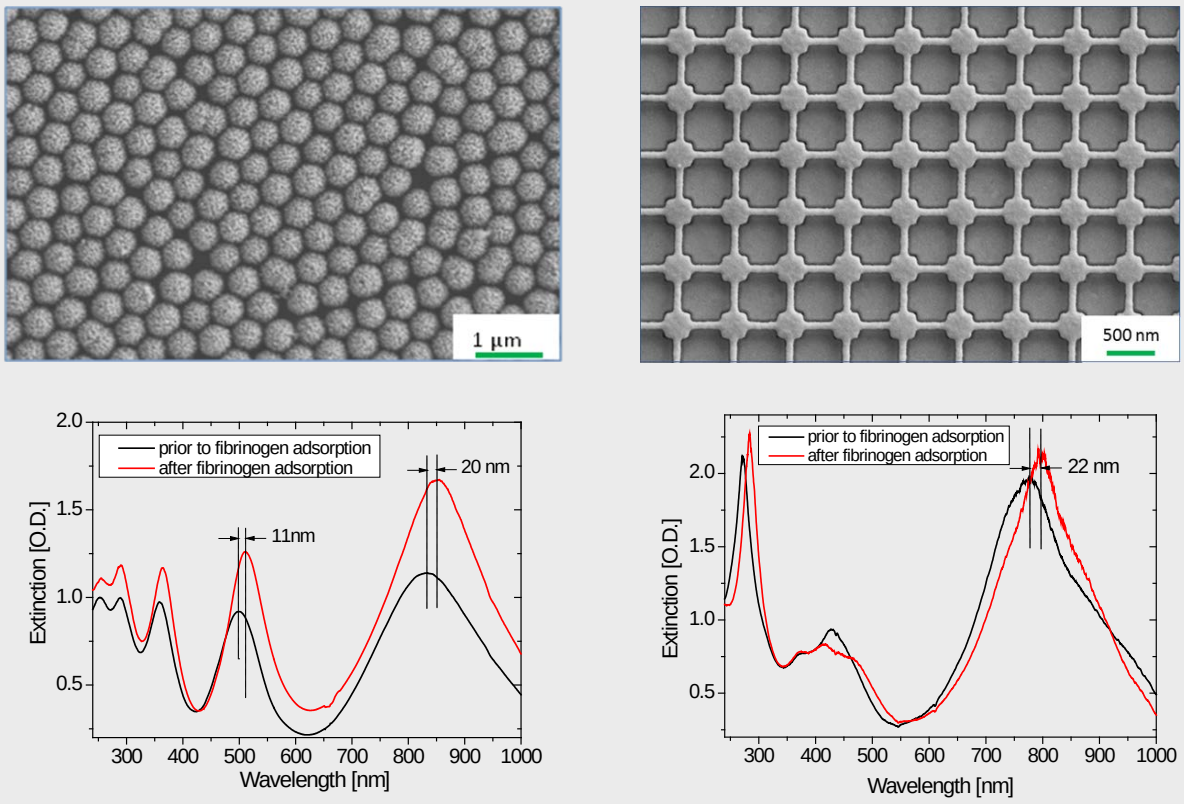

Figure 3: *Scanning electron microscopy images (top) and red-shift of the extinction spectrum upon fibrinogen adsorption (bottom) for nanoparticle films (left) and nanostructures fabricated at KNMF (right).*

Karlsruhe Nano Micro Facility (KNMF)
Karlsruhe Institute of Technology (KIT)
Hermann-von-Helmholtz-Platz 1
76344 Eggenstein-Leopoldshafen
Germany

User Office
Phone: +49 (721) 608-3123
Fax: +49 (721) 608-6273
Email: knmf-useroffice@kit.edu
Web: www.knmf.kit.edu

Scaling of the reference structure by a factor of 0.5 and 2, i.e. the formation of cubes with dimensions of 150 and 600 nm, respectively, clearly shows the most pronounced extinction spectrum for the smallest pattern size (Fig. 4, left). The optical properties can also be improved upon changing from cubes to cuboids whose height is larger than their width and length (Fig. 4, right). Comparative experiments aiming at light reflection from non-structured PMMA films deposited on the same type of substrate clearly show interference effects with significantly smaller peak amplitude than in case of the metallized nanostructures but with a similar peak spacing. We may, thus, conclude that the optical response of the nanostructures is caused by the superposition of optical interference and plasmon excitation, and more pronounced for the higher cuboids.

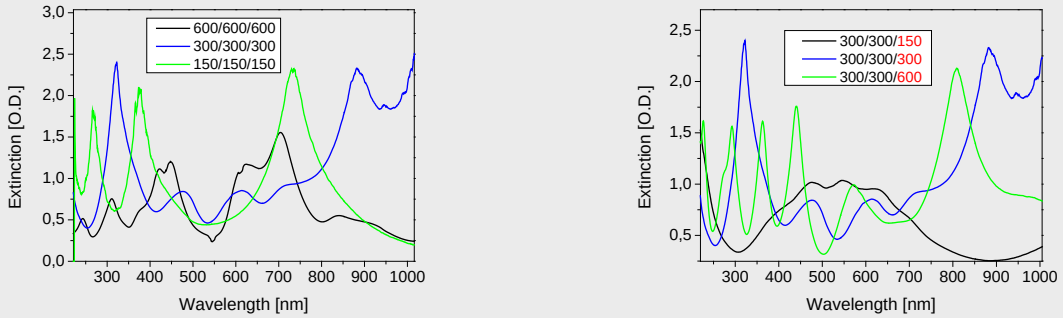

Figure 4: *Extinction spectra of different cube-shaped nanostructures scaled in size (left) and cuboid-shaped nanostructures with the same lateral dimensions but different height (right). In each case, the nanostructures are interconnected as shown in Fig. 3, top right. The numbers l/w/h in the inset indicate the length (l), width (w) and height (h) of the respective cubes/cuboids in nm.*

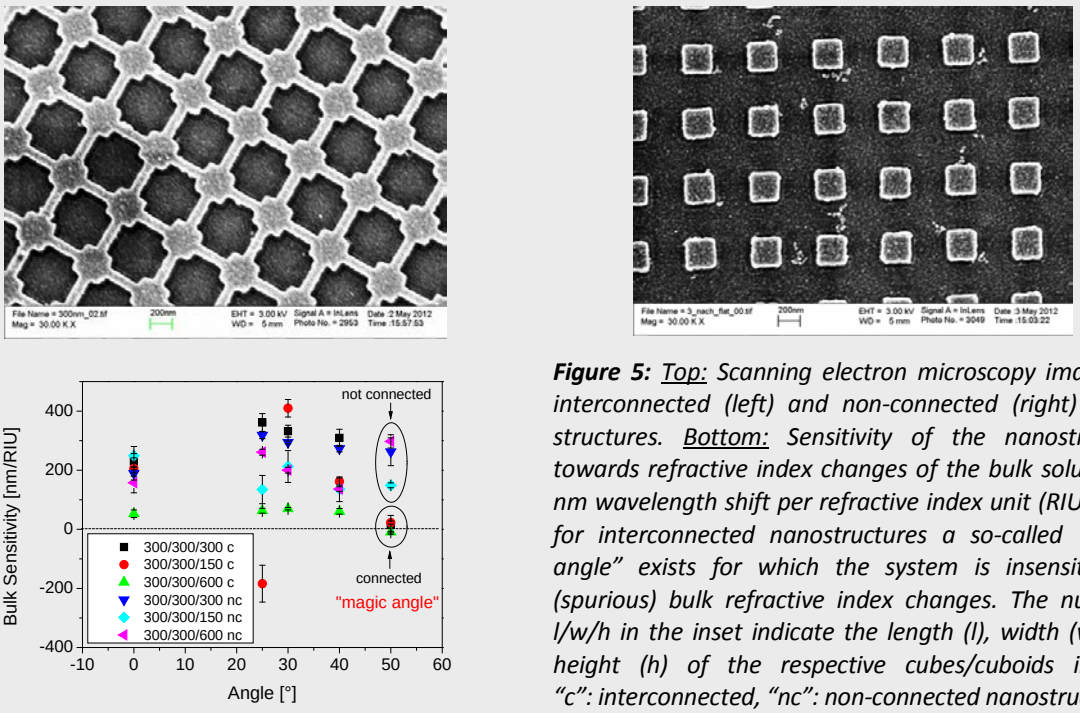

Figure 5: *<u>Top:</u> Scanning electron microscopy images of interconnected (left) and non-connected (right) nano-structures. <u>Bottom:</u> Sensitivity of the nanostructure towards refractive index changes of the bulk solution in nm wavelength shift per refractive index unit (RIU). Only for interconnected nanostructures a so-called "magic angle" exists for which the system is insensitive to (spurious) bulk refractive index changes. The numbers l/w/h in the inset indicate the length (l), width (w) and height (h) of the respective cubes/cuboids in nm. "c": interconnected, "nc": non-connected nanostructures.*

Karlsruhe Nano Micro Facility (KNMF)
Karlsruhe Institute of Technology (KIT)
Hermann-von-Helmholtz-Platz 1
76344 Eggenstein-Leopoldshafen
Germany

User Office
Phone: +49 (721) 608-3123
Fax: +49 (721) 608-6273
Email: knmf-useroffice@kit.edu
Web: www.knmf.kit.edu

A severe problem in plasmon-based biosensing in liquid environments originates from the fact that both molecule adsorption and refractive index changes of the bulk solution contribute to the observed response. Usually, unwanted bulk effects are reduced by working in total reflection geometry accompanied by a (second) reference measurement. In contrast, it has been found that this is not necessary in case of gold-coated nanoparticle films as bulk effects can be eliminated from the optical response by appropriate selection of the angle of incidence.[3] Experiments with the KNMF nanostructures show that they also exhibit this important feature, which provides a clear advantage compared to conventional plasmon-based analysis (Fig. 5). However, it has only been observed for interconnected structures so far. Nanostructures composed of separated cubes miss this property, which emphasizes the importance of nanostructure contact in biosensor design. Utilizing samples with interconnected cuboids we have already been able to identify KNMF nanostructures which show higher sensitivity in *in situ* protein adsorption measurements than the nanoparticle films previously used.

The results of the project may, thus, be summarized as follows:

1) The nanostructures fabricated at KNMF are well-suited for label-free detection of biospecific interactions.
2) They exhibit excellent lateral homogeneity and reproducibility, and provide high structural flexibility for further improvement of optical properties and sensitivity.
3) With respect to optical response, smaller lateral structure size and larger nanostructure height seem to be favorable.
4) Even without optimization, adsorption-induced wavelength shifts are comparable to those found in core-shell nanoparticle systems in air.
5) Enhanced sensitivity is observed in *in situ* measurements under liquids.
6) For nanostructures with connecting units, a “magic angle” is found for which refractive index changes of the bulk can be eliminated from the sensor response while adsorption processes can still be detected.
7) No such “magic angle” has been observed for nanostructures without connecting units.
8) The nanostructures fabricated at KNMF, therefore, appear to be a promising tool for high-throughput medical diagnostics.

3. Publications (please stick to the user guidelines for publications and acknowledgements on www.knmf.kit.edu):

Publication of the results is in preparation. However, prior to manuscript submission, some of the above conclusions will be confirmed and extended in a continuation of the project.

4. Comments (max. 1.800 characters):

We gratefully acknowledge the excellent and friendly support by KNMF, their willingness to always meet the needs of the users as well as the high quality of the fabricated nanostructures.

[1] R. Dahint, E. Trileva, H. Acunman, U. Konrad, M. Zimmer, V. Stadler, M. Himmelhaus, *Biosensors & Bioelectronics*, 2007, **22**, 3174-3181.
[2] P. Buecker, E. Trileva, M. Himmelhaus, R. Dahint, *Langmuir*, 2008, **24**, 8229-8239.
[3] H. Takei, M. Himmelhaus, T. Okamoto; *Optics Lett.*, **2002**, *27*, 342-344.

Proposal 2011-007-000621

Analysis of Interferometric phase contrast imaging for dental imaging and comparison with simulation results

Ciamak Abkai

Sirona Dental Systems GmbH

Germany

Note: *Please fill in this report form and save/print it as a PDF file, then upload it to the KNMF proposal submission system. A cover page containing proposal title, proposer name(s), and technologies selected will be added by the system. A link for the download of the complete report as a PDF file will be displayed in the system.*

Final Report

1. Project goals (max. 1.800 characters):

The main aim of this project was to compare simulation results and real experiment output for polychromatic Xray phase-contrast imaging (XPCI) for a given experimental setup and condition up to **100 keV** design energy.

Another target is to analyse the impact of XPCI for dental imaging, which could not be determined with provided gratings for a design energy of app. 23 keV.

By selecting a design energy of 100 keV and using xray sources powered with up to 125 kV we reach the maximum clinically possible energy for dental medical applications. Higher energies result in a more effective phase-contrast-ratio and reduce the patient effective dose.

2. Project results (max. 7.000 characters + figures):

A simulation and an experimental setup was realized during the project. Different visibilities V, for the different target energies 21.9 and 100 keV have been measured and simulated as shown in Table 1. As one can see the visibility for 100 keV is decreasing. The simulated results doesn't include the photon statistic and thus don't include SNR impact.

Design Energy [keV]	Visibility (Simulation)	Visibility (Experiment)
21.9	0.3688 ± 0.0017	0.1943 ± 0.0230
100.0	0.2447 ± 0.008	0.0546 ± 0.0010

Table1 : Simulated and experimentally obtained visibilities for the used setups

Karlsruhe Nano Micro Facility (KNMF)
Karlsruhe Institute of Technology (KIT)
Hermann-von-Helmholtz-Platz 1
76344 Eggenstein-Leopoldshafen
Germany

User Office
Phone: +49 (721) 608-3123
Fax: +49 (721) 608-6273
Email: knmf-useroffice@kit.edu
Web: www.knmf.kit.edu

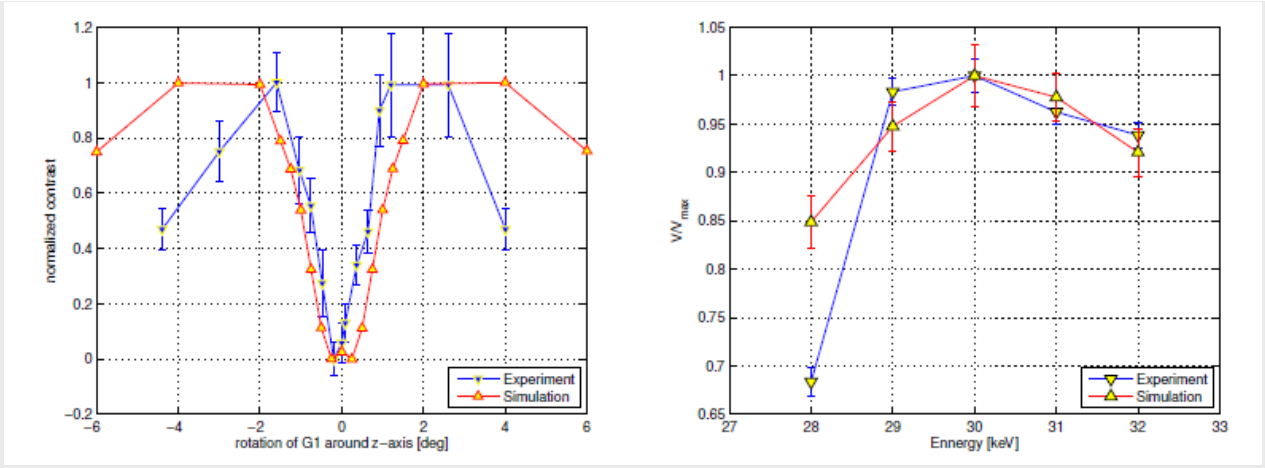

Figure 1: Sensitivity of the system : a) Influence of rotations of G1, b) Influence of tube voltage variations

Different Sensitivities have been examine in simulation and experiment, as shown in Figure 1.

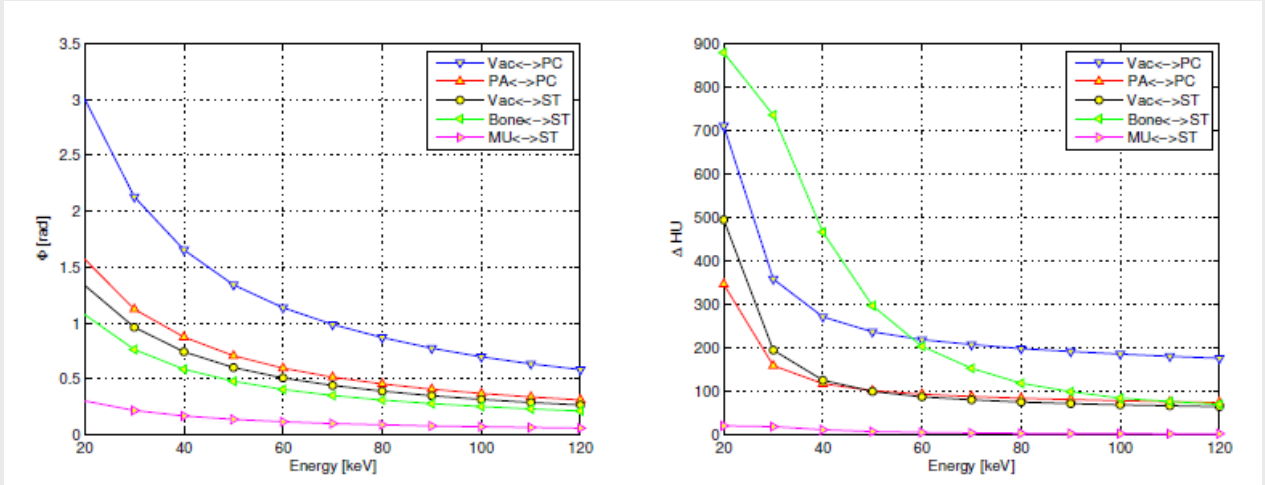

Figure 2: Expected phase shift and absorptions difference for different materials, depending on the mean xray energy.

The expected phase shift for higher energies is decreasing, as shown in Figure 2, for different materials. Experimental phase, absorption and darkfield results are shown in Figure 3. and 4. As one can see the results for 21.9 keV are very interesting, showing many details of the paraffin structure, however for 100 keV due to the bad Visibility, the results for phase-shift and dark-field images contain much less information in comparison to the absorption images.

Karlsruhe Nano Micro Facility (KNMF)
Karlsruhe Institute of Technology (KIT)
Hermann-von-Helmholtz-Platz 1
76344 Eggenstein-Leopoldshafen
Germany

User Office
Phone: +49 (721) 608-3123
Fax: +49 (721) 608-6273
Email: knmf-useroffice@kit.edu
Web: www.knmf.kit.edu

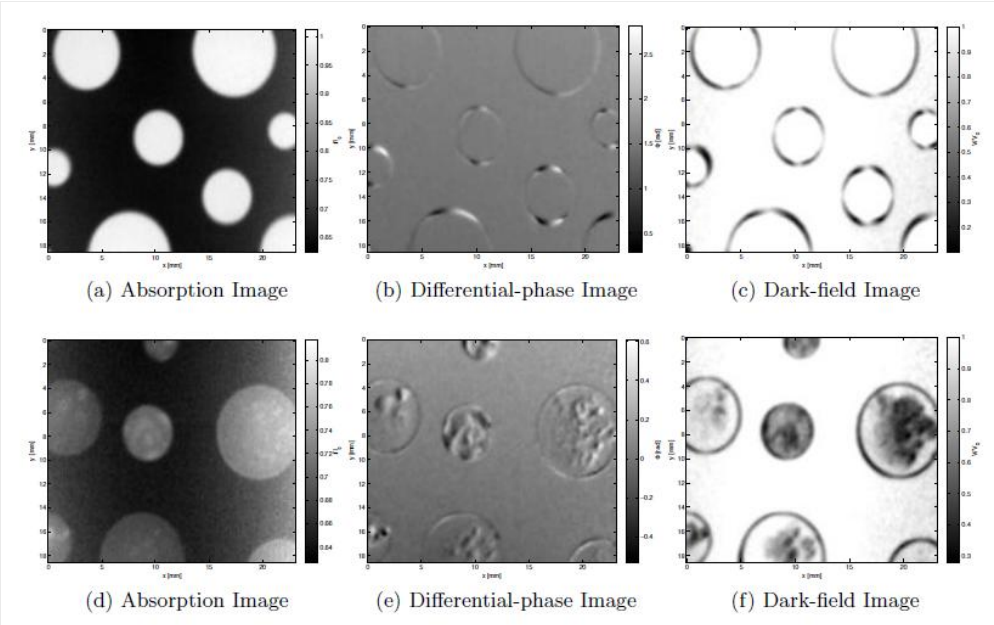

Figure 3: Results for 21.9 keV mean xray energy. Top: air gaps in polycarbonate phantom. Bottom: gaps filled with paraffin.

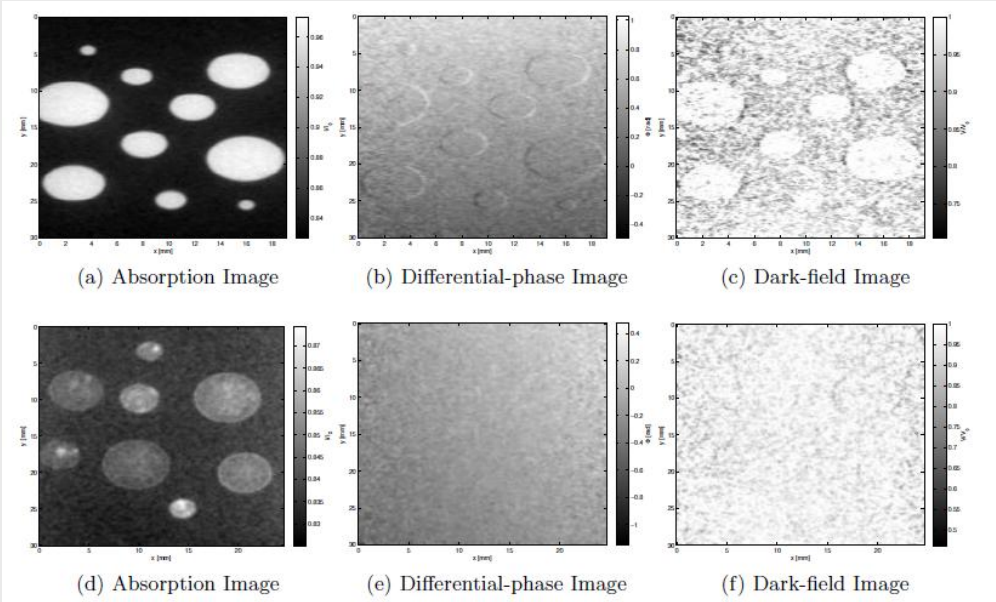

Figure 4: Results for 100 keV mean xray energy. Top: air gaps in polycarbonate phantom. Bottom: gaps filled with paraffin.

3. Publications (please stick to the user guidelines for publications and acknowledgements on www.knmf.kit.edu)**:**

Karlsruhe Nano Micro Facility (KNMF)
Karlsruhe Institute of Technology (KIT)
Hermann-von-Helmholtz-Platz 1
76344 Eggenstein-Leopoldshafen
Germany

User Office
Phone: +49 (721) 608-3123
Fax: +49 (721) 608-6273
Email: knmf-useroffice@kit.edu
Web: www.knmf.kit.edu

Publications are planed are in progress…

C. Guthier , C. Abkai, J. Ulrici, E. Hell, J. Schulz, J. Mohr, J.Hesser	First Interdisciplinary European Symposium on Biomedical Application of X-Ray Phase-Contrast Imaging Hotel Riessersee in Garmisch-Partenkirchen, Friday 13 Jan 2012.	2012

4. Comments (max. 1.800 characters)**:**

According to the experimental and simulated results, we can conclude that with the current limitations of the grating production process, it is not possible to use a system with 100 keV mean xray energy with reasonable contrast expectations for clinical and especially dental usage.

On the other hand the results for 21.9 keV are very promising for soft-tissue imaging, however due to the high z materials (bone, dentin, …) and the necessary high tube power not acceptable for dental applications.

Proposal 2012-009-001153

3D forming of laser patterned foils by micro thermoforming

Alexander Kolew

Cardiff University

United Kingdom

Final Report

1. Project goals:

Introduction

The micro thermoforming process has great potential for replication of 3D shaped foils with micro- and nanofeatured surfaces. Typical replication technologies like injection moulding and hot embossing are limited to replicate structures with oriented features to allow demoulding. Three dimensional parts with a functional surface topography cannot be produced due to the limitations of the demoulding process during tool opening or ejection. For 3D parts which have to be improved by self-cleaning surfaces these replication technologies can be used rarely.

Aim of the project

The Aim of the project is to find the minimum feature size for the 3D shape of micro thermoforming and to compare surface features which have been structured before and after the micro thermoforming process. To find the minimum feature size of micro thermoforming the tool dimensions have to be reduced to below 100 µm of functional features. As laser processing is a micro patterning technology which can generate 3D micro features cost effective. Also the surface characteristics of laser processed parts can be varied which shows a great potential of combining the micro thermoforming and laser processing technologies.

Principal tasks of the project

In this project a micro pattern of holes of different diameters and line and space structures has been produced to test the minimum feature sizes. The design used for this study is shown in figure 1. Holes and lines with a diameter/ width between 700 µm and 30 µm have been laser processed on a steel substrate plate which can be adapted to the micro thermoforming system. 12 different masters have been structured by laser processing using the DMG Lasertec 40 nanosecond laser system. Five masters are shown exemplarily in figure 2.

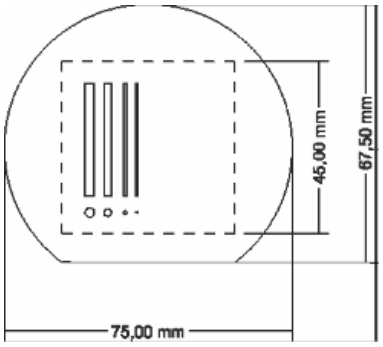

Figure 1: Used pattern design of the micro thermoforming demonstrator

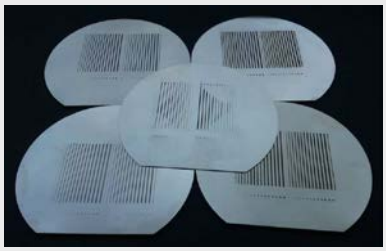

Figure 2: Five structured masks / thermoforming substrates used for microthermoforming experiments. The middle one is processed with cut through channels and holes.

Three of the masters have been structured creating cuts through the substrate; nine were produced by creating surface structures only. The different geometries were measured and used for microthermo-forming.

Karlsruhe Nano Micro Facility (KNMF)
Karlsruhe Institute of Technology (KIT)
Hermann-von-Helmholtz-Platz 1
76344 Eggenstein-Leopoldshafen
Germany

User Office
Phone: +49 (721) 608-3123
Fax: +49 (721) 608-6273
Email: knmf-useroffice@kit.edu
Web: www.knmf.kit.edu

2. Project results:

Description of work

Laser Processing of mask / substrate for micro thermoforming

Twelve masks / substrates for microthermoforming were produced using a variation of process parameters and substrate thickness. This results in different depth of the structures and different sidewall angles, widths and surface quality. Unfortunately all of the samples showed a high roughness around Ra=3-5µm. The widths of the channels varied between 731 µm and 27 µm on the thinner side of a cut through mask. Figure 3 shows one cut through channel by optical microscope at the top and the bottom side. To improve the stability and shape of micro thermoformed part the tool surface was structured by laser processing by ablation of one layer with different processing direction.

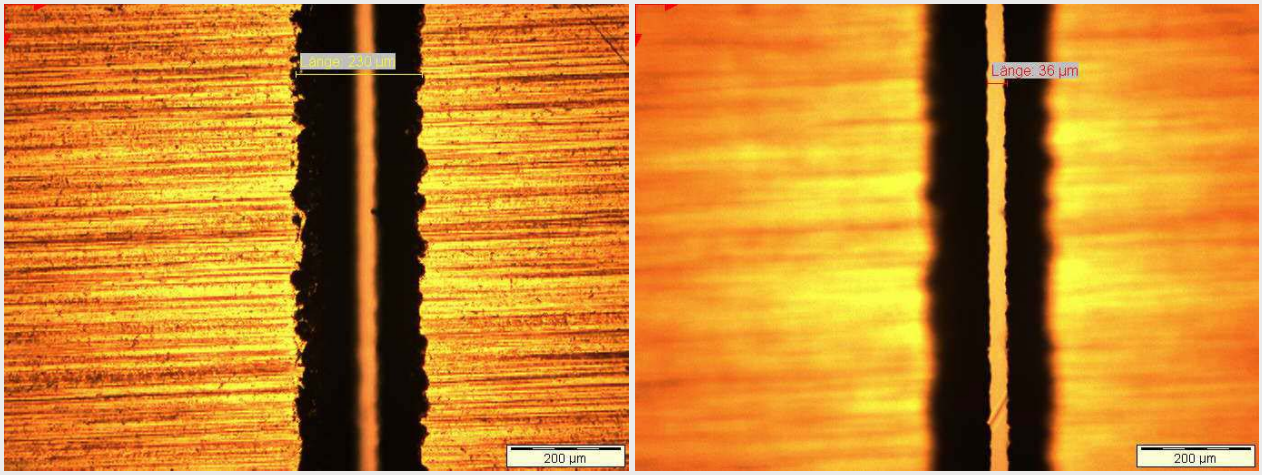

Figure 3: Cut through line of the thermoforming substrate.
The top opening was around 230 µm and the bottom opening around 37 µm.

Microthermoforming of thin foils

Polycarbonate foils of a thickness of 20 µm have been used for the microthermoforming experiments. Figure 4 shows three samples of thermoformed foils. The larger channels were replicated successfully. Due to a high roughness on the channels sidewall and sharp edges on the top side of the substrate small local deformations of the parts were observed. For channels of smaller width than 150 µm no complete demoulding was possible due to rough sidewalls or they haven't been filled completely by using lower thermoforming pressure.

Karlsruhe Nano Micro Facility (KNMF)
Karlsruhe Institute of Technology (KIT)
Hermann-von-Helmholtz-Platz 1
76344 Eggenstein-Leopoldshafen
Germany

User Office
Phone: +49 (721) 608-3123
Fax: +49 (721) 608-6273
Email: knmf-useroffice@kit.edu
Web: www.knmf.kit.edu

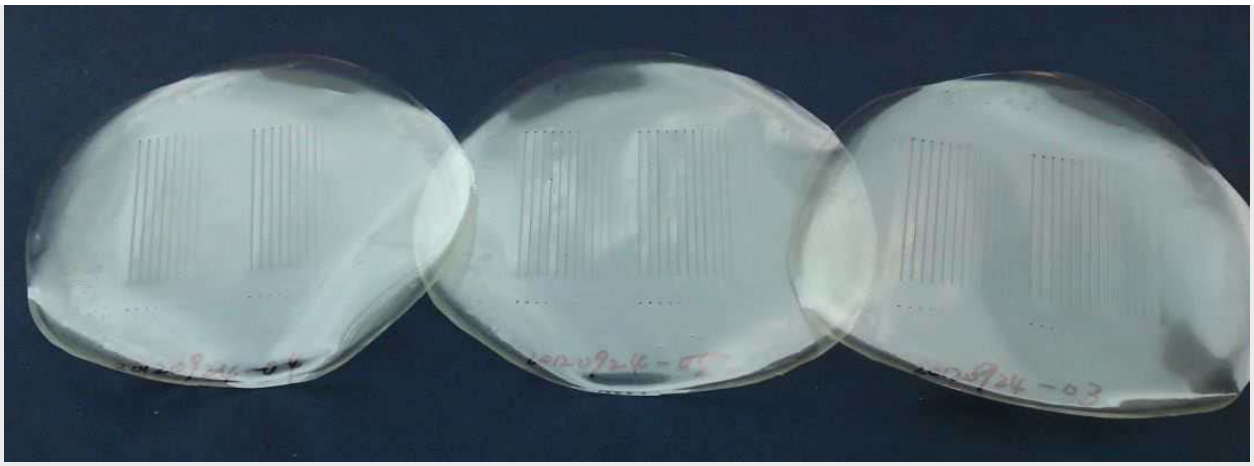

Figure 4: Three polycarbonate foils of 20 µm thickness which have been formed by microthermoforming into laser cut substrate.

Conclusions

As the replication temperature in microthermoforming in lower compared to hot embossing or injection moulding the polymer shows higher viscosity during the forming step. Cavities are not completely filled but the foil is bent and stretched into the micro features. Nevertheless a high roughness limits the demoulding even when the cavities are not completely filled with polymer. Due to the high roughness of the laser material processed mask no demoulding was possible with the smaller channels. The smallest reproducible feature size was 140 µm but the minimum feature size is not yet reached.

We observed a significant influence of the surface characteristics produced by laser processing. Instead of the roughness there was a higher influence of the orientation of laser material removal. Even with lower surface roughness, sliding of the polymer foils was reduced when structuring the surface of the substrate parallel to the channel instead of orthogonal.

3. Publications:

4. Comments:

Project number CIP 3-03 (EUMINAfab cross-infrastructure JRA project).
The EUMINAfab project is co-funded by the European Commission within the 7th Framework Programme.
Project reference is FP7-2008-INFRASTRUCTURES-1-226460

Karlsruhe Nano Micro Facility (KNMF)
Karlsruhe Institute of Technology (KIT)
Hermann-von-Helmholtz-Platz 1
76344 Eggenstein-Leopoldshafen
Germany

User Office
Phone: +49 (721) 608-3123
Fax: +49 (721) 608-6273
Email: knmf-useroffice@kit.edu
Web: www.knmf.kit.edu

Proposal 2012-009-001154

Nanosphere lithography for micro tooling in bulk metallic glass

Nicolas Blondiaux

CSEM SA - Centre Suisse d'Electronique et Microtechnique SA

Switzerland

Project Report

Final Report

1. Project goals:

Short-term: investigate the hot embossing of bulk metallic glass using structured silicon masters as molds.
Long-term: develop new process chains for the fabrication of nanostructured replication molds for hot embossing and injection molding.

2. Project results:

Preliminary work made at CSEM:
The structured silicon masters have been produced by CSEM by means of nanosphere lithography combined with standard microfabrication processes. Two types of structures were made for the project:
structure 1: lateral size of 350nm, interspace 500nm, height 600nm
structure 2: lateral size of 150nm, interspace 300nm, height 400nm
Work carried out at KIT:

- BMG samples purshased from Liquidmetal (grade LM001 & LM601) have been prepared (EDM cut + polishing).
- The hot embossing press was setup to allow very high temperature embossing
- A series of trials was made to identify the best conditions to emboss the bulk metallic glass. the most critical point was to make very fast heating/cooling cycles to avoid a crystallization of the materials (if it stays too long above the Tg).
- We focused mainly on the grade LM001 as the other grade could hardly be embossed.

3. Publications:

With the current results, no publications can be intended.
However, we observed the following points which could be interesting for publication if additional tests are done:

- The samples replicated in the BMG were structured according to the template of the silicon. the aspect ratio of the features was not satisfactory (60nm depth instead of the 600nm expected)
- The high aspect ratio nanostructures were found to be difficult to replicate but the macro microscale features were easily replicated.
- By polishing the samples before embossing, the quality of the parts was greatly improved. one of the problem was the presence of "black spots" that came from the EDM cutting process. we identified by EDX that EDM drastically affect the composition of the material, which loses locally its thermoplastic properties. Polishing allowed the removal of these defects. A second point is the removal of the recast layer and eventually of a top layer oxidized when the material is exposed in air to high temperatures.

4. Comments:

EUMINAfab project number 1089. EUMINAfab is co-funded by the European Commission within the 7th Framework Programme. Project reference is FP7-2008-INFRASTRUCTURES-1-226460.

Karlsruhe Nano Micro Facility (KNMF)
Karlsruhe Institute of Technology (KIT)
Hermann-von-Helmholtz-Platz 1
76344 Eggenstein-Leopoldshafen
Germany

User Office
Phone: +49 (721) 608-3123
Fax: +49 (721) 608-6273
Email: knmf-useroffice@kit.edu
Web: www.knmf.kit.edu